# THE USE OF COHERENT ANTI-STOKES RAMAN SPECTROSCOPY AS A DIAGNOSTIC TECHNIQUE FOR STUDYING THE HYDROGENATION OF CARBON MOXIDE IN A TUBE-WALL REACTOR

BY

RUSSELL JAMES SIMON

B.Sc. (Eng) (Cape Town)

Submitted to the University of Cape Town
in fulfillment of the requirements for the degree of

MASTER OF SCIENCE

University of Cape Town

Department of Chemical Engineering
University of Cape Town
Rondebosch, Cape
South Africa

The University of Cape Town has been given the right to reproduce this thesis in whole or in part. Copyright is held by the author.

The copyright of this thesis vests in the author. No quotation from it or information derived from it is to be published without full acknowledgement of the source. The thesis is to be used for private study or non-commercial research purposes only.

Published by the University of Cape Town (UCT) in terms of the non-exclusive license granted to UCT by the author.

University of Cape Town

## ACKNOWLEDGEMENTS

I would like to express my thanks to my supervisor, Dr Gary Foulds, for his guidance and assistance during the course of this work.

I wish to thank Professor Gerald Robertson, Dr Richard Hutcheon and Dr Steve Driver of the Physics Department for their invaluable assistance in operating the CARS laser system.

The following people are also gratefully acknowledged:

The technical staff, particularly messrs A. Barker and R. Senekal of the Chemical Engineering Workshop for the patient construction of the reactor housing.
The glassblower, Mr C. Ledger, for his applied skills.

## SYNOPSIS

The methanation reaction, discovered in 1902 by Sabatier and Senderens, still remains a subject of intense interest. It is currently used in numerous industrial processes to remove carbon monoxide traces in hydrogen-rich gases of ammonia plants. Since the early 1980's there has been a renewed interest in especially catalytic methanation as it is an important step in the transformation of coal into substitute natural gas - an industrial process that is becoming more attractive to coal-rich developing countries. Current reactors are of the fixed bed type, but there is an interest in using tube-wall reactors in order to reduce the large pressure drops normally associated with fixed bed reactors.

Coherent Anti-Stokes Raman Spectroscopy (*CARS*) is a relatively new laser-based spectroscopic technique which may be used to obtain the concentrations of species in the gas phase. The aim of this work was to study the methanation reaction over various supported metal catalysts in a simple tube-wall flow reactor using *CARS*.

The metals, nickel,cobalt and ruthenium were used to catalyse the methanation reaction. These were loaded onto various amorphous and zeolitic supports using typical ion exchange and incipient wetness techniques. The metal loading of the catalysts were determined by atomic adsorption analysis. Typically, the metal loadings were 7% and 0.5% by mass.

A similar experiment was conducted at the Engineering Sciences and Materials Physics Division, Harwell, U.K., by England et al in 1984 (4). As the *CARS* technique proved to be feasible, the current experiment was designed and performed in order to corroborate the results of the earlier experiment. In the Harwell experiment, however, a multi-mode laser was used with an internal $N_2$ reference in order to obtain relative concentrations of carbon monoxide along the reactor. A laser system which is considered to be more advanced,

incorporating reference cell optics together with a single-mode *Nd:YAG* laser, was used in this experiment.
It was decided to investigate :

i) The integration of reference cell optics, made possible by recent advances in laser technology, into the laser configuration.
ii) The degree of correlation between this experiment and the earlier work by England et al (4).
iii) The methanation activity of the metals, nickel, cobalt and ruthenium.
iv) The effect of varying the reactant flowrates,($H_2$ and CO).
v) The effect of varying the metal loading on the support.
vi) The effect of varying the metal support itself.

Briefly, the method used to obtain the relative concentration of carbon monoxide along the catalyst was as follows:

i) The catalyst was ground and passed through a 25 micron sieve before being slurried onto an inert 15cm long, fine stainless steel mesh. This coated mesh was inserted into the quartz reactor tube, thereby lining the reactor inner wall with the catalyst. The catalyst was reduced in flowing hydrogen at temperatures of typically 400 to 500°C.

ii) The reactor tube was heated by using a heating element wound onto an outer quartz tube. The temperature of the reactor was recorded by using a thermocouple and controlled by varying the current through the heating coils.

iii) The stoichiometric gas flowrates of CO and $H_2$ were fed through an oxygen trap before entering the reactor and accurately controlled by using gas rotameters on each feed stream

iv) In order to position the focus of the laser beams at the required point in the reactor, the mobile reactor configuration was moved axially.

v) After alignment of the beams into the reactor and onto the Optical Multichannel Analyser, the entire system was placed under computer control.

vi) Ninety laser shots at a frequency of 1Hz were fired at a particular point in the reactor. The interaction length (sampling volume length) of the laser beams was approximately 12mm. The resulting *CARS* signal for each of the 90 shots was compared to a reference signal (produced by splitting off 4% of the unaltered exit green beam and passing it through an external reference cell filled with carbon monoxide). The ratio of the sample to reference signals was recorded for each of the 90 shots in order to yield the relative concentration of carbon monoxide.

vii) The relative concentrations of the 90 shots were averaged to yield the average relative concentration for that particular point in the reactor.

viii) The temperature at the focal point of the laser beams was recorded using a thermocouple.

ix) The reactor was moved axially so as to position the laser focus at a new point in the reactor and the process after step (v) was repeated.

In this way, a concentration and temperature profile could be obtained for the conversion of CO along the reactor for each catalyst and set of reactant flowrates used.

In order to determine the best method of referencing, and indeed, whether or not the external referencing technique used in this experiment was more accurate than the internal referencing method employed at Harwell, the following preliminary experiment was carried out. The following three referencing techniques were compared for eventual use in the methanation experiment.

a) External argon referencing,i.e. a series reference in an external cell pressurized to 40 atmospheres.

b) External CO referencing,i.e. a series reference in an external cell at atmospheric pressure. Note that in this option, the sample and reference *CARS* signals were generated by the same molecular species.
c) Internal nitrogen referencing,i.e. the reference signal was generated by nitrogen introduced into the reactor along with the reactant gases.

The method of data acquisition for this preliminary experiment was as described before, except that no catalyst was present in the reactor, and was the same for each referencing technique tested. For each set of 90 shots, the standard deviation of the ratio of sample to reference signal was obtained. For each referencing technique,i.e. for each sequence of (90 shots * 10 points), the average of the relative standard deviations obtained for each sequence was calculated.
The results of these calculations were:

| Referencing Method | Relative Std. Dev. | Average number of counts | |
|---|---|---|---|
| | | Signal | Reference |
| External Ar | 1.09 % | 56 000 | 84 000 |
| External CO | 0.31 % | 54 000 | 29 000 |
| Internal $N_2$ | 1.61 % | 21 000 | 40 000 |

These results clearly demonstrate the advantages of an external reference and hence of a single-mode *Nd:YAG* laser. The larger relative standard deviation for the internal $N_2$ reference can readily be understood, since the sample CO signal and the reference $N_2$ signal are generated by very different regions of the dye laser spectral profile. The profile varies considerably from shot to shot and so provides an additional contribution to the standard deviation. Referencing with an external cell is more satisfactory if a single-mode pump beam is used, otherwise there will be different phase relationships between the input beams in the sample and reference cell, and the two *CARS* signals will not necessarily be proportional.

The referencing for the methanation experiment was carried out with the method that was found to yield the lowest relative standard deviation, namely that with the external carbon monoxide reference. In order to model the methanation reaction over the various supported metal catalysts, a computer program was written, using a rate equation of the form:

$$-r_{CO} = A\, e^{-Ea/RT} p^{X}_{CO} p^{Y}_{H2}$$

This rate equation was utilised in the simple design equation for a plug-flow reactor. The one-dimensional, non-isothermal model was derived from the Navier-Stokes equation of continuity in cylindrical co-ordinates and the assumptions inherent in this were justified by numerous calculations and derivations. The model was seen to fit the experimental data accurately whilst yielding values of A,Ea,X and Y that were in agreement with other researchers findings. The non-isothermal model was necessary as the heating element and reactor tube were of a similar size and thus energy end-losses occured, resulting in an inherent temperature profile along the catalyst section of the reactor. This was overcome by simultaneously solving the mass and energy balances over the reactor.

The following results were obtained for the various supported metal catalysts at 250°C and at 1 atmosphere.

| Metal | Substrate | Loading | A | Ea | X | Y |
|---|---|---|---|---|---|---|
| Ni | $SiO_2/Al_2O_3$ | 11% | 8.75e4 | 24950 | -0.32 | 1.1 |
| Ni | Zeolite-Y | 7% | 5.00e4 | 25250 | -0.32 | 1.0 |
| Ni | Alumina | 7% | 7.50e4 | 25250 | -0.36 | 1.0 |
| * Ni | ZSM-5 | .5% | 8.75e4 | 25100 | -0.30 | 1.3 |
| * Ni | Alumina | 7% | 8.75e4 | 24750 | -0.36 | 0.9 |
| Co | Alumina | 7% | 9.25e4 | 25925 | -0.44 | 1.1 |
| Co | $SiO_2/Al_2O_3$ | 7% | 8.75e4 | 25900 | -0.44 | 1.1 |
| Co | Alumina | 7% | 9.00e4 | 25925 | -0.44 | 1.1 |
| Co | $SiO_2/Al_2O_3$ | .5% | 8.75e4 | 25925 | -0.44 | 1.0 |
| Co | Zeolite-Y | 7% | 1.17e5 | 25900 | -0.44 | 1.2 |
| * Ru | $SiO_2/Al_2O_3$ | 7% | 8.25e4 | 23300 | -0.25 | 1.3 |
| Ru | Alumina | 7% | 4.00e4 | 24800 | -0.26 | 1.6 |
| Ru | Zeolite-Y | 7% | 7.50e4 | 23800 | -0.26 | 1.2 |
| * Ru | Zeolite-Y | 7% | 7.50e4 | 24775 | -0.26 | 1.5 |
| Ru | ZSM-5 | .5% | 8.75e4 | 24500 | -0.26 | 1.5 |

Where the units of Ea are calories and where * denotes those reaction runs performed at flowrates of 13 ml/min and 39 ml/min for CO and $H_2$ respectively. All other reaction runs were performed at flowrates of 6 and 18 ml/min for CO and $H_2$ respectively.

From these results and also from the graphs of the activity as presented in chapter 12, the following conclusions were drawn.

Effect of metal on the rate equation

The parameters A,Ea,X and Y as found to best fit the data for the three metals investigated, whilst differing noticably from metal to metal, are similar enough to indicate that the same mechanism of reaction is occuring on each metal - with the possible exception of ruthenium. The results further suggest that, either hydrogenation of the surface carbon or of a (CH) intermediate is the rate limiting step in the mechanism. The order of the activation energies for the methanation reaction on these metals is : Ru < Ni < Co, and this is inverse to the heats of adsorption of CO on these metals viz. $\Delta H_{ads}(CO)$ = Ru > Ni > Co.

Effect of metal on the methanation activity

The present study confirms the trend in the methanation activity of the metals as decreasing in the order : Ru > Ni > Co.

Effect of the support

The rate equation, and thus the mechanism of reaction, for the same metal, is unaffected by the support. The support does however affect the methanation activity. The zeolitic supports appeared to enhance the activity of Co when compared to the amorphous supports. Nickel on alumina appeared to be a more active methanation catalyst than nickel on Zeolite-Y.

Effect of the metal loading

The mechanism of reaction is not affected by the metal loading on the support. The activity of the catalysts increases for higher metal loadings.

Effect of reactant flowrates

Once again, the mechanism is independant of the reactant flowrates as used in this experiment. The effect of the flowrates on the methanation activity of the catalyst appeared to be conflicting on the metals, nickel and ruthenium. At higher flowrates, the Ni on alumina catalyst yielded a higher CO conversion than at the lower flowrates while the Ru on Zeolite-Y catalyst yielded a higher CO conversion at lower flowrates. More data is needed to corroborate or to refute the trends observed on each metal.

Having successfully demonstrated the use of *CARS* to obtain concentration data in a laboratory reactor, it is felt that the future direction of *CARS* lies increasingly towards systems in which heat and mass transfer effects are important, particularly in hostile environments. Possible future applications for the use of *CARS* in catalytic reactor studies include the following:

(1) The study of turbulent and/or non-isothermal tube-wall catalytic reactors to characterise heat and mass transfer effects.
(2) The study of monolithic reactors on a channel by channel basis.
(3) The study of oscillating chemical reactors.
(4) The study of reactions over precious metal gauzes, where temperature and concentration profiles above and below the catalyst could be studied.

## LIST OF CONTENTS


| TITLE | Page |
|---|---|
| Acknowledgements | |
| Synopsis | (i) |
| List of Figures | (xii) |
| Nomenclature | (xiii) |
| 1. Introduction | 1 |
| 2. CARS Theory | 6 |
| 2.1 Application of the CARS technique to the modelling of a chemical reactor | 6 |
| 2.2 Raman Spectroscopy | 6 |
| 2.3 CARS Laser configuration | 8 |
| 2.4 Analysis of the Anti-Stokes beam | 11 |
| 2.5 Temperature measurement | 14 |
| 3. CARS Equipment | 15 |
| 3.1 General layout | 15 |
| 3.2 Laser system and beam configuration | 15 |
| 3.3 Spectrometer and OMA detector | 17 |
| 3.4 Reference cell | 19 |
| 4. Design of the reactor | 20 |
| 4.1 Constraints on design | 20 |
| 4.2 Reactor configuration used | 20 |
| 4.3 Additional equipment and glassware | 22 |
| 5. Physics of the CARS process | 23 |
| 5.1 Referencing | 25 |
| 6 Referencing | 27 |
| 6.1 Referencing procedure | 27 |
| 6.2 Comparison of techniques | 27 |
| 6.3 Results | 29 |
| 6.4 Discussion | 29 |

7 Kinetics of the methanation reaction 30
7.1 Theoretical rate equation 30

8 Catalyst preparation 33
8.1 Nickel on alumina 33
8.2 Nickel on Zeolite-Y 34
8.3 Nickel on ZSM-5 35
8.4 Nickel on silica-alumina 35
8.5 Preparation of cobalt and ruthenium catalysts 36
8.5.1 Amorphous supports 36
8.5.2 ZSM-5 and Zeolite-Y 36

9 Infrared studies of CO on supported methanation catalysts 38

10 Theoretical modelling of the reactor 44
10.1 Assumptions made 44
10.2 Solution of the mass balance (isothermal case) 46
10.3 Solution of the mass balance (non-isothermal case) 46
10.4 Calculation of the outer heat transfer coefficient 47
10.5 Thermodynamic analysis of the methanation reaction 48

11 Analysis of the results 49
11.1 Derivation of the relative concentrations 49
11.2 Computer simulation 49
11.2.1 User inputs required 49
11.2.2 Sensitivity of the rate equation parameters 50

12 Results and discussion 51
12.1 Effect of metal on the rate equation 55
12.2 Effect of metal on the methanation activity 57
12.3 Effect of the support 57
12.4 Effect of the metal loading 58
12.5 Effect of the reactant flowrates 59
12.6 Catalyst deactivation 59
12.7 Effect of water 60
12.8 Effect of temperature 60

13 Conclusions and recommendations 61

14. List of references 64

**APPENDICES**

No. Title page

1 Derivation of the kinetic rate equation 70

Preparation of:

2 7% Nickel on alumina 73

3 7% Nickel on Zeolite-Y 74

4 0.5% Nickel on ZSM-5 76

5 11% Nickel on silica-alumina 77

6 7% Cobalt on silica-alumina 78

7 7% Cobalt on alumina 79

8 0.5% Cobalt on silica-alumina 80

9 7% Cobalt on Zeolite-Y 81

10 7% Ruthenium on alumina 83

11 7% Ruthenium on silica-alumina 84

12 7% Ruthenium on Zeolite-Y 85

13 0.5% Ruthenium on ZSM-5 86

14 Calculation of the Reynolds number 87

15 Derivation of the plug-flow equation from the Navier-Stokes equation of continuity in cylindrical co-ordinates 89

16 Derivation of the energy balance 91

17 Listing of the modelling program 94

18 Algorithm of the modelling program 104

19 Temperature profile with no gas flows 108

20 Actual and fitted temperature profile curves 109

21 Grashoff and Prandtl number versus temperature curves 110

22 Calculation of the approach to ideal gas behaviour 112

23 Determination of the equilibrium constant as a function of temperature 116

24 Program to calculate the fugacity coefficients 119

| | | |
|---|---|---|
| | Data for the methanation reaction over: | |
| 25 | 11% Nickel on silica-alumina | 121 |
| 26 | 7% Nickel on Zeolite-Y | 122 |
| 27 | 7% Nickel on alumina | 123 |
| 28 | 7% Nickel on alumina | 124 |
| 29 | 0.5% Nickel on ZSM-5 | 125 |
| 30 | 7% Cobalt on alumina | 126 |
| 31 | 7% Cobalt on alumina | 127 |
| 32 | 7% Cobalt on alumina | 128 |
| 33 | 0.5% Cobalt on silica-alumina | 129 |
| 34 | 7% Cobalt on Zeolite-Y | 130 |
| 35 | 7% Ruthenium on silica-alumina | 131 |
| 36 | 7% Ruthenium on alumina | 132 |
| 37 | 7% Ruthenium on Zeolite-Y | 133 |
| 38 | 7% Ruthenium on Zeolite-Y | 134 |
| 39 | 0.5% Ruthenium on ZSM-5 | 135 |
| 40 | Experimental layout | |
| 41 | Modifying the rate for surface reaction | 136 |
| 42 | Calculation of the internal and external diffusion resistances to determine the rate controlling step | 138 |
| 43 | The Methanation reactor | 139 |
| 44 | The Methanation reactor | 140 |
| 45 | The CARS Laser System | 141 |

## LIST OF FIGURES


| Figure | | page |
|---|---|---|
| 2.1 | Vibrational energy level with associated rotational energy levels | 7 |
| 2.2 | Stokes and Anti-Stokes emission lines | 8 |
| 2.3 | Broad band and narrow band beams | 9 |
| 2.4 | Boxcars technique to ensure the conservation of angular momentum | 10 |
| 2.5 | Generation of the Anti-Stokes beam | 10 |
| 2.6 | Typical CARS spectrum | 13 |
| 4.1 | Reactor and heating element | 20 |
| 4.2 | Alignment of reactor, heating element and insulation tube | 21 |
| 4.3 | Cross-sectional profile of the reactor base | 22 |
| 9.1 | Assignment of Infrared bands to surface species for CO chemisorbed on supported Ni samples | 39 |
| 10.1 | Temperature profile along the heating element | 47 |

| | | |
|---|---|---|
| $d\sigma/d\Omega$ | Raman cross-section | |
| $\Gamma_{Rm}$ | Half width of the spontaeous Raman line | $cm^{-1}$ |
| $H_{H2}$ | Heat of adsorption of $H_2$ | $J.mol^{-1}$ |
| $H_H$ | Heat of adsorption of atomic H | $J.mol^{-1}$ |
| $H_{CO}$ | Heat of adsorption of CO | $J.mol^{-1}$ |
| Re | Reynold's number | |
| V | Volume of catalyst section of reactor | $cm^3$ |
| $F_{Ao}$ | Molar flowrate of pure CO | $mol.sec^{-1}$ |
| $x_a$ | Conversion of CO | |
| $h_o$ | Outer heat transfer coefficient | $W.m^{-1}.K^{-1}$ |
| $T_s$ | Temperature of heating wire | K |
| T | Reaction temperature | K |
| $F_t$ | Total molar flowrate | $gmol.sec^{-1}$ |
| $C_p$ | Heat capacity of gas | $cal.gmol^{-1}$ |
| $Nu_D$ | Nusselt number | |
| $Ra_D$ | Radleigh number | |
| Pr | Prandtl number | |
| Gr | Grashoff number | |
| Z | Compressibility factor | |
| K | Equilibrium constant | |
| $G^o$ | Gabbs free energy of formation | $cal.gmol^{-1}$ |
| $\theta_i$ | Fraction of cat. surface covered by i | |
| $\theta_v$ | Fraction of cat. surface uncovered | |
| $K_i$ | Equilibrium constant for the adsorption of species i | |
| $H_f$ | Enthalpy flow into the reactor | $J.sec^{-1}$ |
| $H_e$ | Enthalpy flow out of reactor | $J.sec^{-1}$ |
| Q' | Rate of heat transfer | $J.sec^{-1}$ |
| dH | Accumulation of energy in volume element dV in time dt | |
| $dA_h$ | Effective heat transfer area in volume element dV | |
| dT | Temperature change in time dt | |
| dx | Differential change in conversion | |
| dz | Differential change in axial length along the reactor tube | |

| | | |
|---|---|---|
| $k$ | Thermal conductivity of air | $W.m^{-1}.K^{-1}$ |
| $r$ | Radius of reactor | cm |
| $T_c$ | Critical temperature | K |
| $P_c$ | Critical pressure | atm |
| $w$ | Accentric factor | |
| $T_r$ | Reduced temperature | |
| $P_r$ | Reduced pressure | |
| $\Phi_i$ | Fugacity coefficient of species i | |
| $V_c$ | Critical volume | $cm^3$ |
| $y_i$ | Mole fraction of gas i in mixture | |
| $P$ | Total pressure | atm |
| $I$ | Integration constant | |
| $\alpha_i$ | Heat capacity constant for species i | |
| $\beta_i$ | Heat capacity constant for species i | |
| $\gamma_i$ | Heat capacity constant for species i | |
| $k_m$ | Mass transfer coefficient | |
| $a_m$ | Effective catalyst surface area | m |
| $C_b$ | Bulk concentration | $gmol.l^{-1}$ |
| $C_s$ | Surface concentration | $gmol.l^{-1}$ |
| $\mu_i$ | Viscosity of species i | $Pa.sec^{-1}$ |
| $\rho_i$ | Density of species i | $g.cm^{-3}$ |
| $G$ | Volumetric gas flowrate | $cm^3.sec^{-1}$ |
| $\epsilon_B$ | Void fraction of interparticle space | |
| $M_A$ | Molecular mass of A | g |
| $\Omega_{AB}$ | Collision integral | |
| $k_B$ | Boltzman constant | |
| $D_k$ | Knudsen diffusivity | $cm^2.sec^{-1}$ |
| $D_{AB}$ | Bulk diffusivity of A in mixture | $cm^2.sec^{-1}$ |
| $D$ | Overall diffusivity | $cm^2.sec^{-1}$ |
| $\nu$ | Kinematic viscosity | $cm^2.sec^{-1}$ |

## 1. INTRODUCTION

*CARS* (Coherent Anti-Stokes Raman Spectroscopy) is a laser-based spectroscopic technique which may be used to measure temperature and concentration profiles in the gas phase. This is a technique, originally discovered by Maker and Terhune in 1965 at the Ford Research Laboratories. It remained essentially in the province of non-linear optics until 1973, when Dr J.P. Taran of the French Aerospace Research Centre, ONERA, started applying the technique to gas phase diagnostics. Its versatility in important practical situations such as turbulent combustors(1), internal combustion engines(2) and plasmas(3), has already been demonstrated.

Briefly, *CARS* involves using three laser beams to excite one or more component gases in a mixture, and so produce an emission which can be analysed to yield information about the concentration of the gas or gases in the mixture. Typically, three pulsed laser beams, two at frequency $\omega_1$ and one at frequency $\omega_s$ are focussed and crossed in the measurement volume. If $(\omega_1-\omega_s)$ coincides with a Raman active transition of one of the component gases, a new laser-like anti-Stokes 'signal' is generated such that $(\omega_1-\omega_s) = (\omega_{as}-\omega_1)$. The pencil-like directionality of the *CARS* signal beam facilitates discrimination against high levels of unwanted background light eg. luminescence and flourescence.By using a broad band $\omega_s$, 100-200cm$^{-1}$ of molecular spectrum may be recorded from one laser pulse.

The nature of the *CARS* experiment lends itself to the following special advantages of using *CARS* to study chemical reactors.

1) Because *CARS* uses light beams, all measurements are carried out *in situ* without the use of mechanical sampling probes or thermocouples. This eliminates unquantifiable corrections due to probe perturbations caused by effects such as heat transfer, catalytic reactions and flow disturbances
2) There is no need for sample removal or conditioning prior to chemical analysis, as the measurements are made *in situ*.
3) *CARS* is temporally precise. The *CARS* signal is only produced during the 13ns laser pulse. This is more than adequate to freeze any turbulence,

so that the turbulence field may be evaluated by recording a series of 'snapshots', of concentration of a particular species in a reactor at a chosen point.

4) *CARS* is spatially precise. The *CARS* signal is only generated from the measurement volume, where the focussed laser beams intersect; for this experiment, this volume was typically a 12- to 15mm long cylinder, 200 $\mu$m in diameter.
5) The frequency of the *CARS* beam is shifted up from that of the higher frequency pump beam by an interval, $(\omega_1-\omega_s)$. It is thus easy to discriminate between the *CARS* beam and other radiation.
6) The *CARS* radiation is radiated as coherent, pencil-like beams, whose frequencies are precisely determined by the orientation of the input beam.

The use of *CARS* to model a reactor is a very new technique, and has been successfully applied by W.A. England (4), at AERE Harwell in 1984. Since this experiment was performed, however, advances in laser technology have resulted in the incorporation of reference cell optics in the *CARS* analysis system. This should enable a more accurate concentration profile to be obtained.

Mainly because of this, it was decided to study the methanation reaction over various supported catalysts. Methanation is the production of $CH_4$ from CO and $H_2$:

$$CO + 3H_2 \rightleftharpoons CH_4 + H_2O \qquad \Delta H^\circ_{298} = -206 \text{ kJ/mol}$$

The reaction is currently being used to remove traces of CO from the feedstocks in the Haber process. In the future, it may be used to produce synthetic natural gas from coal-derived synthesis gas. Current reactors are of the fixed-bed type, but there is interest in using tube-wall or monolithic reactors in order to reduce presure drops (5,6)

The methanation reaction was chosen to demonstrate the *CARS* technique because the spectroscopic properties of the components are well established. In addition to this, the *CARS* spectrum of $CH_4$ is simple and does not suffer overlap with other reactant or product molecules.

Furthermore, the kinetics of the reaction are sufficiently simple to permit comprehensive modelling and are well established in the literature.

As a result of the above considerations, it was decided to :

(1) Investigate the integration of reference cell optics into the laser configuration.
(2) Assess the degree of correlation between this experiment and earlier work (4).
(3) Gain working experience with the *CARS* technique.
(4) Study the methanation reaction over a variety of supported metal catalysts in order to :
  (a) compare the methanation activity of the metals, nickel, cobalt and ruthenium.
  (b) determine what the effect is of varying the reactant flowrates.
  (c) investigate the effect of varying the catalyst substrate.
  (d) ascertain what the effect of varying the metal loading on the catalyst would be.

In particular a kinetic and thermodynamic study of the methanation reaction was carried out in order to quantify the effect of changing the experimental parameters.

Briefly, the method used to obtain concentration profiles of CO along the catalyst region of the reactor was as follows :
The optically-accessible reactor was positioned so that two identical lenses focussed the input laser beams at a point in the reactor. (The focal point was fixed while the more mobile reactor was moved along rails). The temperature and gas flowrates in the reactor were accurately controlled. Ninety laser shots were fired at each position and the *CARS* signal so produced was compared to the reference beam signal. The average relative concentration of the ninety shots was recorded.

One of the most important differences between this experiment and the previous work conducted at Harwell was the method of referencing used. Previously, concentrations were obtained from the experimental *CARS* data by

fitting the concentration-dependant features of the spectral curve to the theoretical models of spectral profiles. In this experiment, however, relative concentrations were obtained by using reference cell optics with the added advantage that the same molecular species was used to generate both the sample and reference beams. The advantages of this referencing technique are discussed and clearly demonstrated in chapter 6 of this paper.

The kinetics of the methanation reaction over the supported Ni, Co and Ru catalysts were simulated by using a non-isothermal model incorporating a power-law rate equation of the form :

$$-r_{CO} = Ae^{-Ea/RT}p_{CO}{}^{X}p_{H2}{}^{Y}$$

The mechanism of the reaction was as proposed by Rautavouma and Van der Baan (20), and is supported by literature studies, particularly infrared studies of CO on group VIII supported metal catalysts. This rate equation was used in the design equation for a plug-flow reactor in order to generate the conversion of carbon monoxide at a particular point in the reactor. The plug-flow model was derived from the Navier-Stokes equation of continuity in cylindrical co-ordinates. The assumptions made in this simplification are discussed in chapter 10 and the mathematical justification is provided in appendix 15. Typically, nine experimental points (CO conversion,length into catalyst) were obtained for a particular catalyst at each set of experimental conditions. Practically, this profile of nine points represents a set of conventional total conversion measurements on nine different tube lengths taken simultaneously. In all, fifteen reaction runs were recorded, five for each of the three metals investigated.The chapters in this paper are presented in the order that the *CARS* system would utilize each topic discussed in the various chapters. As an introduction to Anti-Stokes Raman spectroscopy, the basic theory of Raman spectroscopy is discussed in chapter 2, with particular emphasis on the generation and analysis of the Anti-Stokes beam. As this work was performed with a view to comparing the results obtained with those presented by England et al (4), the differences in the methods of analysing the *CARS* spectrum between the two experiments is also discussed in chapter 2. The general layout and the technical specifications of the *CARS* equipment used is presented in chapter 3. The path followed by the emitted

laser beams then determines the order of the chapters from chapter 4 onwards. Chapter 4 itself discusses the problems encountered in designing the optically-accessible reactor and the final reactor configuration is presented. The physics of the *CARS* process, as it occurs inside the reactor is then discussed in chapter 5. As the *CARS* system utilized in this experiment incorporated reference cell optics never used before, a preliminary experiment was performed in order to determine the accuracy of the system. This is discussed in chapter 6. Chapter 7 deals with the kinetics of the methanation reaction and highlights numerous reasons for the reaction mechanism chosen to model the reaction. The preparation of the catalysts used is given in chapter 8. In order to fully discuss the surface reaction, chapter 9, dealing with infrared literature studies of CO on supported metal catalysts, provides a background for the discussion.

The theoretical modelling of the reactor, the assumptions made and the final rate equation used is discussed in chapter 10. This chapter also deals with the actual method of simulation of the iso- and non-isothermal models used in the simulation program. The values obtained from the modelling program for the rate equation parameters as well as the activity graphs (CO conversion versus length into catalyst) are presented and discussed in detail in chapter 12. The conclusions that may be drawn from this experiment are presented in chapter 13 of this paper.

## 2. CARS THEORY

### 2.1 Application of CARS technique to the modelling of a Chemical Reactor

*CARS* has been used to obtain *in situ* CO concentration profiles in an operating methanation reactor (4). The *CARS* technique is based on the integration of Raman spectroscopy with advanced laser optics. This chapter will concentrate on the fundamentals of Raman spectroscopy whilst outlining the difference between the method of analysis of the Anti-Stokes beam as carried out by England et al (4), and in this experiment.

### 2.2 Raman spectroscopy

A Raman emission spectrum results from an interaction of a gas molecule with photons. In this experiment, the photons were provided by three laser beams (as will be described later). If a perfectly elastic collision occurs, there is no change in the frequency of the emitted photon. However, an inelastic collision between the photon and the molecule results in a transfer of energy to the molecule. The frequency of the emitted photon is thus changed. The energy transfer results in rotational and vibrational transitions in the molecule.

The rotational transition results from a two-photon transfer (9), i.e. one photon enters the molecule while another leaves. The rotational transition is characterised by a rotational quantum number, $J$. When a transition occurs, because two photons are involved, the change in the quantum number is such that $J = 0 ; \pm 2$

The vibrational transition requires much more energy than the rotational transistion and thus each vibrational energy level is associated with many rotational energy levels. (see fig. 2.1 overleaf)

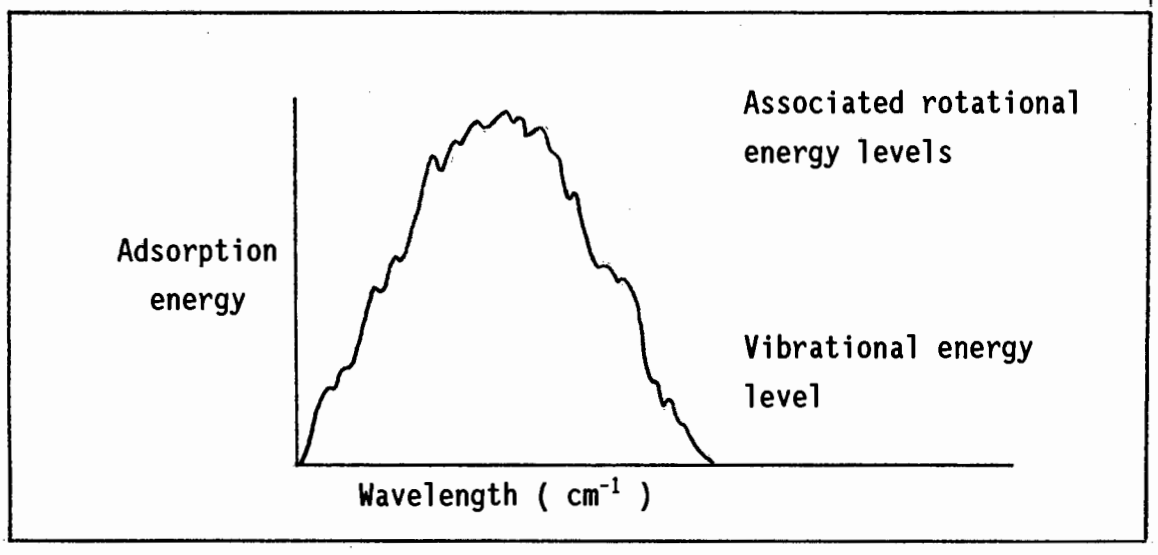


**Figure 2-1 Vibrational Energy level with associated rotational energy levels**

If the molecule gains energy, the scattered photons have less energy such that :

$$\text{Photon energy} = hf - \Delta E$$

where $h$ = Planck's constant
$f$ = emitted photon frequency
$\Delta E$ = difference in energy between vibrational energy levels

The emitted photon produces a new beam, known as the Stokes beam, having a lower frequency than that of the incident photon such that :

$$f = f_o - \Delta E/h$$

where $f$ = emitted frequency
$f_o$ = incident frequency

If the molecule loses energy, the photons have increased energy such that :

$$f = f_o + \Delta E/h$$

This beam is known as the **Anti-Stokes emission line.**

The emissions resulting from the increased and decreased energy of the emitted photons are shown in fig. 2.2 below.

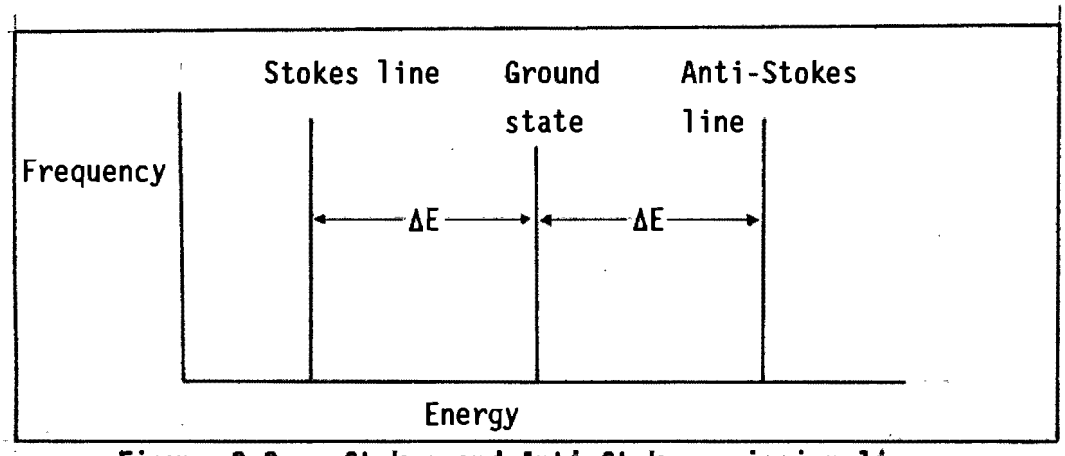


**Figure 2-2 Stokes and Anti-Stokes emission lines**

The detector part of the laser configuration records the Anti-Stokes emission line.

## 2.3 CARS Laser configuration

The purpose of the laser is to provide two beams.

a) A narrow band beam (green beam,$\omega_1$) - the pump beam
b) A broad band beam (orange beam,$\omega_s$) - the Stokes beam

a) The narrow band beam has been so adusted that the frequency range is small (and hence a small wavelength range) and provides sufficient energy so that CO molecules undergo multiple vibrational transitions (10). (The frequency of this beam is manually adjusted so that only the CO molecules are excited).

The pump beam is produced by a *Nd:YAG* laser and has a linewidth of approximately 0.3 $cm^{-1}$. The energy emitted is 280 mJ and it is produced in 13 nanoseconds.

b) The broad band laser is obtained by splitting off 30% of the pump beam to pump a dye laser which provides the Stokes beam. (The laser dye is carried in ethanol) This beam has a wide frequecy range with a corresponding linewidth of approximately 100 $cm^{-1}$. This beam can subsequently excite all other matrix molecules. (the matrix molecules consist of all molecules other than CO)

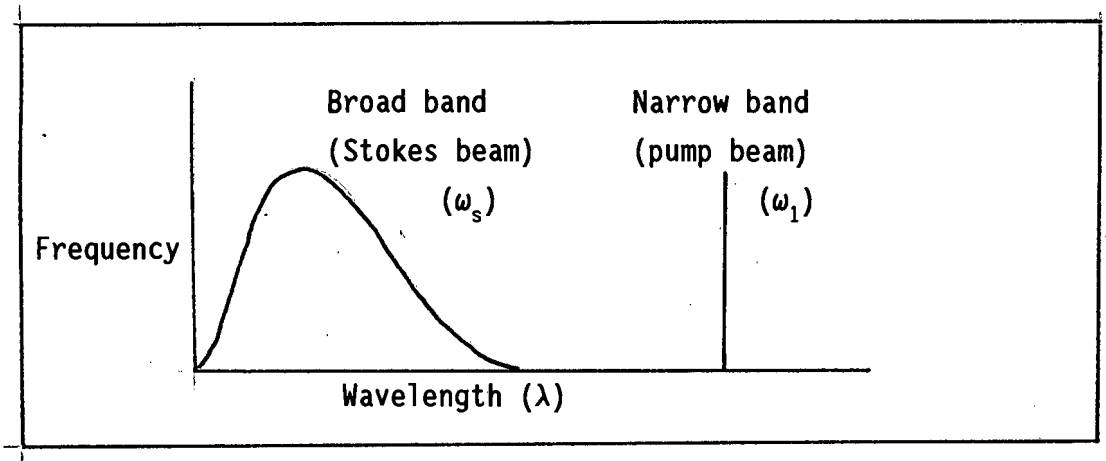


**Figure 2-3 Broad band and narrow band beams**

The pump beam is split into two parallel beams and together with the Stokes beam, are focussed by a converging lens to a point in the reactor. At the point of crossing of the three beams, an Anti-Stokes beam, (as described above) will result. This beam will have a frequency, $\omega_{as}$, such that :

$$\omega_{as} = 2\omega_1 - \omega_s$$

At the point of crossing of the beams, both the angular momentum and energy conservation equations must be satisfied. If each term in the above equation is multiplied by the Planck constant, the energy equation is satisfied.

If $\underline{k}_1$, $\underline{k}_2$ and $\underline{k}_3$ are the wave vectors (denoting the spatial direction of each wave) of the pump, Stokes and Anti-Stokes beams respectively, then the angular momentum may be conserved by using a cross-beam technique known as **BOXCARS**. This may be represented as follows (11):

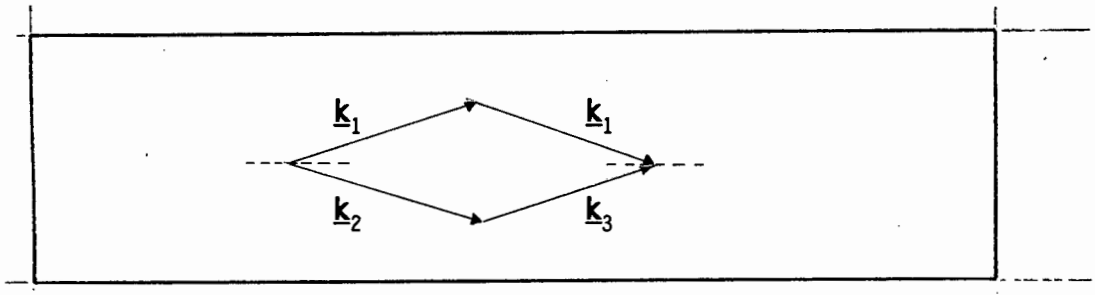


**Figure 2-4 BOXCARS technique to ensure the conservation of angular momentum**

The emitted Anti-Stokes beam is channelled to the detector. As the CO molecule undergoes multiple transitions, its contribution to the intensity of the Anti-Stokes beam will be far greater than that from the matrix molecules and background noise.

Approximately 4% of the unaltered green beam is split off in the detector unit and passed through a cylinder filled with pure CO. This serves as a reference cell. The beam emitted from this reference cell acts as a reference signal to which the Anti-Stokes beam can be compared.

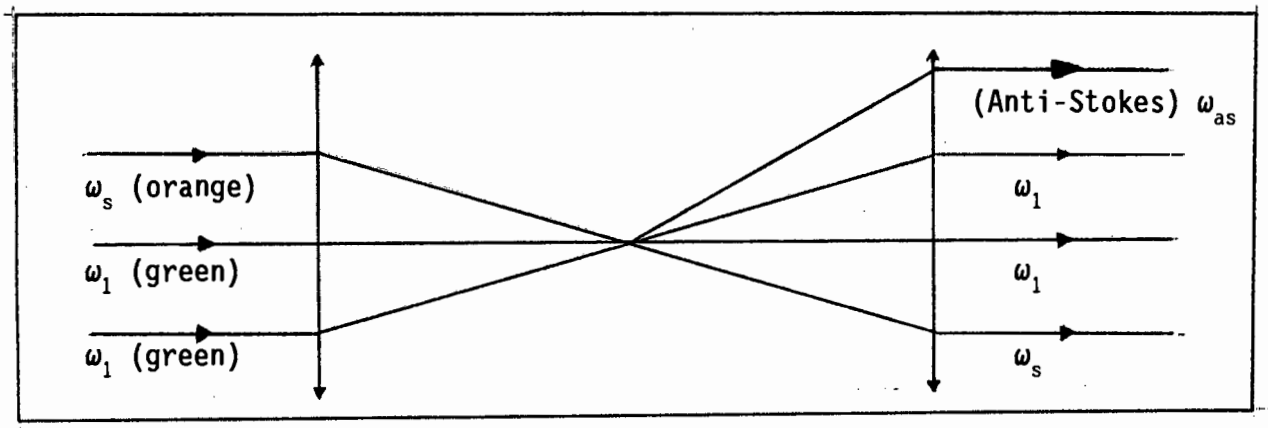


**Figure 2-5 Generation of Anti-Stokes beam**

## 2.4 Analysis of the Anti-Stokes beam

The intensity of the *CARS* signal (Anti-Stokes beam) is given by : (5)

$$(I)\omega_{as} = I\omega_1^2 I\omega_s^2 L^2 \, |\chi|^2 \, 4\pi^2 \, \omega_{as} \, \frac{(\sin \Delta L/2)}{c^2 \, n_{as} \, \Delta L/2}$$

where $\Delta L$ = Interaction length (i.e. crossing length of the laser beams)

$I_i$ = Intensity at frequency i

$\chi$ = Third order non-linear susceptability

The susceptability may be written in terms of a resonant and a non-resonant component such that :

$$|\chi|^2 = |\chi_{NR} + \chi' + i\chi''|^2$$

where $\chi_{NR}$ = Non-resonant component comprising the susceptability of the background noise and matrix molecules.

$\chi'$, $\chi''$ = Resonant component comprising the susceptability of CO

Frequently $\chi'$ and $\chi''$ are combined as follows: $\chi = (\chi', \chi'')$

$\chi_{NR}$ is frequency independent and arises from electronic transitions in the matrix molecules and from background noise. The susceptability, $\chi$, varies with CO concentration.

As the ratio of $\chi_{NR}/\chi$ changes, the shape of the Raman spectrum will alter according to a change in the terms $\chi'$, $\chi''$ and $\chi_{NR}$. Thus $\chi$ is a function of the extent of the reaction and hence the determination of this value is very important (10).

It was found that $\chi = f(\Gamma^{-1})$ where $\Gamma$ = linewidth of the rotational sublevels associated with a particular vibrational energy level (15). England et al, have shown that the linewidths are dependent on :

a) the rotational quantum number
b) the temperature
c) the gas composition
d) the susceptability
e) the molecular weight

Since no Raman linewidth data were available, England et al(4) used infrared linewidth data based on the assumption that the values were similar. This assumption was checked for CO using a diode laser. Excellent agreement existed between the two sets of results. Thus infrared linewidth data was used and corrected to higher temperatures using the formula :

$$\Gamma_j(\Gamma_2) = \Gamma_j(\Gamma_1)\ (\Gamma_1/\Gamma_2)^n$$

Typically n has a value between 0.5 and 1. For the linewidth of pure CO, n has a value of 0.66.

For the species present in the reactor, the linewidths were approximated as follows :

a) $CO/CH_4$ linewidths are approximately 10% greater than CO/CO linewidths
b) $CO/H_2O$ = 1.5 $CO/NH_3$ = 1.5 CO/CO linewidths
c) CO/CO and $CO/N_2$ linewidths are approximately the same.

Using the above approximations, the susceptabilities of each molecule could be obtained. The total non-resonant susceptability, $\chi_{NR}$ is given by :

$$\chi_{NR} = \sum x_i \chi_i$$

where $x_i$ = mole fraction of molecule i
$\chi_i$ = susceptability of molecule i

Using the susceptability values, the intensity can be solved for. This yields a typical CARS spectrum as shown below :

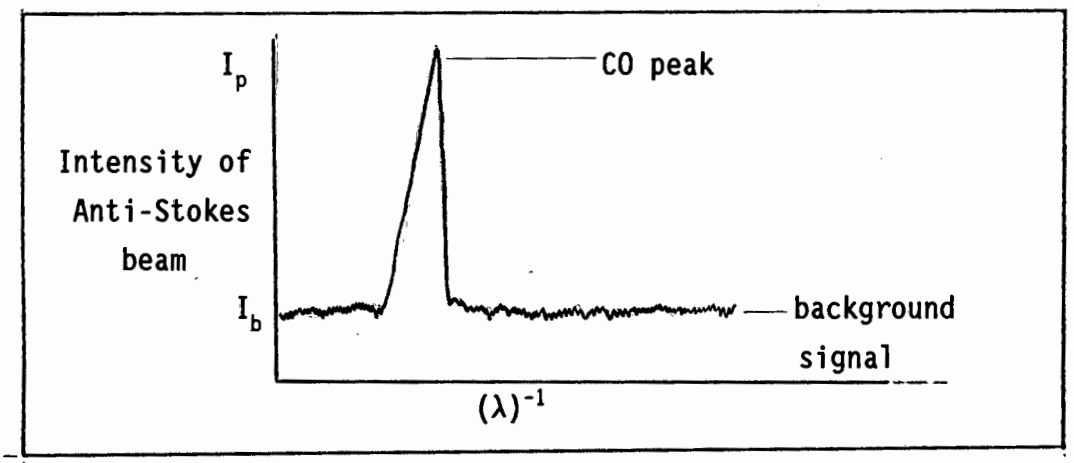


**Figure 2-6 Typical CARS spectrum**

Two methods of analysing the spectrum to obtain a concentration of CO exist:

a) The first is a ratioing technique and involves the ratio of the peak intensity (CO peak), $I_p$, to the average background intensity, $I_b$. As the CO concentration changes, so the CO peak value changes. The following relation holds : (9)

$$( \chi_{co}/\chi_{NR} )^2 = ( I_p/I_b ) = K$$
$$\text{therefore : } ( \chi_{co}/\chi_{NR} ) = K^{0.5}$$

Since $\chi_{co}$ is directly proportional to the number density ( the number of molecules per unit volume ), it follows that a plot of $K^{0.5}$ versus concentration will be nearly linear . As the concentration of CO decreases, the value of K tends to unity and hence K can be related to the extent of the reaction.

b) The second technique involves integrating the signal and reference curves to obtain the area beneath each curve. As the reference curve is for pure CO, the area under this curve will be the maximum possible. The ratio of the two areas will thus yield the relative concentration. Knowing the inlet and outlet concentrations, the extent of the reaction can be calculated using the stoichiometry of the methanation reaction.

In this experiment, the second of these techniques was utilized. As described in the experimental procedure, ninety laser shots were fired at each position in the reactor. By calculating the relative concentration for each shot, an average value and a standard deviation could be calculated for the relative concentration at each point. The accuracy of the concentration measurement at a particular point could subsequently be obtained.

## 2.5 Temperature measurement

The rotational energy levels associated with each vibrational energy level are strongly dependent on temperature (12). Thus using a broad band laser, all rotational components of the molecule under observation can be excited. The scattered light signal is then detected with a spectrograph. The spectrum is stored in a mini-computer and later analysed to give the temperature.At present, the temperature resolution of the *CARS* system is limited by the available library of recorded spectra and by the speed of the mathematical computations needed to analyse these spectra. Due to this, the system is not accurate enough to allow it to be used for work where the variation in temperature is of the order of one degree. In this experiment, a thermocouple was used to record the temperature in the reactor at the exact point of crossing of the laser beams. The design of the reactor allowed this to be done without disturbing the flow pattern of the reactants in the reactor tube itself.

## 3. CARS EQUIPMENT

### 3.1 General Layout

The pump and Stokes beams were focussed into the tubular catalytic reactor by two lenses. The *CARS* beam was generated by the carbon monxide, coherently scattered in the forward direction and analysed by a spectrometer/OMA combination. The input beams were then passed through a reference cell filled with CO under pressure. This generated a second *CARS* signal from the same molecular species used to generate the main (sample) signal, which was used to normalize the main signal against its dependance on the input laser power and dye laser spectral profile. Appendix 40 contains a diagramatic representation of the general layout.

### 3.2 Laser system and beam configuration

The pump and Stokes input beams were produced by a commercial CARS system built by SOPRA. The pump beam was generated initially by an *Nd : YAG* laser with an oscillator and two amplifiers and passively Q-switched by a saturable dye. The beam was then frequency doubled to produce a green beam. The Stokes beam was generated by a dye laser. The green pump beam passed through two beam splitters, with total reflectances of 10 and 25 per cent, to generate pumping beams for the dye laser oscillator and amplifier respectively. The energy of this green beam when it reached the reactor was approximately 110mJ/pulse. This beam was a single-mode beam due to two Fabry-Perot etalons mounted in the oscillator cavity. The dye laser had an oscillator and amplifier with Rhodamine 610 dissolved in ethanol as the lasing medium for both components. The dye concentrations were 458mg/l and 115mg/l for the oscillator and amplifier respectively. The emission profile peaked at 605nm and had a half-width of 6nm. This covers the $\nu$=0 to 1 Q branch of CO, which was the only branch of significant intensity used in this work. The energy of this beam was 2.2mJ/pulse. The pulse length of both beams was approximately 13ns FWHM. The beams left the laser system accurately parallel.

The beams had a diameter of 8mm and were focussed into the reactor by a Clerault lens (achromatic doublet with one plane outer face) with a focal length of +750mm, and recollinated after the reactor by a second identical lens. The beams are in the planar **BOXCARS** configuration (fig.2.4). The **BOXCARS** configuration was used to improve the spatial resolution. In the basic collinear configuration where the pump beam is not split, and both beams coincide, the *CARS* beam is generated in significant intensity only in the focal region. In **BOXCARS** configuration, the *CARS* beam is generated only in the much smaller region where the beams cross. This argument can be expressed more precisely as follows :

The laser beams have Gaussian intensity profiles and hence can be focussed down into a focal spot of diameter :

$$\phi = 4\lambda f/\pi d \qquad .....(3.1)$$

The beam diameter is :

$$L_r = \pi\phi^2/2\lambda \qquad .....(3.2)$$

In these expressions,

$\lambda$ is the laser wavelength
f is the focal length
$\phi$ is the beam diameter

Theoretical calculations (13) predict that 75% of the *CARS* power is generated within a distance :

$$6L_r = 48(\lambda/\pi)*(f/d)^2 \qquad ....(3.3)$$

where equations (3.1) and (3.2) have been used. This is defined as the spatial resolution for the collinear configuration. By taking $\lambda$=0.6 mm, f=750 mm and d=8 mm, we obtain, $6L_R \simeq 80$ mm. This collinear resolution is clearly much too long for a reactor of effective length = 150 mm. The spatial resolution in the **BOXCARS** configuration can be estimated by

approximating the beams to cylinders (this is justified below) and then assuming that the distance over which there is overlap between these cylinders is $2\phi/\theta$, where $\theta$ is the angle at which the beams cross. Since the beam separation before focussing is 9.5 mm, we have $\theta$ = 9.5/750 and hence a spatial resolution of 12 mm. Since this is much less than $L_R$, the cylinder approximation is justified. This follows because the diameter of the beam at an axial distance L, from the focal spot is given by :

$$\phi_L^2 = \phi_o^2 \left( 1 + L^2/2L_R^2 \right) \quad ....(3.4)$$

This greatly improved resolution is achieved at the cost of a reduced *CARS* signal. There are two reasons for this. First the pump beam is split into two and thus the term $P_p$ in equation (5.1) is halved. Secondly, the interaction volume is smaller. This reduces the *CARS* power by a factor $(d/e)^2$, where e is the separation of the input beam axes. In this experiment, d=8mm and e=9.5 mm. In practice, the *CARS* intensity is reduced by a larger factor, the discrepancy is due to the approximations in deriving this result. Conducting the experiment in the **BOXCARS** mode is at the limit of current techniques. If the laser power is increased, breakdown occurs in the reactor. If the laser power is reduced, the **BOXCARS** signal becomes too weak to detect.

Note that the power of the *CARS* beam does not depend on the focal length of the focussing lens, but the focal length of the interaction region, and hence the resolution as well. The power remains constant because, as the focal length increases, the interaction volume becomes larger but the input beams in this region are less intense and the two effects cancel. A schematic representation of the *CARS* laser is shown in appendix 45.

### 3.3 **Spectrometer and OMA detector**

The input laser beams, still effectively at full strength, and the *CARS* beam from the reactor (the sample beam) strike the dichroic, $D_1$, which transmits the *CARS* beam but reflects the input beams. The *CARS* beam is focussed by an achromatic convex lens, f= +120mm, onto a slit of width 50mm. The beam then expands to fill the aperture of a circular concave

the aperture of a circular concave holographic grating with the following parameters :

| | | |
|---|---|---|
| Diameter of grating | : | 60mm |
| Number of grooves | : | 2100 |
| Radius of curvature | : | 1000mm |

Because the grating is holographic, it focusses a spectrum not along the clasical Rowland circle but along a plane inclined at 5.5° to the normal to the diffracted beam. This spectrum now serves as the object of an expanding telescope, with magnification=2, which focusses the magnified image onto an EGG type 1641 OMA detector. This has a one dimensional array of 1024 pixels, each with dimensions 2mm by 0.025mm. The spectral dispersion of the final image is about $0.3cm^{-1}$ per pixel and the resolution is approximately 3 to 4 pixels FWHM. The spectrometer was set to monitor the Raman frequency window between about 2080 and $2150cm^{-1}$.

The input beams reflected from the dichrioc $D_1$ are focussed into the reference cell by an achromatic lens with focal length $^{+}300mm$. A yellow filter prevents any of the sample *CARS* beam reflected from the dichroic from entering the reference cell. The beams leaving the reference cell (input laser beams and reference *CARS* beam) are recollinated by a second achromatic lens and strike another dichroic $D_2$, which again reflects the input laser beams, this time into a dump, and transmits the reference *CARS* beam.This *CARS* beam enters the spectrometer and is analysed.

The sample and reference *CARS* beams are analysed by the same OMA. Thus overlap of the two spectra had to be avoided. This was achieved by tilting the spectrometer slit so that the two beams entered the slit at different heights and horizontal positions. The diffracted beams were focussed, again at different heights and horizontal positions onto a quartered mask with each quarter alternately clear and opaque. This suppressed horizontal overlap.

The two spectra, still at different heights, were brought side by side into the same horizontal plane by translation plates. They were then focussed onto the OMA as described above. Each half of the OMA array thus recorded the sample and reference *CARS* signal respectively. The spectra were then digitized and processed by computer.

### 3.4 Reference cell

The reference cell is a stainless steel tube, internal diameter 25mm and external diameter 50mm, and can be pressurised up to 50 atmospheres. It has two windows with thickness 16mm, diameter 26mm and has an anti-reflection coating (for 532nm) on all cell faces.

# 4. DESIGN OF REACTOR

## 4.1 Constraints on design

(1) The region in the reactor along the catalyst-lined walls had to be optically accessible to the laser beams.
(2) The focal length of the lenses used to focus the laser beams was 75cm, and as this determined the sampling volume, it placed a constraint on the reactor length.
(3) As the width of the laser beam was 8mm, this constrained the inner diameter of the reactor tube.
(4) The entire reactor configuration had to be transversely mobile as the more bulky laser system was too large to move practicably.

## 4.2 Reactor configuration used.

A quartz reactor tube (10mm I.D.) was used. In order to achieve a constant temperature zone of approximately 120mm, an outer quartz tube was wound with Ni/Cr (80% Nickel, 20% Chrome) resistance wire.(resistance of 13.5 ohms per meter)

The resistance wire was wound on a quartz tube (17mm I.D., 20mm O.D.). The length of the outer tube was 255mm while the heating wire was wound over 234mm.The ends of the heating wire were secured to the tube by aluminium clamps. This configuration is shown below.

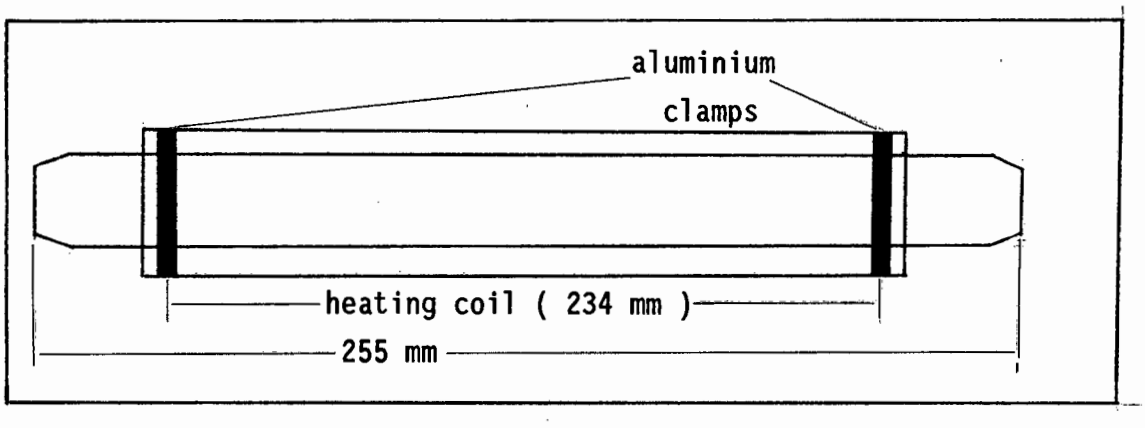


**Figure 4-1 Reactor and heating element**

The inner diameter of the heating tube was chosen such that a thermocouple could be easily inserted in the space between the reactor and heating tubes. The outward radial heat loss from the heating wire was minimised by winding asbestos lagging along the length of the heating tube. (this also prevented movement of the resistance wire due to expansion) A pyrex tube enclosed the asbestos lagging.

The heating element was centered inside the pyrex tube using two aluminium discs (mounted internally). The reactor tube itself was centered and fixed so that lateral movement was prohibited by using two externally mounted aluminium discs.

This configuration is shown diagramatically below.

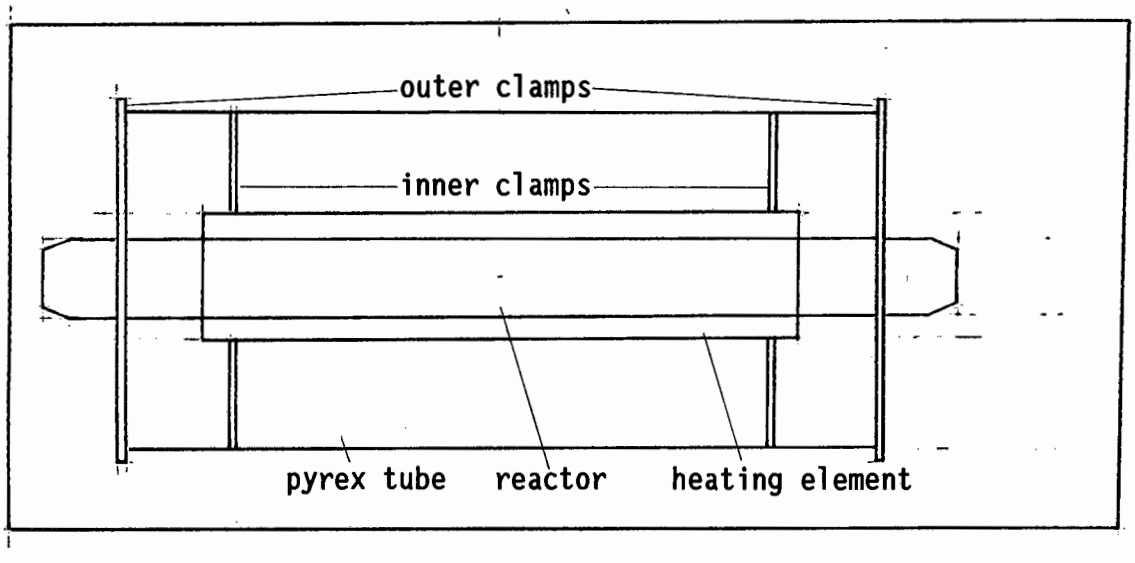


**Figure 4-2 Alignment of reactor , heating element and insulation tube**

End joints containing screw-on threads with quartz windows, angled at the Brewster angle to prevent the internal reflection of the beams, facilitated the entry and exit of gases as well as the easy removal of the reactor tube. Appendices 44 and 45 contain detailed drawings of the entire reactor configuration.

## 4.3 Additional equipment and glassware

Gas chromatograph bombs at inlet and outlet points served to sample entry and exit gases. Gas flowrates were controlled by using gas rotameters (range 4-40 ml/min, type F1100). The rotameters were fed with reactant gases from two cylinders containing pure CO and $H_2$. Accurate control was maintained via needle valves and regulators. Tygon tubing was used to transport the reactant and product gases to and from the reactor respectively. The final product gases were vented to an extraction fan.

The current in the resistance wire was controlled using a variac. Low resistance wire conducted current from the variac to the heating element. An Iron-Constantin thermocouple was used (type J). The thermocouple was accurate up to 800 °C. The thermocouple junction potential was amplified via an electronic transducer in order to obtain a significant volt meter reading.

The entire reactor configuration was mounted on a movable aluminium trolley. This, in turn, moved on aluminium rails, fixed to an accurately adjustable solid base.For a diagramatic representation of the base, see figure 4-3 below.

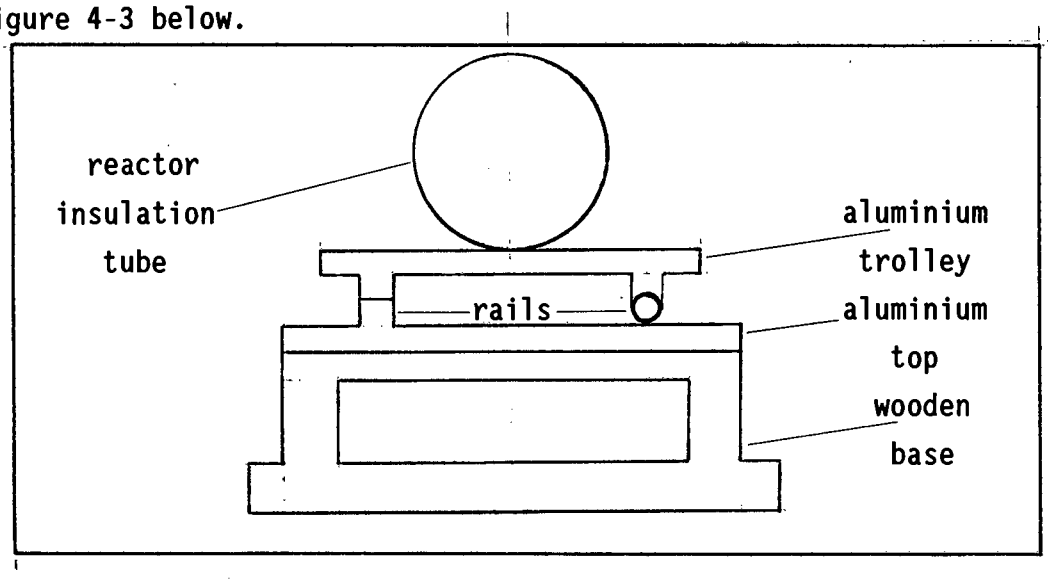


**Figure 4-3 Cross sectional profile of reactor base**

## 5. PHYSICS OF THE CARS PROCESS

In a *CARS* experiment, as mentioned before, intense laser beams of frequency $\omega_p$ and $\omega_s$ ($\omega_p > \omega_s$), known as the 'pump' and 'Stokes' beams, are focussed into the measurement volume. Since the electromagnetic fields of the laser beams are so intense, the polarisation of any molecules in the experimental volume becomes non-linear. It may be shown that if the frequency difference ($\omega_p - \omega_s$) coincides with a Raman active transition of these molecules, an intense coherent laser-like beam is generated at a frequency, $\omega_{as} = \omega_p + (\omega_p - \omega_s)$. This is commonly known as the **anti-Stokes beam**. Thus the input beams interact through the third order non-linear susceptibility of the molecule to generate a beam at a higher frequency than either the input beams. An alternative description is that the beat frequency of the laser beams drives the molecular oscillations.

The intensity of the *CARS* (anti-Stokes) beam may be calculated as follows. Consider the following case:

a) The input beams are Gaussian.
b) The focal region is approximated by a cylinder of diameter, $\omega_o = 4\lambda f/\pi\omega$ and length, $l = \pi\omega_o^2/2\lambda$ . Where :
   $\lambda$ is the wavelength of the beams
   f is the focal length of the lens
   $\omega$ is the diameter at which the beam intensity has dropped to $1/e^2$ of its peak value.

The power of the CARS beam is then :

$$P_{CARS} = \left(\frac{2}{\lambda}\right)^2 \frac{256\ \pi^4\ w_p^{\ 2}}{n_p^{\ 2}\ n_s\ n_{as}\ c^4} * |\chi_{CARS}(\lambda)| * P_p^{\ 2} - P_s(\lambda) \quad ..(5.1)$$

In this expression :
$\lambda$ is the beam wavelength. For this term the difference in beam wavelength is ignored and the wavelength ofthe pump beam adopted.

n is the refractive index.
$\chi_{CARS}$ is the bulk CARS susceptibility i.e. per unit volume
P is the beam power.

The subscripts 'p', 's' and 'as' denote the pump, Stokes and anti-Stokes beams respectively.

This expression assumes perfect phase matching throughout the volume. Note that various authors adopt different definitions of $\chi_{CARS}$ and this affects the numerical factors in the equation above. In this work, the definition adopted by Nibler and Knighten (14) will be followed. The bulk *CARS* susceptibility $\chi_{CARS}$, may be written :

$$\chi_{CARS} = \frac{( N_n - N_k ) n_p c^4}{2 h n_s \omega_s^4} \left(\frac{d\sigma}{d\Omega}\right) \frac{1}{\omega_{Rm} - \omega_p + \omega_s - i\Gamma_{Rm}} \quad ..(5.2)$$

In this expression :

The subscripts 'n','k' denote the lower and upper states of the Raman transition.
$N_a$ is the population density of the molecules in state 'a'
$d\sigma/d\Omega$ is the Raman cross-section
$\omega_{Rm}$ is the Raman frequency
$\Gamma_{Rm}$ is the half width of the spontaneous Raman line.

Thus $\chi_{CARS}$ can be expressed as the sum of the real and imaginery parts i.e.

$$\chi_{CARS} = \chi^{i}_{CARS} + \chi^{ii}_{CARS} \quad ....(5.3)$$

Now equation (5.3) can be written in the form :

$$|\chi_{CARS}|^2 = \frac{A}{\Gamma} * \chi^{ii}_{CARS} \quad ...(5.4)$$

So far the non-resonant *CARS* from other transitions in the molecule or from ther species present has not been considered.In this case the line profile is given by :

$|\chi^{(3)}|^2$ where,

$$|\chi^{(3)}|^2 = |\chi_{NR} + \chi^{i}_{CARS} + \chi^{ii}_{CARS}|^2$$

$$= \chi^2_{NR} + 2\chi_{NR}*\chi^{i}_{CARS} + \chi^{i}_{CARS} + \chi^{ii}_{CARS} \quad ..(5.5)$$

Thus the presence of significant concentrations of other species can distort the CARS profile through the $X_{NR}$ term. At high pressures, the CARS profile is modified by the phenomenon of "collisional narrowing" (15). This effect is negligable at the low pressures used in this experiment.

## 5.1 Referencing

It may be seen from equation (5.1) that the power of the *CARS* signal depends on the power $P_p$, of the pump beam and the power and the wavelength profile of the Stokes beam. One must therefore normalize against these terms to extract the information of diagnostic interest which is embedded in the susceptibility term, $\chi_{CARS}$. This may be done by generating a second signal as a reference. In the SOPRA system utilized in this experiment, the reference signal was generated in an external reference cell.

The reference signal is commonly generated from the inert gas, argon, in an external cell. The signal arises from the non-resonant susceptibility $X_{NR}$, which does not depend significantly on wavelength in the relevant range. Thus the intensity can be written as $P_{REF}(\lambda)$, and the ratio as : $P_{CARS}(\lambda)/P_{REF}(\lambda)$, and is proportional to the resonant susceptibility. As will be discussed later, the reference signal was generated from CO at atmospheric pressure. In this case, the intensity ratio is proportional to the ratio of the squares of the bulk susceptibilities : this, in turn, is proportional to the ratios of the squares of the concentrations, provided that only the resonant *CARS* susceptibility is significant.

These results assume that the phase relationships between the beams are the same in both the sample and reference cell. This is possible only if the pump beam is single-mode.

## 6. REFERENCING

In order to provide proper shot-to-shot referencing, three different methods of referencing were compared in a prelimimary experiment to determine which was the most accurate. This is described below.

### 6.1 Referencing procedure

The referencing for the methanation experiment was carried out with the method that was found to yield the lowest relative standard deviation, namely that with the external carbon monoxide reference. This was used consistently throughout the methanation experiment. After each run of 90 shots (at one position in the reactor), the relative standard deviation was obtained from the analysis program. Typically the value was 1%.

### 6.2 Comparison of techniques

The following three referencing techniques were compared for use in the methanation experiment :

a) External argon referencing, i.e. a series reference in an external cell pressurised to 40 atmospheres.

b) External CO referencing, i.e. a series reference in an external cell at atmospheric pressure. Note that in this option, the sample and reference *CARS* signals are generated by the same molecular species.

c) Internal nitrogen referencing, i.e. the reference signal is generated by nitrogen introduced into the reactor.

For each referencing technique, 90 laser shots were fired at each of a series of 10 points along the reactor. The reactor was maintained at 250°C whilst flowing pure carbon monoxide through it at 20ml/min. No catalyst was present in the reactor at this stage. For each of the 90 shots, the ratio 'R', was obtained,where :

$$R = \left\{ \frac{\text{Area under sample signal}}{\text{Area under reference signal}} \right\}^{0.5}$$

As shown previously, R is proportional to the concentration. In the expression above :

The area under the sample signal is defined as the total number of counts for all pixels up to 20 pixels (i.e. 6.2 $cm^{-1}$) on each side of the peak. The area under the reference signal for carbon monoxide and nitrogen, where the signal arises from a resonant *CARS* interaction, is defined in the same way. For the argon reference, where the *CARS* signal is non-resonant, the area under the reference signal is defined as the total number of counts for the corresponding pixels.

At the temperatures used in this experiment, a total window width of 41 pixels was enough to include the whole of the resonant signals. The signals were corrected for background noise as follows :

The counts for all the other pixels monitoring the sample or reference signals as appropriate were summed and the average count per pixel was subtracted from each pixel. For the non-resonant signal, this was not possible and this introduced an error into the signal strength calculations. Fortunately, the background correction is small, typically about 1% of the total signal strength.

For each run of 90 shots then, the standard deviation of the ratio,R, was obtained. For each technique, i.e. for each sequence of (10 runs*90 shots) per run, the average of the relative standard deviations obtained for each point (i.e. series of 90 shots) was calculated.

## 6.3 Results

The results of these calculations were :

| Referencing Method | Relative Std. Dev. | Average number of counts | |
|---|---|---|---|
| | | Signal | Reference |
| External Ar | 1.09% | 56 000 | 84 000 |
| External CO | 0.31% | 54 000 | 29 000 |
| Internal $N_2$ | 1.61% | 21 000 | 40 000 |

## 6.4 Discussion

These results clearly demonstrate the advantages of an external reference and hence of a single-mode *Nd : YAG* laser. The larger relative standard deviation for the internal $N_2$ reference can be readily understood, since the sample CO signal and the reference $N_2$ signal are generated by very different regions of the dye laser spectral profile (the Q branch of the $J$=0 to $J$=0 transition lies at 2330 $cm^{-1}$ for $N_2$ and 2143 $cm^{-1}$ for CO). The profile varies considerably from shot to shot and so provides an additional contribution to the standard deviation. Referencing with an external cell is more satisfactory if a single-mode pump beam is used, otherwise there will be different phase relationships between the input beams in the sample and in the reference cell, and the two *CARS* signals will not necessarily be proportional.

The external CO reference gives a lower relative standard deviation than the external Ar reference. (Using an Ar reference leads to some ambiguity about the base line because it is not possible to correct for the background). Both the external references yield lower standard deviations than internal nitrogen referencing.

## 7. KINETICS OF THE METHANATION REACTION

The methanation reaction involves the production of methane from carbon monoxide and hydrogen, using metal catalysts (on different supports). The stoichiometric equation for the reaction is :

$$CO + 3H_2 \rightleftharpoons CH_4 + H_2O \qquad \Delta H^\circ_{298} = -206 \text{ kJ/mol}$$

### 7.1 Theoretical rate equation

Different reaction mechanisms have been proposed - all based on different rate-limiting steps (16),(17). From literature studies, it has been found that the methanation reaction typically follows a zero order in carbon monoxide concentration and near first order in hydrogen concentration over a specified pressure range.(16) From this data it has been assumed that the catalyst surface is "nearly completely" covered with strongly adsorbed carbon monoxide, while the hydrogen competes for adsorption on the small number of remaining metal sites.

Both CO and $H_2$ adsorption on group VIII metals are typically non-activated and monolayer coverages at temperatures above 25°C are found to decrease. It has been found (16,17) that both carbon monoxide and hydrogen adsorption, particularly the former, are enhanced at 200°C thus providing an indication that not all the metal surface is readily accessible for adsorption at lower temperatures. Literature studies show that the catalyst surface is "almost totally" covered by CO (18). The following comparison of the heats of adsorption of CO and $H_2$ support this view.

For Nickel on different supports, the activation energy of the methanation reaction lies between 70 and 130 kJ/mol. This value drops from 130 to 70 kJ/mol for a temperature increase from 473K to 623K. The enthalpies of adsorption for dissociatively adsorbed hydrogen and carbon monoxide (i.e. H and C) are related to the enthalpies of adsorption of the $H_2$ and CO molecules such that :

$$H_{H2,D} = 2*H_H$$
$$H_{CO,D} = 2*H_C + E_{CH2} - E_{H2O}$$

By evaluating the different parameters it was found that :

$$H_{H2,D} = -32^{\pm}6 \text{ kJ/mol}$$
$$H_{CO,D} = -84^{\pm}25 \text{ kJ/mol}$$

As the energy released when CO adsorbs is much greater than when $H_2$ adsorbs, the CO molecule will adsorb more quickly and strongly than $H_2$.

Earlier studies of the mechanism of the methanation reaction have suggested that, as the activation energy of the hydrogenation of carbon deposited from the reaction of CO into molecular C (71.1 kJ/mol) differs from that of the methanation reaction (83.7 kJ/mol - 105 kJ/mol), the hydrogenation of the surface carbon could not possibly be the rate determining step. However, it has been shown (19) that the true activation energy of the methanation reaction is approximately 71 kJ/mol. This is in excellent agreement with the activation energy of the hydrogenation of surface carbon deposited from the CO disproportionation reaction on the metal surface. Thus, it can be concluded that the rate determining step of the methanation reaction is probably the hydrogenation of the surface carbon.

The formation of methane can thus be described by a reaction sequence as follows (20):

* = vacant site on the catalyst surface

$$CO_{(g)} + * \rightleftharpoons CO_{(ads)} \quad \text{(i)}$$
$$CO_{(ads)} + * \rightleftharpoons C_{(ads)} + O_{(ads)} \quad \text{(ii)}$$
$$H_{2\,(g)} + 2* \rightleftharpoons 2H_{(ads)} \quad \text{(iii)}$$
$$C_{(ads)} + yH_{(ads)} \rightleftharpoons CH_{y\,(ads)} + y* \quad \text{(iv)}$$
$$CH_y + (4-y)H_{(ads)} \rightleftharpoons CH_{4\,(g)} + (5-y)* \quad \text{(v)}$$
$$O_{(ads)} + 2H_{(ads)} \rightleftharpoons H_2O_{(g)} + 3* \quad \text{(vi)}$$

Appendix (1) contains a derivation of the kinetic rate expression based on the above mechanism. The final kinetic rate equation is as follows :

$$-r_{co} = \frac{K' p_{co}^{-y/2} p_{H2}^{y/2}}{(1 + K'' p_{co} + K''' p_{H2})^{(y+1)}} \qquad \ldots(A)$$

where $K' = k_{CHy}^{1/2} k_{co}^{1/2} k_{H2} k_{H2O}^{1/2}$

$K'' = K_{CO}^{1/2} k_{H2O}^{1/2} k_{CHy}^{-1/2}$

$K''' = K_{H2}^{1/2}$

At low temperatures,(less than 320°C), Klose and Baerns (17), have suggested that $K'' >> K''' p_{H2}^{1/2}$
Therefore equation (A) reduces to :

$$-r_{co} = Ae^{-E/RT} p_{co}^{-y/2} p_{H2}^{y/2} \qquad \ldots(B)$$

where $Ae^{-E/RT}$ has been equated to $K'$

Thus a general power law of the form :

$$-r_{co} = Ae^{-E/RT} p_{co}^{X} p_{H2}^{Y}$$

may be fitted. From equation (B) it may be expected that the absolute values of X and Y will be the same. In practice, however, it has been found that the absolute values of X and Y differ slightly. As an example, it has been found that at 275°C, the values of X and Y are 0.7 and -0.5 respectively for a Nickel on alumina catalyst (18)

## 8. CATALYST PREPARATION

### 8.1 Supported nickel on alumina (7% nickel by mass)

It has been reported by Huang and Schwarz (21), that the catalytic performance of $Ni/Al_2O_3$ catalysts depend on their preparation procedures. A standard incipient wetness technique was used to prepare the $Ni/Al_2O_3$ catalyst utilized in this work. For $Ni/Al_2O_3$ catalysts prepared by incipient wetness, the weight loading of the catalysts can be determined solely on the basis of of the impregnation solution variables, i.e. nickel concentration, ionic strength and impregnant pH. (22) The dispersion, activity, selectivity and poison resistance have been found to correlate with metal loading (23).

It has also been reported in recent literature (21-23), that the following general trends exist for the preparation of $Ni/Al_2O_3$ catalysts by the incipient wetness technique. The dispersion of nickel on the catalyst support decreases with increasing nickel weight loading or nickel impregnant pH. On the other hand, the methanation activity (turnover frequency) increases with either nickel weight loading or impregnant pH. The activation energy for the methanation reaction increases with increasing nickel weight loading or decreasing initial impregnant pH.

The reagents used in the synthesis of the catalysis used in this work were:
3.728g $Ni(NO_3)_2.6H_2O$ and 10g $\gamma$-$Al_2O_3$ (Ruhrchemie chemicals). These were added together in a $HNO_3$ solution of pH=1 to produce a slurry upon attaining incipient wetness. The powdered catalyst was then dried at 130°C for 3 hours. The particles were sieved and passed through a 25 micron mesh. Appendix 2 contains the calculations of the reagents used in the synthesis. An Atomic Absorption analysis yielded a nickel weight loading of 7.03% by mass.

The catalyst was slurried onto a 15cm long stainless steel wire mesh and this was inserted into the central portion of the reactor.(The stainless steel mesh on its own, under normal reaction conditions proved to be completely inert and thus did not affect the catalyst or reaction in any way.) In experiments before the mesh was used, the catalyst would flake off the quartz reactor wall during firing of the laser through the reactor and occlude the optical path through the reactor. All the powdered catalysts used in this work were inserted into the reactor in this way.

The $Ni/Al_2O_3$ catalyst was activated under the following conditions.A reduction procedure was used in which the catalyst was subjected to a stream of flowing $H_2$ (40 ml/min) for :

30 min at 120°C
30 min at 260°C
160 min at 450°C

(Vannice, M.A., 1975, (18))

## 8.2 Nickel on Zeolite Y (6.76%)

The Zeolite Y contained 13% sodium oxide (by mass) and as an ion-exchange technique was used, this was the maximum attainable loading.

The catalyst was prepared as follows:
Exactly 3.0 grams of sodium Zeolite Y was added to 5.49g of $Ni(NO_3)_2 \cdot 6H_2O$ in 100ml of distilled water. The slurry was agitated and refluxed for 15 hours. The resulting slurry was washed and filtered until the filtrate was entirely clear in order to ensure that only the ion-exchanged nickel remained in the catalyst. A small quantity of the precipitate was dried in a furnace at 180°C for 3 hours. An atomic absorption analyses performed on this sample yielded a weight loading of 6.76% nickel.

Appendix 3 contains the calculations of the actual quantities of the reagents used. The catalyst was reduced under the following conditions in a stream of hydrogen (40ml/minute).

60 min at 200°C
30 min at 300°C
130 min at 450°C

## 8.3 Nickel on ZSM-5 (0.527%)

The method of preparation involved an ion exchange of positive ammonium ions on the surface of the ZSM-5 support with the nickel ions (from $Ni(NO_3)_2 \cdot 6H_2O$) in solution. The ammonium ions constituted 1% (by mass) of the ZSM-5, and hence this was the maximum loading possible by ion exchange.

The catalyst was prepared as follows:
50ml of a 1M solution of nickel nitrate was added to 3.0g of ammonium ZSM-5. The solution was agitated and refluxed for 15 hours. The final solution was vacuum filtered and thoroughly washed to yield a precipitate of nickel loaded ZSM-5. 0.1595g of this precipitate was sampled and dried in a furnace at 180°C for 3 hours. This dry sample was then dissolved in 250$cm^3$ of distilled water. An atomic analysis of this solution yielded a nickel loading of 0.527%.

Appendix 4 contains the detailed amounts of the reagents used in the synthesis of this catalyst. The catalyst was calcined onto the mesh inside the reactor under the following conditions in a stream of flowing hydrogen (40ml/min).
60 min at 200°C
30 min at 300°C
130 min at 450°C.

## 8.4 Nickel on Silica-Alumina (11.17%)

As with nickel on alumina, an incipient wetness technique was used to prepare this catalyst.

Exactly 6.1175g of nickel nitrate hexahydrate was added to 10g of silica alumina by preparing a slurry in a $HNO_3$ solution of pH≈1. Upon

incipient wetness, the powdered catalyst was dried in a furnace at 130°C for 3 hours. Exactly 0.1524g of this dried catalyst was dissolved in 1 litre of distilled water (using HF acid). This was diluted ten times and an atomic analysis performed on the latter solution yielded a loading of 6.98% nickel (by mass).

Appendix 5 contains the detailed calculations of the quantities of reagents used in this synthesis. The catalyst was reduced in the reactor as follows:

30 min at 120°C
30 min at 260°C
160 min at 450°C

in a stream of hydrogen flowing at 40 ml/min.

## 8.5 Preparation of the cobalt and ruthenium catalysts

### 8.5.1 Amorphous supports

The catalyst preparation procedure for the cobalt and ruthenium catalysts was largely the same as for the nickel catalysts and hence it will not be discussed. The amorphous supports were loaded with cobalt or ruthenium from $Co(NO_3)_2 \cdot 6H_2O$ and $Ru_3(CO)_{12}$ respectively using a standard incipient wetness technique with n-hexane being used as a solvent in the case of ruthenium. Upon incipient wetness, the powdered catalyst was dried, and a sample was used for an atomic analyses to determine the exact metal loading of the catalyst. Appendices 6 to 9 contain the exact calculations of the reagents used in the synthesis of these catalysts.

### 8.5.2 ZSM-5 and Zeolite Y

Although, as with the amorphous supports, the ammonium Zeolite Y and the sodium ZSM-5 were ground to sub-25 micron size to eliminate intraparticular diffusional effects, an ion exchange technique was used to load the zeolite supports with cobalt or ruthenium.

Typically, a solution of the metal ions was prepared and the support was added before refluxing the slurry for 15 to 24 hours. The resulting solution was then vacuum filtered and thoroughly washed (until the filtrate was clear) in order to remove the surface-loaded metal ions. The powdered catalyst was then dried and a sample was used for an atomic analysis to determine the exact metal loading.

Appendices 10 to 15 contain the exact amounts of the reagents used in the synthesis of these catalysts.

## 9. INFRARED STUDIES OF CO ON SUPPORTED METHANATION CATALYSTS

Infrared spectra of carbon monoxide and hydrogen chemisorbed on nickel, iron, and cobalt have produced important evidence as to the existence and nature of surface complexes of possible importance in catalytic methanation. Spectra of carbon monoxide on nickel and other metals were first described in 1954 (24).

Bands attributed to CO bonded to a single nickel metal atom were found at 4.92 and 5.24$\mu$. The admission of $H_2$ to a sample with chemisorbed CO was reported to shift the major bands towards longer wavelengths by about 0.05$\mu$ and broaden the bands. The spectra were interpreted to show that there are two types of bonds to single metal atoms when CO is bonded to nickel and palladium. Moreover, the broadness of these bands was taken as evidence that there are greater differences among the bonds contributing to each band than there are in the case of CO on Pt. The theory that carbon monoxide is chemisorbed as a molecule and bonded to the metal through the carbon appeared to be confirmed by infrared spectra.

More detailed studies (25,26) were made with emphasis on the effect of varying the surface coverage. It was found that the spectra of CO on Ni and on Pd showed a number of bands with increasing surface coverage, indicating a heterogeneity of the surface. The 5.0$\mu$ region was regarded as a dividing line between bands due to linear and bridged CO. The longer wavelength bridged CO is the most strongly held. The results were interpreted as a measure of the relative importance of surface heterogeneity, interaction between adjacent molecules and changes in work function of the surface.

The IR spectra of CO chemisorbed on nickel were further studied with emphasis on the effect of nickel concentration (27). An assignment of IR bands to surface species for CO chemisorbed on nickel samples at room temperature was made as shown in Table 9.1 overleaf.
A new technique was reported (28) for the preparation of porous, high area, unsupported metal films which are suitable for IR absorption studies of chemisorbed CO. Reduction was accomplished by CO instead of $H_2$ so as to preclude the influence of sorbed $H_2$.A further structure was proposed from these studies :

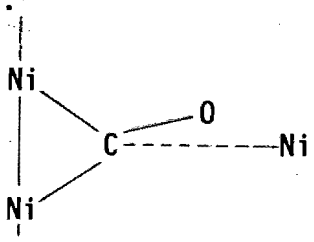


The presence of adsorbed and dissolved hydrogen influences the properties of nickel towards the sorption of carbon monoxide. The dissolved hydrogen is thought to alter the electronic properties of the metal, and the view was expressed (27) that electrons are tranferred to the nickel.

**Fig 9.1 Assignment of Infrared bands to Surface Species for CO chemisorbed on supported Ni samples at room temperature**

| Band | Frequency ($cm^{-1}$) | Species | Site | Strength of adsorption |
|---|---|---|---|---|
| A | 1915 | O<br>C<br>Ni Ni | Crystalline Ni | Very strong |
| C | 2035 | O<br>C<br>—Ni— | Crystalline Ni | Very strong |
| B | 1963 | O O O<br>C C C<br>Ni Ni | Crystalline Ni | Moderate |
| D | 2057 | O<br>C<br>—Ni— | Semi-Crystalline Ni | Moderate |
| E | 2082 | O<br>C<br>—Ni— | Dispersed Ni | Weak |

Treatment of samples of CO chemisorbed on Ni with $H_2$ at room temperature shifts the band due to linear carbon monoxide to a lower frequency and increases the relative amount of bridged CO. Removal of $H_2$ from nickel at 350°C resulted in spectra, when CO was subsequently sorbed, with most of the CO appearing as a linear structure. The significance was believed related to the observation that metals which chemisorb CO in the bridged form (Ni and Pd) are better catalysts for hydrogenation to methane than are metals (Cu and Pt) which chemisorb CO in linear form.

There has been some doubt expressed as to the existance of bridged bonds. Calculation (30) by the molecular orbital method showed that all available data on the IR spectra of chemisorbed CO can be explained by assuming only a linear form of bonding. Likewise, from considerations distinguishing between surface sites and surface atoms, the spectra of CO on various nickel catalysts can be described (with reference to the relative number of various types of nearest neighbor surface atoms) on the assumption that only linearly bonded CO is present (31).

The question of linear and bridged bonds have also been discussed when CO is adsorbed on iron (32,33). Blyholder and Neff (34) reported IR spectra of surface complexes when silica-supported iron samples were exposed to CO and $H_2$ at temperatures ranging up to 180°C. A number of workers have found that in experiments from -80 to 97°C on various iron, nickel, and cobalt catalysts, preadsorption of a small amount of CO enhances the quantity of $H_2$ subsequently adsorbed, while a large CO preadsorption inhibits $H_2$ adsorption. The enhancement effect has led to the proposal that complexes such as :

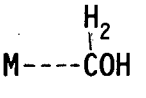


are formed on the surface. Eischens (24) in an investigation of the effect of hydrogen on CO chemisorbed on silica-supported iron, found no IR bands in the 2 to 7.5$\mu$ range which could be attributed to such complexes.

In agreement with Eischens, Blyholder and Neff (35) found no interactions between CO and $H_2$ to the extent of C-H or O-H band formation at or near room temperature. In fact, no interaction was found until the iron surface was hot enough to desorb chemisorbed CO rapidly.

However, IR spectra were obtained at 180°C which can be interpreted as giving evidence for the existence of oxygenated complexes on the surface. This arises from the fact that bands are observed indicating the presence of C-H and O-H bonds in species on the surface. Previously they found (34) that water or mixtures of water and hydrogen do not give O-H bands on silica supported iron at 20 or 180°C. Therefore, they presumed the O-H groups to be attached to carbon atoms. More work is desirable to establish the nature of the surface complexes in the system.

In contrast to the situation with iron, surface complexes formed by the interaction of $H_2$ and CO on nickel at temperatures up to 180°C were not found (34) even though products of the reaction of $H_2$ and CO were readily detected. It was speculated that in order to build up a long hydrocarbon chain it is necessary that the reacting species be firmly enough anchored to the surface that a number of chain-building steps can occur before desorption. It was suggested that the reaction species are much less firmly bonded to the nickel than to the iron catalyst, and this is why the former is better for methanation and the latter for Fischer-Tropsch synthesis.

One of the most important chemical features of chemisorbed CO is it's lack of reactivity at room temperature. In fact, experiments showed no reaction of CO with hydrogen until temperatures high enough to desorb chemisorbed CO were reached.

Spectra of CO adsorbed on evaporated films of cobalt are not dissimilar to those of CO on iron, with weaker bands at ca. 2030 $cm^{-1}$ and stronger bands near 1970 $cm^{-1}$. However, the supported metal samples, unlike those of Fe, show a number of additional linear-CO bands between 2050 and 2100 $cm^{-1}$, and are in general, dominated by absorptions in the linear CO region. Heal (36) assigned the two or three bands in the 2100 to 2000 $cm^{-1}$ region to multi - linear species of the $M(CO)_n$ type.

Bands near 2180 $cm^{-1}$ were attributed to CO adsorbed on incompletely reduced Co (36). It seems that it is difficult to reduce Cobalt, or alternatively, that adsorbed carbon monoxide is partly dissociated at room temperature leading to re-oxidation of the surface.

A considerable number of studies have been carried out using supported Ruthenium. There is a consistency in the wavenumbers of bands observed above 2000 $cm^{-1}$, viz. ca. 2140 $cm^{-1}$ and ca. 2030 $cm^{-1}$. In Lynds' original investigation (37) only the two higher wavenumber bands occurred. Dalla Betta (38) showed that the lowest wavenumber band of the three was the strongest, or the only band, when large metal particles were present. Brown and Gonzalez (39), aiming at accounting for differences previously obtained, showed that the 2030 $cm^{-1}$ band was much the strongest for a newly reduced Ru sample, but that the 2080 $cm^{-1}$ absorption became the strongest after controlled re-oxidation of metal samples. The most straightforward interpretation is that the ca. 2030 $cm^{-1}$ band is attributable to the linear and dominant species on fully reduced Ru, the ca. 2080 $cm^{-1}$ band is from linear CO on partially oxidised Ru, and the ca. 2140 $cm^{-1}$ band is from CO on strongly oxidised Ru, eg. ruthenium oxide. Earlier suggestions that $Ru(CO)_n$ species (n>2) give rise to the higher frequency bands seems to be less probable.

The adsorption of carbon monoxide on electron-deficient palladium crystallites on amorphous silica-alumina and on zeolite Y has been studied (40) by infrared spectroscopy. The observed shift toward higher frequencies of the CO band as the metal becomes more electron deficient reflects a decrease in pi-bonding between the metal and adsorbed carbon monoxide and hence a decrease in electron density on the oxygen. Similar shifts have been observed (41) for carbon monoxide adsorbed on ruthenium as the acidity of the support increases. Following the correlation of Joyner and Roberts (52), relating oxygen (1s) binding energies in carbon monoxide to its heat of adsorption on a variety of metals, it is expected that carbon monoxide will adsorb less strongly on ruthenium as the metal particles become more electron deficient and the extent of backbonding decreases. Hydrogen will then compete more successfully with carbon monoxide for the available

adsorption sites, resulting in an increased surface concentration and an enhanced reaction rate. This pattern is also consistent with the suggestion by Vannice (18) that a weakening of the metal-carbon monoxide bond results in a higher activity for carbon monoxide hydrogenation.

Brown and Gonzalez's conclusions (39) are consistent with Dalla Betta's results (38) if it is assumed that the smaller metal particles are less thoroughly reduced or are modified by proximity to the surface of the oxide support. This is reminiscent of the situation with nickel. Only a few weak bands have been observed for ruthenium in the bridged - CO region, with the exception of results by Kobayashi and Shirasaki (40), wherein a strongish absorption band was reported to occur just below 2000 $cm^{-1}$; but in this case, the experimental procedures did not allow for in situ examination of the spectra of the sample in an evacuated infrared cell.

## 10. THEORETICAL MODELLING OF THE REACTOR

Two approaches to modelling the tube wall reactor were possible. The first involved a detailed model which included the effects of radial mass transport (two dimensional model). The second model was a plug flow model, based on the integration of the kinetic rate expression over the length of the reactor tube. (one dimensional model)

### 10.1 Assumptions made

(i) Fully developed laminar flow along the entire catalyst section (from Appendix 14 it may be seen that, even at the highest flowrates used in this experiment, this assumption is valid )

(ii) Negligible axial diffusion (the absence of a catalyst packing eliminated almost all axial diffusion )

(iii) Interparticle gradients were smaller than experimental
* accuracy and hence were neglected.

*(iv) No intraparticle temperature gradients occured (see appendix 42)

(v) Concentration gradients within the catalyst particles could generally be excluded due to the small particle sizes used. (all catalyst particles passed through a 25 micron sieve) (see appendix 42)

* Confirmed by studies conducted by Klose and Baerns,(17)

In order to ascertain whether or not the radial concentration profile was negligable, a preliminary experiment was performed in which pure CO was allowed to flow through a catalyst-free reactor. The reactor was positioned so that the laser sampling-volume was generated at three radial positions in the reactor. The carbon monoxide relative concentrations obtained from these positions were indentical within the expected exerimental error of 1%. The radial concentration profile was thus confirmed to be negligable under the conditions of this experiment. The reactor was then positioned so that the laser-sampling volume was generated at eight positions along the axis of the reactor. The relative concentrations of CO obtained in this way also did not differ by more than the experimental error of 1%.England

et al(4), at Harwell, compared the one and two dimensional models and found them to be identical. They also found that the radial concentration profile was negligible, thus the results of the fully detailed model, including radial, diffusive mass transfer, laminar flow and a heat balance could be duplicated by using only the simple plug flow model. This indicates that under laminar conditions, diffusive resistance was negligible compared to kinetic resistance.
In this experiment, a plug flow model, using isothermal and non-isothermal conditions was compared. The latter was considered necessary because of the large heat of reaction. (-206 kJ/mol)

The characteristic plug flow design equation for a homogeneous reaction (See appendix 15 for derivation)

$$\frac{V}{F_{Ao}} = \int \frac{dx_a}{-r_{co}} \quad ..(A)$$

where V = reactor volume ( catalyst section )
$F_{Ao}$ = flowrate of pure CO
$x_a$ = conversion
$-r_{co}$ = rate of reaction

was used with a rate expression of the form

$$-r_{co} = Ae^{-Ea/RT} p_{co}^{X} p_{H2}^{Y} \quad ....(B)$$

where X,Y,A,$E_a$ are all variables.

Using equations (A) and (B), it was possible to solve the mass balance and hence obtain a concentration versus length profile in the reactor under isothermal conditions.

For the non-isothermal case, an energy balance had to be incorporated. This energy balance accounted for rates of:

i) Radial heat transfer from the reactor
ii) Heat of reaction

iii) Energy efflux from the reactor due to gas flowrates.

iv) End loss effects

The energy balance, as derived in Appendix 16, is shown below :

$$\frac{dT}{dz} = \frac{\pi d\, h_o (T_s - T) - r_{co} H_{rxn} \pi d^2/4}{F_t\, C_p} \qquad \ldots(C)$$

where $\frac{dT}{dz}$ = variation of temperature with length

$d$ = diameter of reactor tube

$h_o$ = outer heat transfer coefficient

$T_s$ = temperature of heating wire

$T$ = Reaction temperature

$F_t$ = total molar flowrate

$C_p$ = heat capacity of gases

In order to evaluate the variables $A, E_a, X$ and $Y$ in the rate expression (B), a Basic computer program was written. A listing and an algorithm of this program is provided in Appendices 17 and 18.

## 10.2 Solution of the mass balance (Isothermal case)

Values of conversion (x) were generated and, using different values of $A, E_a, X$ and $Y$, the mass balance was solved to yield a theoretical length versus conversion profile of the reactor.

## 10.3 Solution of the mass balance (Non-isothermal case)

A temperature profile along the reactor was obtained with no reaction occuring. This gave the wall surface temperature at any point along the reactor. (A profile existed since the reactor was not much longer than the heating element and thus introduced end heat losses.)

This profile was obtained at 50°C and at 200°C and is graphically illustrated in Appendix 19. In order to obtain a similar profile at any other temperature by an interpolation technique, curves were fitted to the above measured profiles as seen in appendix 20. This procedure was necessary since $T_s$ in equation (C) is a function of the reactor length.

A simultaneous solution of the mass and energy balances (equations(A), (B) and (C) respectively) was performed using a Runge-Kutta numerical integration technique. This simultaneous solution yielded a theoretical temperature and conversion versus length profile along the reactor.

## 10.4 Calculation of the outer heat transfer coefficient

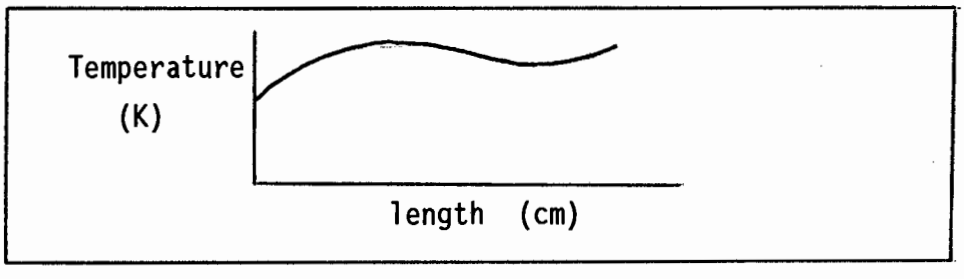


**Figure 10-1 Temperature along the heating element**

Due to a temperature profile along the heating element, the heat transfer coefficient varied along the reactor tube.

The equation used to determine $h_o$ was :

$$Nu_D = \left[ 0.6 + \frac{.387\ Ra_D^{0.1667}}{[1 + (.559/Pr)^{.5625}]^{.2963}} \right]^2$$

This equation incorporates the dimensionless quantities **Gr** and **Pr** which are functions of temperature. In order to obtain the parameters at any temperature, curves were fitted to these values covering a temperature range from 250K to 1000K. (see Appendix 21) Thus the Nusselt number could be obtained at any temperature corresponding to any distance along the reactor and subsequently $h_o$ could be obtained. This value was then used in the energy balance.

## 10.5 Thermodynamic analysis of the methanation reaction

In order to determine the theoretical conversion at any temperature, the equilibrium constant for the reaction was determined. Since the pressure was low (approximately 1 atm) and the temperature high (approximately 500 K), the gases and gas mixture were assumed to be ideal. This was evident from the fact that the fugacity coefficient and the value of **Z** in the ideal gas equation was practically equal to one. The calculations are performed in Appendix 22. The equilibrium constant could then be determined as a simple ratio of the product of the product gas partial pressures to the product of the reactant gas partial pressures.

Appendix 23 contains calculations of the equilibrium constant (as a function of temperature). By rewriting the partial pressures in terms of conversion and equating the resulting ratio to the equilibrium constant, the conversion could be obtained. This calculation is performed in Appendix 22.
The feasibility of the reaction was investigated by calculating the Gibbs free energy for the methanation reaction as a function of temperature.

Examples of the above calculations are shown in Appendix 23.

## 11. ANALYSIS OF RESULTS

### 11.1 Derivation of relative concentrations

The number density of the gas molecules varies as the inverse of the square root of the absolute temperature at any point in the reactor. Thus, at higher temperatures, the number density of a gas species as indicated by *CARS* is lower than the true value of the number density that would be indicated at a lower (true) temperature. This may be illustrated by analogy with a fixed number of gas molecules expanding to fill the available volume as the temperature is increased. The correction factor that was thus applied to the results is :

Corrected Conc.= Relative Conc.*$(T_{actual}/T_{ref})^{1/2}$

iff, $T_{actual} > T_{ref}$, where $T_{actual}$ = T reaction and Tref = Temperature at the start of the catalyst section.

Thus, the corrected relative concentration, averaged over 2cm before the start of the catalyst section of the reactor was regarded as being the 'true' relative concentration. The CO conversion was then obtained by linearly ratioing the relative concentrations with this 'true' relative concentration. It was necessary to average the two concentrations just before the start of the catalyst section as the measurement volume had a length of approximately 12mm whilst the reactor was moved by only 10mm at a time.

### 11.2 Computer simulation

#### 11.2.1 User inputs required

The inputs required by the modelling program are :

A set of data points of the form :

(Distance into catalyst (cm), Conversion of CO)

A selection of : A - Isothermal modelling

B - Non-isothermal modelling

c - A comparison of (A) and (B)

The temperature at the start of the catalyst section (K);$T_{ref}$

Flowrates of CO and $H_2$ in ml/min.
Initial estimates of :
The exponent of the partial pressure of CO; X
The exponent of the partial pressure of $H_2$; Y
The pre-exponential factor ; A
The activation energy of the reaction (cal); Ea
The step size (cm) for non-isothermal modelling (typically 0.5cm)
The conversion of CO at the start of the catalyst section.

The data will be output in the form of a table or graph of CO conversion versus length into the catalyst and a parameter with a numerical value will be displayed. This parameter is the sum of the differences between the actual and the theoretical curves and must be minimised in order to yield the best fit values of the parameters A, Ea, X and Y in the rate equation.

### 11.2.2 Sensitivity of the rate equation parameters

The rate equation parameters were varied by fixing three of the four variables and then optimizing the fourth variable. This was done in a random order to try to overcome any within-parameter variation or dependance i.e. any effect that varying eg. Ea has on X etc.
Typically it was found that:
A, the pre-exponential value affected the vertical displacement of the curve.
Ea, the activation energy, was the most sensitive variable and affected the slope of the theoretical curve i.e. the lower the activation energy, the more steep the slope.
X, the exponent of the partial pressure of CO affected the shape of the curve i.e. more linear or more curved (concave downwards).
Y, the exponent of the partial pressure of $H_2$ had very little effect on the modelling and did not affect the shape or displacement of the curve to any great degree.

## 12. RESULTS AND DISCUSSION

Using the program to model the reactor (listing in appendix 17), a rate equation of the form :

$$-r_{CO} = A\, e^{-Ea/RT} p_{CO}^{X} p_{H2}^{Y}$$

was fitted to the data presented in appendices (25-40). A modified. non-linear least squares fit yielded the following results for the hydrogenation of carbon monoxide at 250°C and at 1 atmosphere.

| Metal | Substrate | Loading | A | $E_a$ | X | Y |
|---|---|---|---|---|---|---|
| Ni | $SiO_2/Al_2O_3$ | 7% | 8.75e4 | 24950 | -.32 | 1.1 |
| Ni | Zeolite-Y | 7% | 5.00e4 | 25250 | -.32 | 1.0 |
| Ni | Alumina | 7% | 7.50e4 | 25250 | -.36 | 1.0 |
| *Ni | ZSM-5 | .5% | 8.75e4 | 25100 | -.30 | 1.3 |
| *Ni | Alumina | 7% | 8.75e4 | 24750 | -.36 | 0.9 |
| Co | Alumina | 7% | 9.25e4 | 25925 | -.44 | 1.1 |
| Co | $SiO_2/Al_2O_3$ | 7% | 8.75e4 | 25900 | -.44 | 1.1 |
| Co | Alumina | 7% | 9.00e4 | 25925 | -.44 | 1.1 |
| Co | $SiO_2/Al_2O_3$ | .5% | 8.75e4 | 25925 | -.44 | 1.0 |
| Co | Zeolite-Y | 7% | 1.17e5 | 25900 | -.44 | 1.2 |
| *Ru | $SiO_2/Al_2O_3$ | 7% | 8.25e4 | 23300 | -.25 | 1.3 |
| Ru | Alumina | 7% | 4.00e4 | 24800 | -.26 | 1.6 |
| Ru | Zeolite-Y | 7% | 7.50e4 | 23800 | -.26 | 1.2 |
| *Ru | Zeolite-Y | 7% | 7.50e4 | 24775 | -.26 | 1.5 |
| Ru | ZSM-5 | .5% | 8.75e4 | 24800 | -.26 | 1.5 |

In the table above :

A has the units of ($mol/m^2$ sec)

$E_a$ has the units of (cal/mol).

* indicates the runs performed with reactant flowrates of :

CO Flowrate = 13 ml/min, $H_2$ Flowrate = 39 ml/min

All other runs were performed with carbon monoxide and hydrogen flowrates of 6 and 18 ml/min respectively.

The pre-exponential factor A, has been modified for surface reaction (see appendix 41).

The graphs on the next three pages show the relative conversion of carbon monoxide along the catalyst tube.

# Conversion vs length data

## 11% Ni on silica-alumina

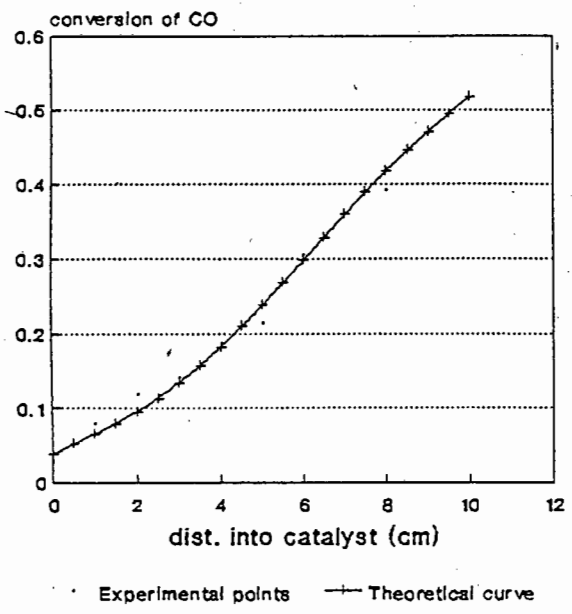


## 7% Ni on Zeolite-Y

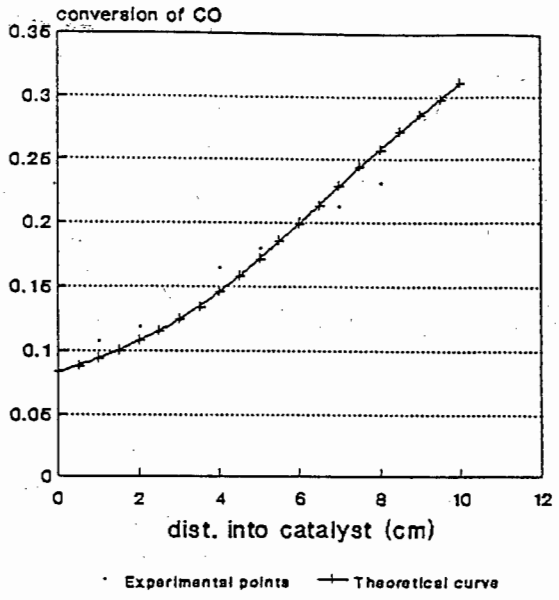


## 7% Ni on alumina

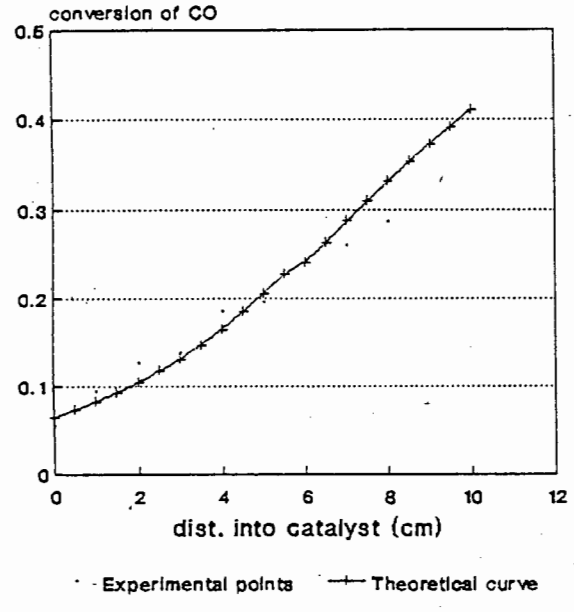


## 0.5% Ni on ZSM-5

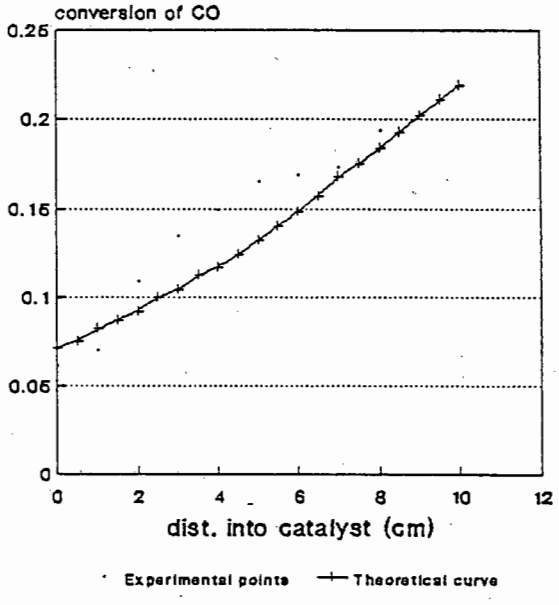


## 7% Ni on alumina

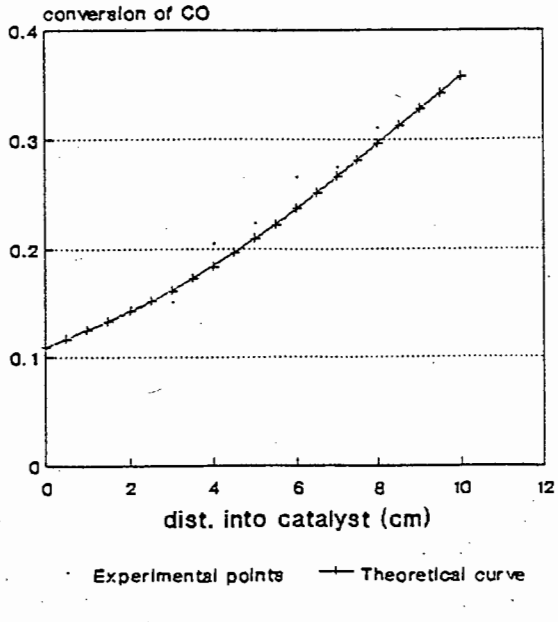

## 7% Co on alumina

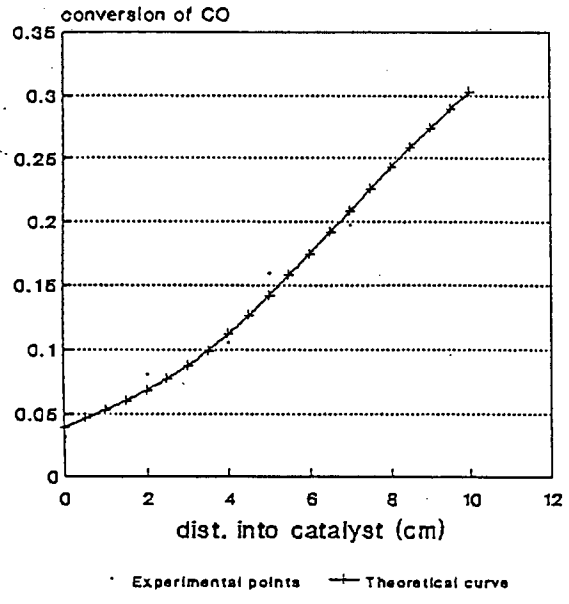


## 0.5% Co on silica-alumina

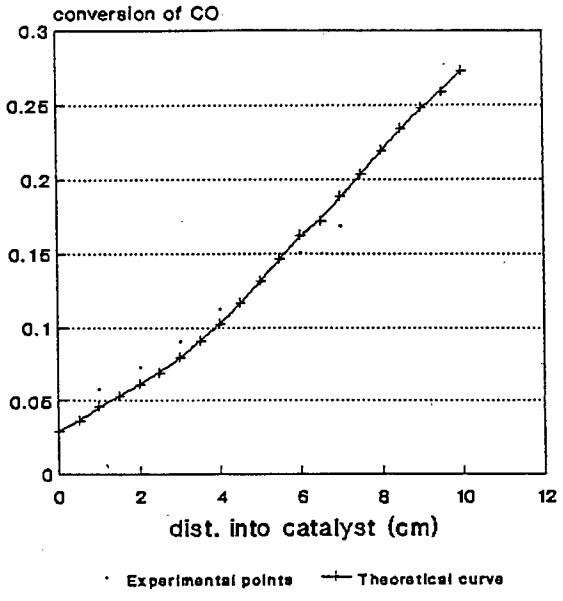


## 7% Co on alumina

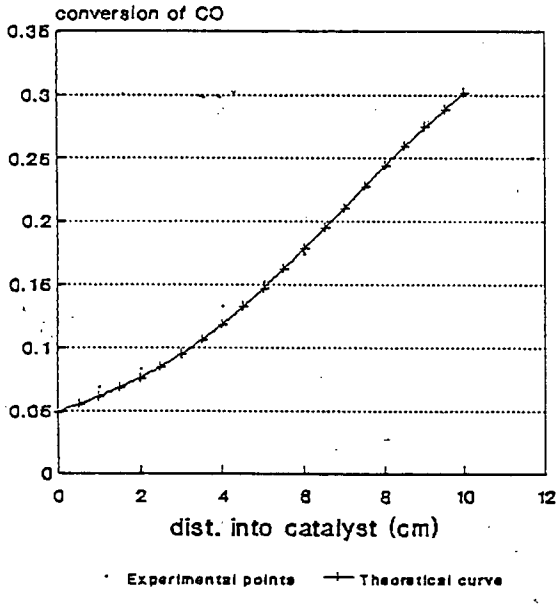


## 7% Co on silica-alumina

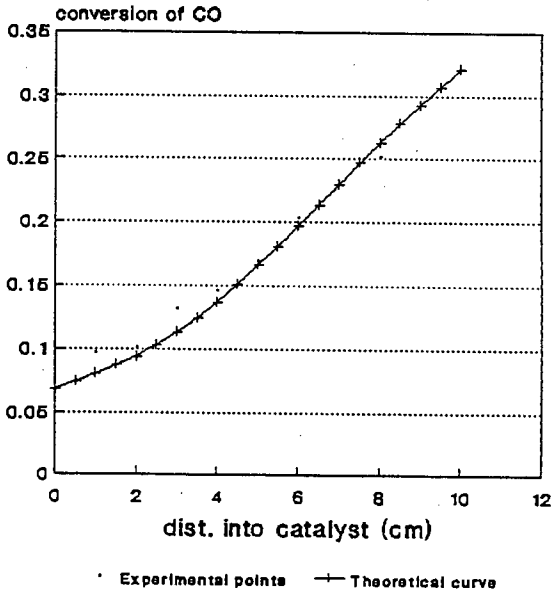


## 7% Co on Zeolite-Y

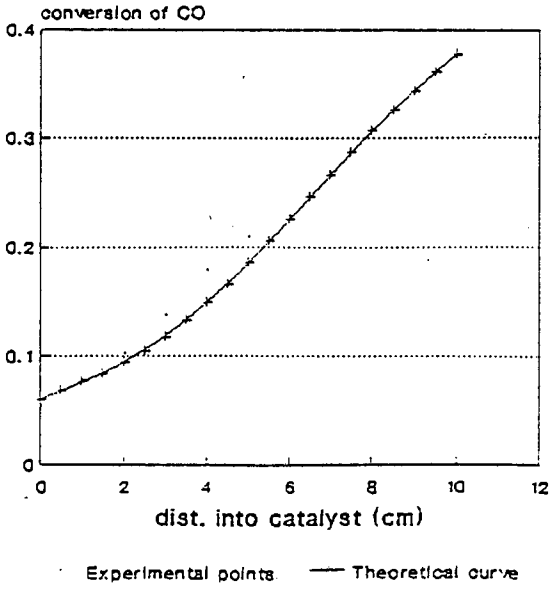

## 7% Ru on silica alumina

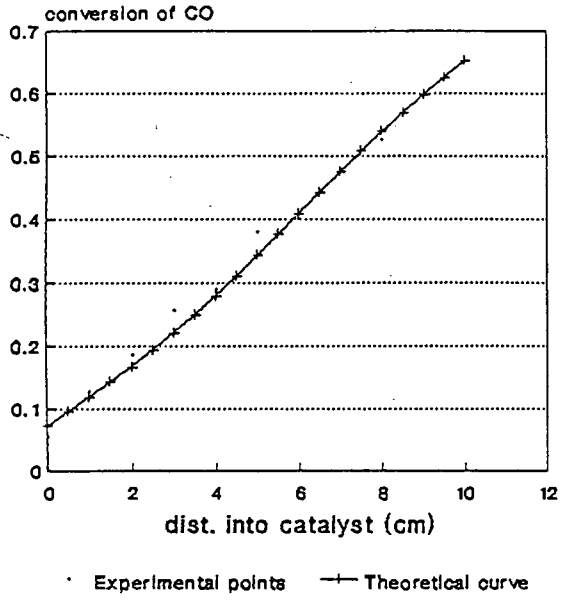


## 7% Ru on alumina

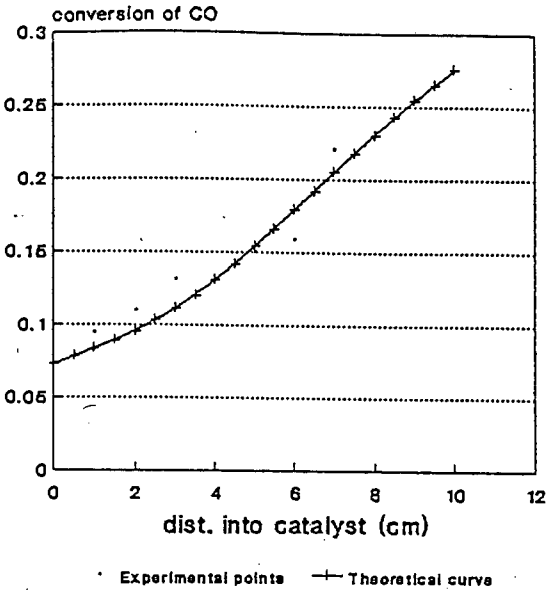


## 7% Ru on Zeolite-Y

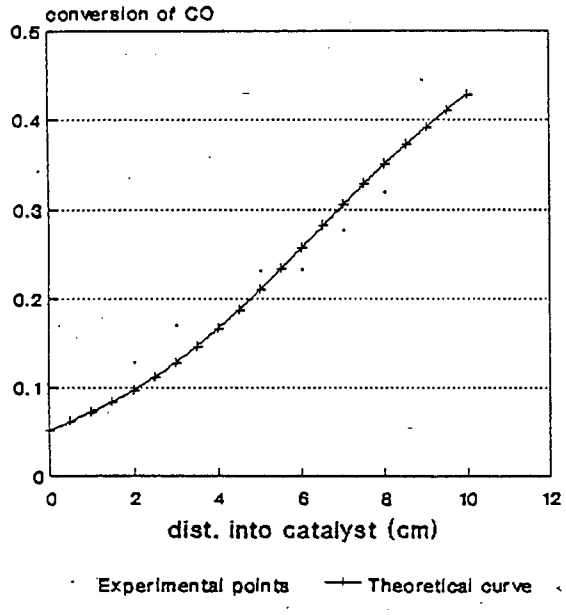


## 7% Ru on Zeolite-Y

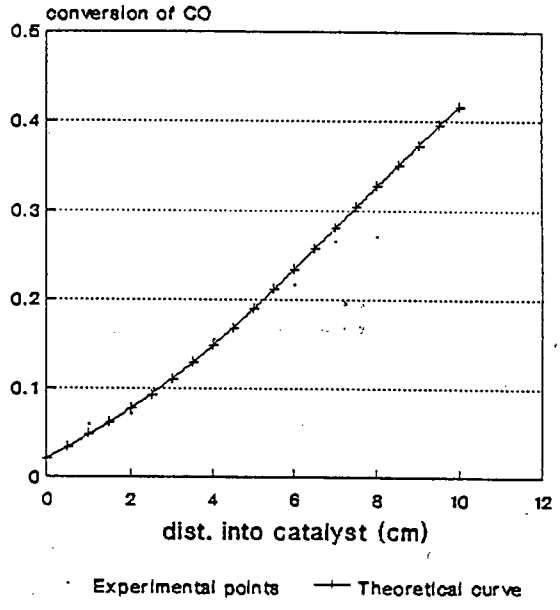


## 0.5% Ru on ZSM-5

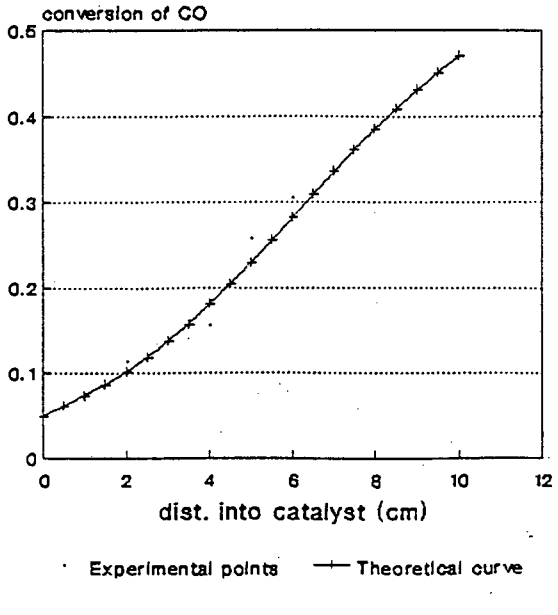

From the results of the rate equation parameters and the activity graphs, the following points can be highlighted:

## 12.1 Effect of metal on the rate equation

The parameters A,$E_a$,X and Y as found to best fit the data for the three metals, whilst differing noticably from metal to metal, are similar enough to indicate that the same mechanism of reaction is occurring on each metal. Nickel and cobalt are the most similar, with ruthenium exhibiting the most deviation. In particular, the role of hydrogen in the reaction over supported ruthenium appears to be more significant than either cobalt or nickel. McKee (47) found that, for a 0.5% Ru on alumina catalyst at 220°C, the reaction rate was proportional to : $p_{CO}^{-.13}p_{H2}^{1.33}$ which is in agreement with the power of the partial pressure of hydrogen found in this work. Furthermore, the results of Vannice (48) for a 5% $Ru/Al_2O_3$ catalyst are consistent with the scenario that the rate determining step involves the reaction of the adsorbed carbon atom with four hydrogen atoms. Dalla Betta et al (49), also reported that the number of hydrogen atoms reacting with the adsorbed carbon atom is greater than two. It is thus possible that, in the case of ruthenium, the mechanism or at least the rate determining step is different from that suggested here. Dalla Betta and Shelef (46) made *in situ* measurements of infrared spectra during methanation on a 5% Ru on alumina catalyst. At 250°C, the main feature was a C-O stretching band at |2000$cm^{-1}$ observed in pure CO and in $H_2$ + CO mixtures. In a similar study on ruthenium by Kellner and Bell (53), it was found that thye surface was heavily covered with CO as a linearly adsorbed species, a diadsorbed $Ru(CO)_2$ form and a bridged structure [Ru(CO)Ru]. The bridged form was present in only minor amounts and the $Ru(CO)_2$ species in moderate amounts. The diadsorbed structure did not hydrogenate rapidly.

Cobalt and nickel are active methanation catalysts, resembling Ru in many ways. One marked difference is that Co and Ni form carbonyls more readily than Ru. Since 1950, there has not been very much research on Co catalysts. Agrawal et al (54) studied the kinetics of methanation on alumina supported cobalt. He suggested that a mechanism involving a surface-carbon

intermediate with the addition of the first hydrogen to the carbon as the rate determining step was the most appropriate. In earlier studies of the methanation reaction, principally over supported nickel, it was apparent that there was a great deal of uncertainty concerning the nature of the reaction intermediate. Since 1975, it has become accepted that the previously accepted concept that CHOH species were intermediate in the methanation reaction is generally unfounded. It is now widely recognised and accepted that, as suggested by the mechanism used in this work, and by the results of Araki and Ponec (41) and Rabo et al (42), that the surface species taking part in the reaction over nickel and cobalt are carbon atoms formed by the dissociative adsorption of CO.

From past studies it has been found that the synthesis reaction in general and the methanation reaction in particular, are frequently close to zero order in CO concentration and near first order in $H_2$ concentration over a specified pressure range (16,17,18). From this data therefore, it has been suggested that the catalytic surface is 'almost completely' covered with strongly adsorbed CO, while the more weakly bound $H_2$ competes for adsorption on the small number of available metal sites remaining. Rautavuoma and van der Baan (20) have reported that. in experiments in which the surface products of reaction on cobalt catalysts were stripped off, more than 95% of the surface was covered by a carbon-containing species. Calculations based on these results indicated that if the surface were 'almost completely' covered in adsorbed CO, then much stronger negative orders in CO in the rate equation :

$$-r_{CO} = Ae^{-Ea/RT}p_{CO}{}^{X}p_{H2}{}^{Y}$$

should be obtained than those found experimentally. In order to explain this, the authors put forward a plausible theory : that there are two types of carbon-species on the surface :

i) Precursors of the rate-determining step i.e. adsorbed CO and surface carbon
ii) All other(i.e. inactive for rate-determination) carbon-containing surface intermediates.

If this is assumed, then the coverage of the carbonaceous species together may easily form an 'almost total' coverage.

In studies conducted by Biljoen et al (44), it was concluded that CO dissociation is very rapid and hence unlikely to be the rate limiting step and that $CH_x$ (X=0-3) species constitute the most reactive $C_1$ surface species. The present results also suggest that, either hydrogenation of the surface carbon or of a (CH) intermediate is the rate limiting step for the hydrogenation of CO over supported nickel and cobalt catalysts. This is in accordance with the recent findings of Dalmon and Martin (19), who, from studies of the activation energy of the methanation reaction, deduced that the active intermediate is the surface carbon - and that the rate determining step is the hydrogenation of the intermediate. It is worth noting that the adsorption of CO on the metal appears to play a role in the mechanism as the order of the activation energies of the metals is : Ru<Ni<Co and this is inverse to the heats of adsorption of CO : $\Delta H_{ads}(CO)$=Ru>Ni>Co.

## 12.2 Effect of metal on the methanation activity

If it is assumed that the mechanism for all three metals is similar, it is possible to determine the methanation activity of the metals in this study. Although dispersion studies were not carried out on the catalysts, they were all ground to sub-25 micron particles before being used in the experiment. The surface areas of the catalysts thus, should be comparable. This is also bourne out by the fact that the pre-exponential factors obtained for all the catalysts used in this study are of the same order of magnitude. Bearing these assumptions in mind, the results of the present study confirms the trend in the methanation activity of the metals as suggested by Vannice (18) and earlier by Fischer et al (50) i.e. decreasing in the order Ru>Ni>Co.

## 12.3 Effect of support

The results of the present study suggests that the support does not affect the rate equation for any of the three metals and thus it appears that the

mechanism, for the same metal, is unaffected by the support. The supported Co catalysts, with the exception of 0.5% Co on silica-alumina, allow the activities for the same metal, under the same conditions of reactant flowrate and metal loading to be compared. Two types of metal-support interactions are possible, (a) electronic interactions and (b) geometric interactiona. However, due to the extremely small size of the molecules, the contribution from any geometric effects will be very small. The zeolite support appears to enhance the methanation activity of Co when compared to the amorphous alumina or silica-alumina supports. Bhatia et al (55) studied supported Ni catalysts for methanation. Nickel on alumina was more active in methanation than Ni on Zeolite-Y.

This was confirmed by the results of the present study where a 7% Ni loaded alumina yielded a CO conversion of 28.62% as opposed to a conversion of 23.14% for a 7% Ni on Zeolite-Y catalyst. Vannice (56) reported that, with alumina as a carrier, the activities declined in the order Ru>Ni>Co, while with silica as a carrier, the activity order was different and declined in the order Co>Ru>Ni. The results of the present study also show a similar increase for the activity of Co on Zeolite-Y as opposed to the same loading of Ru and Ni. Ruthenium yielded a total conversion of 31.89%, while cobalt yielded a value of 30.84%, and nickel only 23.14% for the conversion of CO.

## 12.4 Effect of metal loading

As mentioned before, the rate equation parameters are similar for each metal and it thus appears as though the metal loading does not affect the mechanism of the reaction. It is obvious however, that the metal loading on the support does affect the methanation activity. It is expected that, for a higher metal loading the total conversion of CO should be greater, since the reactant gases effectively 'sees' more active metal sites. This is indeed the case as can be seen by examining the results of the 7% Co on silica-alumina and the 0.5% Co on silica-alumina catalysts. The rate equation parameters for these catalysts are alomst identical, suggesting no change in the mechanism. The activities, however, are markedly different. The 7% Co on silica-alumina catalyst yielded an overall CO conversion of

23.62% while the 0.5% Co catalyst on the same support yielded only 16.70% CO conversion.

## 12.5 Effect of reactant flowrates

Two sets of reactant flowrates were used in this study:

i) CO : 6ml/min and $H_2$ : 18ml/min (low flowrate)

ii) CO : 13ml/min and $H_2$ : 39ml/min (high flowrate)

As expected, the reactant flowrate did not affect the mechanism of the reaction as can be seen by the similarity in the rate equation parameters. The 7% Ni on alumina and the 7% Ru on Zeolite-Y catalysts allow the effect of reactant flowrate to be examined. For Ni and Ru, the activities appear to be affected in contrasting ways. At the higher flowrates, the Ni on alumina catalyst yielded a CO conversion of 31.06% as opposed to 28.62% at the lower flowrates. Firstly, it must be noted that these results are not vastly different and it may be that the effect is not significant. However, as the conditions of the experiment were well below equilibrium conditions, it is likely that increased acitivity (and hence CO conversion) should occur with higher flowrates. The Ru catalyst, however, yielded results that showed a different trend. At the higher flowrates, a conversion of 26.99% was obtained, while at the lower reactant flowrates, a CO conversion of 31.89% resulted. It is possible that, because of the shorter residence time, a decreased conversion resulted, however, more data is needed to confirm a definite effect of reactant flowrate on the methanation activity.

From the results of this study, these are the effects that are most easily examined, however, a few other factors need to be discussed in order to fully appreciate the influences on the results obtained. These are :

## 12.6 Catalyst deactivation

In order to eliminate any effect of deactivation or carbide deposition, the catalyst was replaced with fresh catalyst after each run at a particular temperature. The reproducibility of the results appears to be excellent as can be seen by the similar activity and rate equation parameters obtained from the 7% Co on alumina catalysts under identical conditions. Due to the

high reactivity of Ru, especially, this was considered necessary. Elliot and Lunsford (57) prepared Ru catalysts bu ion exchange an NaY and CaY. In all cases, the Ru content was 0.5%. In methanation at 280°C, the catalysts aged rapidly.

## 12.7 Effect of water

In studies conducted by Anderson (58), it is noteworthy that, in the case of iron catalysts, the partial pressure of water usually appears in the rate equations. In view of the fact that Fe oxidises much more readily than Ru,Ni or Co, the sensitivity to $H_2O$ is understandable. Nevertheless, water should be expected to chemisorb on these three metals and so compete with CO and $H_2$ for catalyst sites. This has been reported in one case by Saletore (59), for a nickel catalyst. The present study utilized the rate equation in the form as used by England et al (4) in order to directly compare the rate equation parameters obtained. Because of the strong correlation and the degree of fit between the experimental points and the predicted (theoretical) curve, it was not considered necessary to include the effect of $H_2O$ in the rate equation.

## 12.8 Effect of temperature

In the published literature, the kinetic equations for methane synthesis do not present a uniform picture. Generally, the exponent of the partial pressure of hydrogen varies from zero to two, and for carbon monoxide, from one to minus one. Dalla Betta et al (49) observed constant initial turnover numbers on Ru on alumina with average sizes of Ru particles varying from less than 10 to 91A. At 240°C, the $H_2$ and CO orders were 1.28 and -0.47 respectively and at 300°C, 1.70 and -0.93. These results suggest possible inadequacies of the power rate law. For Ru on alumina at elevated pressure and at 235°C, Pannell et al (60) obtained power rate law exponents of 0.22 and -0.32 for $H_2$ and CO respectively. In detailed studies by Sughrue and Bartholomew (61), for Ni on alumina, reported parameters of the power rate law that varied widely and irregularly from 200 to 350°C. The CO exponent varied from -0.87 to -0.04 and the $H_2$ power from 0.66 to 1.04. No single fundamental rate equation was useful over the entire temperature range.

## 13. CONCLUSIONS AND RECOMMENDATIONS

Coherent Anti-Stokes Raman Spectroscopy (*CARS*) lends itself well to the study of catalytic reactions as the non-intrusive technique is very effective in obtaining accurate concentration measurements when using reference cell optics.

After comparing the three methods of referencing, viz:

1) External argon referencing
2) External CO referencing, and
3) Internal nitrogen referencing,

it is evident that the external CO reference gives a lower relative standard deviation than the external argon reference. Using an argon reference leads to some ambiguity about the base line because it is not possible to correct for the background signal. Both the external references yielded lower standard deviations than internal nitrogen referencing. Referencing with an external cell is more satisfactory if a single-mode pump beam is used, otherwise there will be different phase relationships between the input beams in the sample and in the reference cell, and the two *CARS* signals will not necessarily be proportional.

England et al (4), used the *CARS* technique with an internal nitrogen reference. The results for the supported nickel catalysts used in this study agrees well with the rate equation parameters found at Harwell by England and his team. This, together with the fact that the referencing method utilized in this study is clearly more accurate than that used by England et al, suggests that the data obtained for the cobalt and ruthenium catalysts is accurate.

The use of a tube-wall catalytic reactor has allowed the justification of numerous simplifying assumptions in the derivation of the one dimensional plug-flow equation from the Navier-Stokes equation of continuity in cylindrical co-ordinates. These were :

i) Fully developed laminar flow along the catalyst section.
ii) Negligable axial diffusion.

iii) Interparticular gradients were smaller than experimental error.
iv) No intraparticular temperature gradients occurred.
v) Concentration gradients within the catalyst particles could be excluded.

The excellent agreement between the experimental points and the theoretical curves as well as the general agreement of this work with other researchers findings has further justified the use of these assumptions.

It has been confirmed that the characteristic plug-flow equation :

$$\frac{V}{F_{A_o}} = \int \frac{dx_{CO}}{-r_{CO}}$$

when used with a rate equation of the form :

$$-r_{CO} = Ae^{-Ea/RT} p_{CO}{}^{X} p_{H2}{}^{Y}$$

may be used to succesfully model the methanation reaction over supported nickel, cobalt and ruthenium catalysts.

From the results of the rate equation parameters and activity graphs obtained, the following conclusions may be drawn.

<u>Effect of metal on the rate equation</u>

The parameters A,Ea,X and Y as found to best fit the data for the three metals investigated, whilst differing noticably from metal to metal, are similar enough to indicate that the same mechanism of reaction is occurring on each metal - with the possible exception of ruthenium. The results also suggest that, either hydrogenation of the surface carbon or of a (CH) intermediate is the rate limiting step in the mechanism. The order of the activation energies for the methanation reaction on these metals is : Ru < Ni < Co, and this is inverse to the heats of adsorption of CO on the metals where : $\Delta H_{ads}(CO)$ = Ru > Ni >Co

<u>Effect of metal on the methanation activity</u>

The present study confirms the trend in the methanation activity of the metals as decreasing in the order : Ru > Ni > Co.

## Effect of the support

The rate equation, and thus the mechanism of reaction, for the same metal, is unaffected by the support. The support does however appear to affect the methanation activity of the metals. The zeolitic supports appeared to enhance the activity of cobalt when compared to the amorphous supports. Nickel on alumina was a more active methanation catalyst than nickel on Zeolite-Y.

## Effect of the metal loading

The mechanism of reaction is not affected by the metal loading on the support. The activity of the catalyst increases for higher metal loadings.

## Effect of reactant flowrates

Once again, the mechanism is independant of the reactant flowrates. The effect of the reacant flowrates on the activity yields conflicting results for nickel and ruthenium catalysts. More data is needed to corroborate or refute the apparent trends observed on these metals.

Having demonstrated the use of *CARS* to obtain concentration measurements in a laboratory reactor, it is felt that the future direction of *CARS* lies increasingly towards systems in which heat and mass transfer effects are important, particularly in hostile environments. Possible future directions for the use of *CARS* in a catalytic reactor studies include the following:

(1) The study of turbulent and/or non-isothermal tube-wall catalytic reactors to characterise heat and mass transfer effects.
(2) The study of monolithic reactors, on a channel by channel basis.
(3) The study of oscillating chemical reactors.
(4) The study of reactors over precious metal gauzes, where temperature and concentrations profiles above and below the catalyst could be studied.

## 14. LIST OF REFERENCES


1) Greenhalgh,D.A.,Porter,F.M., and England,W.A., Comb. Flame, vol.49, 171, (1983)

2) Stenhouse,I.A.,Williams,D.R.,Cole,J.B., and Swords,M.D., Appl. Optics, vol.18, 3819, (1979)

3) Pealat,M.,Taran,J.P.E.,Taillett,E.,Bacak,M., and Bruneteau, A.B., J.Appl.Phys., vol.52, 2687, (1987)

4) England,W.A.,Glass,D.H.W.,Brennan,G, and Greenhalgh,D.A., Journal of Catalysis, vol.100, 103-117, (1986)

5) Jarri,G.A.,Mayo,K.B.,and Bartholomew,C.H., Chem. Eng. Commun., vol.4, 325, (1980)

6) Pennline,H.W.,Schehl,R.R., and Haynes,W.P., Ind. Eng. Chem. Process. Des. Dev., vol.18, 156, (1979)

7) England,W.A.,Milne,J.M.,Jenny,S.W.,Greenhalgh,D.A., "Application of CARS to an Operating Chemical Reactor", Applied Spectroscopy, vol 8, No.6, 867-875, (1984)

8) Greenhalgh,D.A., "Gas Phase Temperature and Concentration Diagnostics with Lasers", January 1983, AERE Report, Harwell

9) Laidler,K.T., and Meiser,J.H., "Physical Chemistry", Benjamin Cummings, Calif., U.S.A., (1982)

10) England,W.A.,Greenhalgh,D.A.,Jenny,S.N.,Milne,J.A., "Coherent Anti-Stokes Raman Spectroscopy of Carbon Monoxide in an Operating Chemical Reactor", ICORS 8 Proceedings, J.Wiley and sons, (1982)

11) Tolles,W.M.,and Harvey,A.B., "Introduction to non-linear phenomena", (1985)

12) Taran,J.P.E.,Regnier,P.E., "On the possibility of Measuring Gas Phase Concentrations by Stimulated Anti-Stokes Scattering", Appl.Phys.Lett., (1973), vol. 23

13) Druet,S.,and Taran,J.P.E., "Chemical and Biological Applications of Lasers", (C.B.Moore,Ed.), Academic Press, (1979)

14) Nibler,J.W. and Knighten,G.V., "Coherent Anti-Stokes Raman Spectroscopy", Chapter 7 in Weber,A.,Ed.,Topics in Current Physics, Springer-Verlag, Stuttgart,(1979)

15) Hall,R.J. and Eckbreth,A.C., "Laser Applications", Eds. J.F.Ready and R.K.Erf, Academic Press, Ch.5,(1984)

16) Vannice,M.A., "The Catalytic Synthesis of Hydrocarbons from $H_2$/CO Mixtures over the Group VIII Metals", Journal of Catalysis, Vol.37, 462-473, (1974)

17) Klose,J. and Baerns,M., "Kinetics of the Methanation of Carbon Monoxide on an Alumina-Supported Nickel Catalyst", Journal of Catalysis, vol.85, 105-116,(1984)

18) Vannice,M.A., "The Catalytic Synthesis of Hydrocarbons from $H_2$/CO Mixtures over the Group VIII Metals", Journal of Catalysis, vol.44, 152-162, (1976)

19) Dalmon,J.A. and Martin,G.A., "The Kinetics and Mechanism of Carbon Monoxide Methanation over Silica-Supported Nickel Catalysts", Journal of Catalysis, vol.84,45-54, (1983)

20) Rautavouma,A.O. and van der Baan,H.S., "Some Observations on the Kinetics of the Hydrogenation of Carbon Monoxide", Journal of Catalysis, vol.71,423-425, (1981)

21) Huang,Y.J.,and Schwarz,J.A.,Applied Catalysis,32,(1987),59-70

22) Huang,Y.J.,Barret,B.T.,and Schwarz,J.A.,Applied Catalysis, 30, (1986), p.241

23) Huang,Y.J., and Schwarz,J.A., Applied Catalysis, 30, (1987), 239

24) Eischens,R.P.,Pliskin,W.A. and Francis,S.A., J.Chem. Phys.,vol.22, 1786, (1954)

25) Eischens,R.P.,Pliskin,W.A. and Francis,S.A., J.Chem. Phys.,vol.60, 194, (1956)

26) Eischens,R.P., Advan. Catal., vol.10, (1958)

27) Yates,J.T. and Garland,C.W., J.Phys.Chem.,vol.65, 617, (1961)

28) Garland,C.W.,Lord,R.C.,Troivano,P.F.,J.Phys.Chem., vol.69, 1188, (1961)

29) Eischens,R.P., "The Surface Chemistry of Metals and Semiconductors", (H.C.Gatos, Ed.), Wiley, New York, (1960)

30) Blyholder,G., J.Phys.Chem., vol.68, 2772, (1964)

31) Van Hardewell,F. and Hartog,F., "4th International Congress on Catalysis", Paper No. 70,(1968)

32) Koelbel,H.,Schoettle,E. and Hammer,H., Z.Phys.Chem. (Frankfurt),vol.46,88, (1965)

33) Koelbel,H.,Mueller,K.H., Z.Electrochem., vol.67, 212, (1963)

34) Blyholder,G. and Neff,L.D., J.Phys.Chem., vol.66, 1464, (1962)

35) Blyholder,G. and Neff,L.D., Journal of Catalysis, vol.2, 138, (1963)

36) (a) Heal,M.J.,Ph.D. Thesis, University of Cape Town, South Africa,(1976),(b) Heal,M.J.,Leisegang,E.C. and Torrington,R.G., Journal of Catalysis, vol.51, (1978)

37) Lynds,L., "Spectrochim.Acta.", vol.20., 1369, (1964)

38) Dalla Betta,R.A., J.Phys.Chem., vol.79, 2519, (1975)

39) Gonzalez,R.D. and Brown, M.F., J.Phys.Chem., vol.80, 1731, (1976)

40) Kobayashi,M. and Shirasaki,T., J.Catal., vol.28, 289, (1973); vol.32, 254, (1974)

41) Araki,M. and Ponec,V., Journal of Catalysis, vol.44, 439, (1976)

42) Rabo,J.A.,Risch,A.P. and Poutsma,M.L., Journal of Catalysis, vol.53, 295, (1978)

43) Low,G. and Bell,A.T., Journal of Catalysis, vol.57, 397, (1979)

44) Biljoen,P.,Helle,J.N. and Sachtler,W.M.H., Journal of Catalysis, vol.58, 95, (1979)

45) Zagli,A.E.,Falconer,J.L. and Keenan,C.A., Journal of Catalysis, vol.56, 453, (1979)

46) Dalla Betta,R.A. and Shelef,M., Journal of Catalysis, vol.49, 383, (1977)

47) McKee,D.W., Journal of Catalysis, vol.8, 240-249, (1967)

48) Vannice,M.A., Journal of Catalysis, vol.37, 449, (1975)

49) Dalla Betta,R.A.,Piken,A.G. and Shelef,M., Journal of Catalysis, vol.35, 54, (1974)

50) Fischer,F.,Tropsch,H. and Dilthey,P., Brennst. Chem., vol.6, 265, (1925)

51) Smith,J.M. and Van Ness,H.C., "Introduction to Chemical Engineering Thermodynamics", McGraw-Hill, Singapore, (1975)

52) Joyner,R.N., and Roberts,M.W., J.Chem. Soc.Faraday Trans., 70 1819, (1974)

53) Kellner,C.S., and Bell,A.T., Journal of Catalysis, 71, p.296, (1981)

54) Agrawal,P.K., Katzer,J.R., and Manogue,W., Ind.Eng.Chem.Fundam. 21,p.385,(1982)

55) Bhatia,S., Bakhshi,N.N., and Matthews,J.F., Can.J.Chem.Eng., 59, p.492,(1981)

56) Vannice,M.A., Catal. Rev.,14(2),p.153, (1976)

57) Elliot,D.J., and Lunsford,J.H., Journal of Catalysis, 57, 11, (1979)

58) Anderson,R.B., Catalysis vol.IV,(Emmet,P.),New York,Reinhold,1976

59) Saletore,D.A., and Thornson,W.J., Ind.Eng.Chem.Process Des.Dev., 16(1), 70, (1977)

60) Pannell,R.B.,Kibby,C.L., and Kobylinski,T.P., Proc.Int.Congr. Catal, 7th, (1980) (Ed. T.Seiyama and K.Tanabe) p.447, Elsevier, Amsterdam, (1981)

61) Sughrue,E.L., and Bartholomew,C.H., Applied Catalysis, 2, p.239, (1982)

## APPENDIX 1

Derivation of the kinetic rate equation to describe the methanation reaction.

The formation of methane can be described by a reaction sequence as shown below :

* = vacant site on the catalyst surface

$$CO_{(g)} + * \rightleftharpoons CO_{(ads)} \qquad (i)$$
$$CO_{(ads)} + * \rightleftharpoons C_{(ads)} + O_{(ads)} \qquad (ii)$$
$$H_{2\,(g)} + 2* \rightleftharpoons 2H_{(ads)} \qquad (iii)$$
$$C_{(ads)} + yH_{(ads)} \rightleftharpoons CH_{y\,(ads)} + y* \qquad (iv)$$
$$CH_y + (4-y)H_{(ads)} \rightleftharpoons CH_{4\,(g)} + (5-y)* \qquad (v)$$
$$O_{(ads)} + 2H_{(ads)} \rightleftharpoons H_2O_{(g)} + 3* \qquad (vi)$$

Equation (iv) is the slow step and hence is the rate determining step (RDS)

Using the RDS, the rate may be written as :

$$-r_{co} = k_{CHy}\, \theta_c\, \theta_H^y \qquad \text{.....(A)}$$

Combining equations (i) and (ii) :

$$CO_{(g)} + * \rightleftharpoons CO_{(ads)}$$
$$CO_{(ads)} + * \rightleftharpoons C_{(ads)} + O_{(ads)}$$

$$CO_{(g)} + 2* \rightleftharpoons C_{(ads)} + O_{(ads)} \qquad \text{.....(B)}$$

Equation (B) represents the surface reaction and hence the rate may be written as :

$$-r_{a,co} = k_{a,co} \left( p_{co}\theta_v^2 - \frac{\theta_c \theta_o}{K_{co}} \right)$$

At equilibrium, $r_{a,co} \rightarrow 0$

Hence : $$K_{co} = \frac{\theta_c \, \theta_o}{p_{co}\theta_v^2}$$

$$\theta_c = \frac{K_{co} p_{co} \theta_v^2}{\theta_o} \qquad \ldots\ldots\ldots(C)$$

From (iii) $$r_{a,H} = k_{a,H} \left( p_{H2} \, \theta_v^2 - \frac{\theta_H^2}{K_{H2}} \right)$$

At equilibrium, $r_{a,H} \rightarrow 0$

Hence : $$K_{H2} = \frac{\theta_H^2}{p_{H2}\theta_v^2}$$

$$\theta_H = (K_{H2} \, p_{H2} \, \theta_v)^{1/2} \qquad \ldots\ldots\ldots(D)$$

Substituting equations (C) and (D) into equation (A) :

$$-r_{co} = k_{CHy} \left( \frac{K_{co} \, p_{co} \, \theta_v^2}{\theta_o} \right) (K_{H2} \, p_{H2} \, \theta_v^2)^{y/2}$$

Rearranging gives :

$$-r_{co} = k_{CHy} \, K_{co} \, K_{H2} \, p_{co} \, p^{y/2} \, \frac{1}{\theta_o} \, \theta^{y+2} \qquad \ldots\ldots(E)$$

If the formation of ethane is neglected : $-r_{co} = r_{H2O} = r_{CH4}$
(confirmed by gas chromatograph analysis of product streams)

Then : $\theta_o = \frac{k_{CHy}}{k_{H2O}} \theta_c$

Substituting into equation (C) :

$$\theta_o = \frac{k_{CHy}^{1/2} K_{co}^{1/2} p_{co}^{1/2} \theta_v}{K_{H2O}} \qquad \text{.....(F)}$$

Substituting equation (F) into equation (E) and rearranging :

$$-r_{co} = k_{CHy}^{1/2} K_{co}^{1/2} K_{H2}\ k_{H2O}^{1/2} p_{co}^{1/2} p_{H2}^{y/2} \theta^{y+1} \qquad \text{....(G)}$$

Now $\theta_v + \theta_c + \theta_H = 1$ .....(H)

Substituting equations (C) and (D) into equation (H) :

$$\theta_v = 1/(1 + K_{co}^{1/2} k_{H2O}^{1/2} k_{CHy}^{-1/2} p_{co}^{1/2} + K_{H2}^{1/2} p_{H2}^{1/2}) \qquad \text{...(I)}$$

Substituting equation (I) into equation (G)

$$-r_{co} = \frac{k_{CHy}^{1/2} K_{co}^{1/2} K_{H2}^{1/2} k_{H2O}^{1/2} p_{co}^{-y/2} p_{H2}^{y/2}}{(1 + K_{co}^{1/2} k_{H2O}^{1/2} k_{CHy}^{-1/2} p_{co}^{1/2} + K_{H2}^{1/2} p_{H2}^{1/2})^{y+1}}$$

The above equation may be simplified by combining constants as follows :

$$-r_{co} = \frac{K' p_{co}^{-y/2} p_{H2}^{y/2}}{(1 + K'' p_{co} + K''' p_{H2})^{y+1}}$$

where $K' = k_{CHy}^{1/2} K_{co}^{1/2} K_{H2}\ k_{H2O}^{1/2}$

$K'' = K_{co}^{1/2} k_{H2O}^{1/2} k_{CHy}^{-y/2}$

$K''' = K_{H2}^{1/2}$

## APPENDIX 2

Quantitative preparation of Nickel on alumina to give a 7% loading using an incipient wetness technique.

Reagents i) $Ni(NO_3)_2 6H_2O$ Molar mass : 290.811 g

ii) $Al_2O_3$ Molar mass : 101.961 g

percentage of Ni by mass in $Ni(NO_3)_2 6H_2O$ = $\frac{58.710}{290.811}$

= 20.188 %

For a 7% loading : $\frac{\text{mass Ni}}{\text{mass Ni}/Al_2O_3} = 0.07$

Therefore 10 g $Al_2O_3$ requires $x/(x+10) = 0.07$ grams of Ni

solving gives $x = 0.753$g Ni

Therefore (0.753/.20188) = 3.728g of $Ni(NO_3)_2 6H_2O$

Calculation of the loading

0.1447 g per 250 $cm^3$ of $Ni/Al_2O_3$ was diluted ten fold to give 0.01447 g in 250 $cm^3$ of distilled water and HF acid.

AA reading : 4.068ppm = 0.00406g/l

Loading:

| | | |
|---|---|---|
| 0.018 g | 1 l | 250 $cm^3$ |
| l | 4*250 $cm^3$ | 0.01447 g |

= 7.03% loading

## APPENDIX 3

Quantitative breakdown of the preparation of Nickel on Zeolite-Y together with a calculation of the actual loading.

Reagents used i) $Ni(NO_3)_2 6H_2O$ Molar mass : 290.811 g
ii) Sodium Zeolite-Y (13 % $Na_2O$ by mass)

The catalyst was prepared by an ion exchange of the Sodium ions withthe Nickel ions.A three fold excess of Nickel nitrate was added based on a 100% exchange of sodium ions.

Molar mass of $Na_2O$ : 61.97 g
Basis : 3 grams of sodium Zeolite-Y

In 3 g of Zeolite-Y, mass of $Na_2O$ = 0.39 g
Moles of $Na_2O$ : 0.39/61.97 = 0.006293 moles

For a one to one exchange rate of sodium oxide with Nickel, mass of Nickel nitrate hexa-hydrate required was :

0.006293 * 290.811 = 1.830 g Ni

For a three fold excess, mass of $Ni(NO_3)_2 6H_2O$ required was :

3 * 1.830 = 5.49 g

Thus 3 g of Zeolite-Y was added to 5.49 g of $Ni(NO_3)_2 6H_2O$

## Calculation of the actual loading

In order to check the loading obtained by ion exchange, the concentration of $Na^+$ ions in solution was calculated.

Basis : 100% exchange rate of $Na_2O$ with Ni ions
moles of $Na_2O$ : 0.006293 moles
moles of $Na^+$ ions : 2*0.006293 = 0.01259 moles
volume of solution : 100 ml
concentration : 0.1259 mol/litre of $Na^+$
= 2.895 g/litre of $Na^+$

AA reading : 192 ppm $Na^+$ ions
= 0.192 g/litre of $Na^+$ ions

Loading by ion exchange : 0.192/2.895 = 6.63%

Loading of Ni/Zeolite-Y :

mass of catalyst in 250 $cm^3$ : 0.04068 g

AA reading : 11.4ppm
= 0.01142 g/litre
= 0.00286 g/250 $cm^3$

loading : 0.00286/0.04068 = 7.02%

Loading by impregnation technique : 7.02 - 6.63 = 0.39%

## APPENDIX 4

Quantitative breakdown of the reagents used to prepare nickel on ZSM-5.

Reagents (i) $Ni(NO_3)_2 6H_2O$ Molar mass : 290.811 g

(ii) ZSM-5 (1% by mass of $NH_4$ ions)

Mass of reagents used :

(a) 1 M $Ni(NO_3)_2 6H_2O$ dissolved in 50 $cm^3$ of distilled water
= 0.05 * 290.811 g
= 14.54 g of $Ni(NO_3)_2 6H_2O$

(b) 3 g ZSM-5

**Calculation of the actual loading**

mass of Ni/ZSM-5 in 250 $cm^3$ : 0.1595 g
AA reading : 3.36ppm = 0.00336g/litre
= 0.00084g/250 $cm^3$

Loading : 0.00084/0.1595 = 0.527%

## APPENDIX 5

Quantitative preparation of nickel on silica-alumina to give an 11% loading using an incipient wetness technique.

Reagents used : i) $Ni(NO_3)_2 6H_2O$ Molar mass : 290.811g
ii) $SiO_2$-$Al_2O_3$ Molar mass : 162.046g

% of Ni by mass in $Ni(NO_3)_2 6H_2O$ = 58.71/290.811 = 20.188%

For a 7% loading : $\frac{\text{Mass Ni}}{\text{Mass Ni and } SiO_2.Al_2O_3} = 0.11$

Therefore 10g SiO2/Al2O3 requires $x/x+10 = 0.11$g Ni

$x = 1.235$g Ni

$= \frac{1.235}{0.20188}$

$= 6.1175$g $Ni(NO_3)_2 6H_2O$

**Calculation of the loading**

0.1524g per 250 $cm^3$ of Ni - $SiO_2/Al_2O_3$ was diluted ten fold to give 0.01524g in 250 $cm^3$ of distilled water and HF acid.

AA Reading : 6.81 = 0.006811 g/l

Loading : $\frac{0.006811 \text{ g} \quad 1l \quad 250cm^3}{1 \quad 4*250cm^3 \quad 0.01524g}$ = 11.17%

## APPENDIX 6

Quantitative preparation of cobalt on silica-alumina to give a 7% loading using a standard incipient wetness technique.

Reagents used : i) $Co(NO_3)_2 6H_2O$ Molar mass : 291.034g
ii) $SiO_2 \cdot Al_2O_3$ Molar mass : 162.046g

% by mass of Co in $Co(NO_3)_2 6H_2O$ = 58.933/291.034 = 20.25%

**Basis** : 5g of $Co(NO_3)_2 6H_2O$
For a 7% loading : 1.01247g = 0.07(x)
x = 14.4639g

Thus Co + $SiO_2 \cdot Al_2O_3$ - $Co/SiO_2 \cdot Al_2O_3$
1.01247g + x - 14.4639g catalyst
x = 13.45147g $SiO_2 \cdot Al_2O_3$

Thus 5g $Co(NO_3)_2 6H_2O$ requires 13.45147g $SiO_2 \cdot Al_2O_3$

**Calculation of the loading :**

0.1603g per 250 $cm^3$ of $Co(NO_3)_2 6H_2O$ was diluted to give 0.01603g per 250 $cm^3$.

AA Reading : 4.51 = 0.00451 g/l

| | | |
|---|---|---|
| 0.00451 g | 1l | 250$cm^3$ |
| 1 | 4*250$cm^3$ | 0.01603g |

= 0.0704

Loading $Co/SiO_2 \cdot Al_2O_3$ = 7.04%

## APPENDIX 7

Quantitative preparation of cobalt on alumina to give a 7% loading using a standard incipient wetness technique.

Reagents used :(i) $Co(NO_3)_2 6H_2O$ Molar mass : 291.034g
(ii) $Al_2O_3$ Molar mass : 101.961g

% by mass of Co in $Co(NO_3)_2 6H_2O$ = 58.933/291.034 = 20.25%

**Basis** : 5g of $Co(NO_3)_2 6H_2O$
For a 7% loading : 1.01247g = 0.07(x)
x = 14.4639g

Thus Co + $Al_2O_3$ - $Co/Al_2O_3$
1.01247g + x - 14.4639g catalyst
x = 13.45147g $Al_2O_3$

Thus 5g $Co(NO_3)_2 6H_2O$ requires 13.45147g $Al_2O_3$

**Calculation of the loading :**

0.2053g per 250 $cm^3$ of $Co(NO_3)_2 6H_2O$ was diluted to give 0.02053g per 250 $cm^3$.

AA Reading : 5.69 = 0.00569 g/l

| | | |
|---|---|---|
| 0.00569 g | 1l | 250$cm^3$ |
| 1 | 4*250$cm^3$ | 0.02053g |

= 0.0693

Loading $Co/Al_2O_3$ = 6.93%

## APPENDIX 8

Quantitative preparation of cobalt on silica-alumina to give a 0.5% loading using a standard incipient wetness technique.

Reagents used :(i) $Co(NO_3)_2 6H_2O$ Molar mass : 291.034g
(ii) $SiO_2 \cdot Al_2O_3$ Molar mass : 162.046g

% by mass of Co in $Co(NO_3)_2 6H_2O$ = 58.933/291.034 = 20.25%

**Basis** : 5g of $Co(NO_3)_2 6H_2O$
For a 0.5% loading : 1.01247g = 0.005(x)
x = 202.494g

Thus Co + $SiO_2 \cdot Al_2O_3$ - $Co/SiO_2 \cdot Al_2O_3$
1.01247g + x - 202.494g catalyst
x = 201.481g $SiO_2 \cdot Al_2O_3$

Thus 5g $Co(NO_3)_2 6H_2O$ requires 201.481g $SiO_2 \cdot Al_2O_3$

**Calculation of the loading :**

Mass of $Co/SiO_2 \cdot Al_2O_3$ in 250 $cm^3$ : 0.142g

AA Reading : 2.9 = 0.0029 g/l

| | | |
|---|---|---|
| 0.00290 g | 1l | 250$cm^3$ |
| 1 | 4*250$cm^3$ | 0.1420g |

= 0.00511

Loading $Co/SiO_2 \cdot Al_2O_3$ = 0.511%

## APPENDIX 9

7% Co on Zeolite-Y : Quantities of reagents used.

Reagents used : i) $Co(NO_3)_2 6H_2O$ Molar mass : 291.034g
ii) Sodium Zeolite-Y (13% $Na_2O$ by mass)

Molar mass of $Na_2O$ : 61.97g
**Basis** : 3 grams of Na/Zeolite-Y

In 3g of ZY, mass of $Na_2O$ = 0.39g
moles of $Na_2O$ : 0.39/61.97 = 0.006293 moles

Hence, from a one-to-one exchange of $Na_2O$ with cobalt, the mass of cobalt required was :

0.006293 * 58.933 = 0.3707g Co

% Co in $Co(NO_3)_2 6H_2O$ = 20.25%
Hence mass of $Co(NO_3)_2 6H_2O$ required = 0.3707/0.2025
= 1.8306g $Co(NO_3)_2 6H_2O$

A three-fold excess of $Co(NO_3)_2 6H_2O$ was used. Thus,
3g of Na/Zeolite-Y was added to 5.492g of $Co(NO_3)_2 6H_2O$

**Calculation of the actual loading :**

In order to check the loading obtained by ion exchange, the concentration of $Na^+$ ions in solution was calculated.

**Basis** : 100% exchange of $Na_2O$ with Co ions
Moles $Na^+$ ions : 2 * 0.006293 moles = 0.01259 moles
Volume of solution : 100ml
Concentration : 0.1029 mol/litre of $Na^+$ ions
= 2.366 g/l of $Na^+$ ions

AA Reading : 164 ppm $Na^+$ ions

Loading by ion exchange : 0.164/2.366 = 6.93%

**Loading of Co/Zeolite-Y :**

Mass of catalyst in 250 $cm^3$ : 0.01292g

AA Reading : 3.66 ppm
= 0.00366 g/l
= 0.000916 g/250 $cm^3$

Loading : 0.000916/0.01292 = 0.0709
= 7.09%

Loading by impregnation : 7.09% - 6.93%
= 0.16%

## APPENDIX 10

Ruthenium on alumina(7%).Calculation of the amounts of reagents used and confirmation of the metal loading.

Reagents used : i) $Ru_3(CO)_{12}$ Molar mass : 639.330g
ii) $Al_2O_3$ Molar mass : 101.961g

% of Ru by mass in $Ru_3(CO)_{12}$ : 303.21/639.33 = 47.43%

**Basis** : 2g of $Ru_3(CO)_{12}$

For a loading of 7% Ru : 0.9485g = 0.07(x)

$x = 13.55g$

$$Ru + Al_2O_3 = Ru/Al_2O_3$$
$$0.9485g + Y = 13.55g \text{ catalyst}$$
$$Y = 12.6015g\ Al_2O_3$$

Thus : 2g of $Ru_3(CO)_{12}$ requires 12.6015g $Al_2O_3$

**Calculation of the loading :**

0.114g of catalyst in 250 $cm^3$
AA Reading : 31.6 ppm = 0.0316 g/l

Catalyst metal loading = 6.94%

## APPENDIX 11

Ruthenium on silica-alumina(7%).Calculation of the amounts of reagents used and confirmation of the metal loading.

Reagents used : i) $Ru_3(CO)_{12}$ Molar mass : 639.330g
ii) $SiO_2 \cdot Al_2O_3$ Molar mass : 162.046g

% of Ru by mass in $Ru_3(CO)_{12}$ : 303.21/639.33 = 47.43%

**Basis** : 2g of $Ru_3(CO)_{12}$

For a loading of 7% Ru : 0.9485g = 0.07(x)

$x = 13.55g$

$$Ru + SiO_2 \cdot Al_2O_3 = Ru/SiO_2 \cdot Al_2O_3$$
$$0.9485g + Y = 13.55g \text{ catalyst}$$
$$Y = 12.6015g\ SiO_2 \cdot Al_2O_3$$

Thus : 2g of $Ru_3(CO)_{12}$ requires 12.6015g $SiO_2 \cdot Al_2O_3$

**Calculation of the loading :**

0.109g of catalyst in 250 $cm^3$
AA Reading : 31 ppm = 0.031 g/l

Catalyst metal loading = 7.12%

## APPENDIX 12

Ruthenium on Zeolite-Y.Calculation of the amounts of reagents used and confirmation of the metal loading.

Reagents used :

(i) $(Ru_3(NH_3)_4(H2O)_2)Cl_3$ Molar mass : 639.330g

(ii) Na-Zeolite-Y (13% $Na_2O$ by mass)

The catalyst was prepared by an ion exchange of $Na^+$ ions with the $Ru^{3+}$ ions. A 2.5-fold excess of $(Ru_3(NH_3)_4(H2O)_2)Cl_3$ was added, based on 100% exchange of $Na^+$ ions.

**Basis** : 2g of sodium Zeolite-Y

Molar mass of $Na_2O$ : 61.97g

Moles of $Na_2O$ present in 2g : $0.26/61.97 = 4.1956*10^{-3}$

$= 2(4.1956*10^{-3})$ moles $Na^+$

$Ru^{3+} = 2/3 * (4.1956*10^{-3}) * 2.5 * 311.581$

$= 2.1787$ g

Thus : 2g of sodium Zeolite-Y requires 2.1787g $(Ru_3(NH_3)_4(H2O)_2)Cl_3$

**Calculation of the loading :**

0.103g of catalyst in 250 $cm^3$

AA Reading : 29.4 ppm = 0.0294 g/l

Catalyst metal loading = 7.14%

## APPENDIX 13

Ruthenium on ZSM-5.Calculation of the amounts of reagents used and confirmation of the metal loading.

Reagents used :

i) $(Ru_3(NH_3)_4(H2O)_2)Cl_3$ Molar mass : 639.330g

ii) $NH_4$-ZSM-5 (1% $NH_4$ by mass)

The catalyst was prepared by an ion exchange of $NH_4^+$ ions with the $Ru^{3+}$ ions. A 4-fold excess of $(Ru_3(NH_3)_4(H2O)_2)Cl_3$ was added based on 100% exchange of $NH_4^+$ ions.

**Basis** : 5g of $NH_4$-ZSM-5

Mass of $NH_4^+$ ions : 0.01 * 5g = 0.05g

Moles of $NH_4^+$ present in 5g : $0.05/18.0383=2.772*10^{-3}$

$Ru^{3+} = 1/3 * (2.772*10^{-3}) * 4.0 * 311.581$

= 1.1516g Complex

Thus : 5g of $NH_4^+$-ZSM-5 requires 1.1516g $(Ru_3(NH_3)_4(H2O)_2)Cl_3$

**Calculation of the loading :**

0.193g of catalyst in 250 $cm^3$

AA Reading : 3.9 ppm = 0.0039 g/l

Catalyst metal loading = 0.511%

## APPENDIX 14

Calculation of the Reynolds number for different flowrates at different temperatures.

diameter of the reactor tube = 0.010 m

cross sectional area of tube = $\pi r^2$

= $\pi(0.5)^2$

= 0.7854 $cm^2$

Conversion of flowrate (ml/min) to velocity (m/s)

| ml | l | 1000 $cm^3$ | | min | m |
|---|---|---|---|---|---|
| min | 1000 ml | l | 0.7854 $cm^3$ | 60 sec | 100 cm |

| Flowrate (ml/min) | Velocity (m/s) |
|---|---|
| 16 | $3.395*10^{-3}$ |
| 52 | $1.1035*10^{-2}$ |

Tabulation of kinematic viscosity ($m^2/s$)

Kinematic viscosity ($*10^{-5}$)

Temperature (K)

| | 400 | 450 | 500 | 550 |
|---|---|---|---|---|
| CO | 2.6021 | 3.1899 | 3.8215 | 4.4945 |
| $H_2$ | 17.723 | 21.573 | 25.683 | 35.012 |

Mole fraction averaged kinematic viscosity :

$$(\text{kin. vis})_{\text{mixture}} = (X_{co})(\text{kin. vis})_{co} + (X_{H2})(\text{kin. vis})_{H2}$$

$$= (.333 * 2.6021 + .667 * 17.723) * 10^{-5}$$

$$= 12.6886 * 10^{-5}\ m^2/s$$

(using the smallest kinematic viscosity values)

**Calculation of Reynolds number**
(using largest velocity)

$$Re = \frac{D\ v}{(kin.vis)}$$

$$= \frac{0.01 * 1.1035*10^{-2}}{12.6886*10^{-5}}$$

$$= 0.8527$$

This is the largest Reynolds number encountered and is well within the laminar regime.

## APPENDIX 15

Derivation of the characteristic plug-flow design equation as used to model the reactor.

From the Navier-Stokes equation of continuity in cylindrical co-ordinates :

$$\frac{\delta C_A}{\delta t} + \frac{V_r \delta C_A}{\delta r} + \frac{V_h \delta C_A}{r\,\delta\theta} + \frac{V_z \delta C_A}{\delta z} = D_{AB}\left\{\frac{1\delta}{r\delta r}\left[\frac{r\delta C_A}{\delta r}\right]\right\} + \frac{1\delta^2 C_A}{r^2\delta\theta^2} + \frac{\delta^2 C_A}{\delta z^2}\Bigg\} - R_A$$

If we plot the concentration profile of carbon monoxide (a) along the length of the reactor, and (b) radially we find :

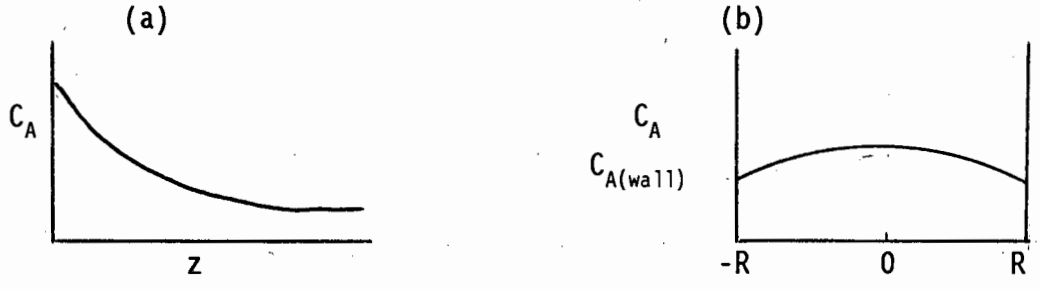


From these plots: it is clear that the following boundary conditions apply :

(i) $\delta C_A/\delta r\big|_{r=0} = 0$ (Radial symmetry about axis)

(ii) $C_A(r,\theta,z)\big|_{z=inlet} = C_{Ao}$ (Inlet concentration)

(iii) $R_A\big|_{volume} = R_A{}^*(R/2)\big|_{surface}$ (Reaction at wall surface)

(See Appendix 41)

Now, if the conversion (x) of carbon monoxide is defined by:

$$x_A = (C_{Ao}-C_A)/C_{Ao}$$

then $$C_A = C_{Ao}-C_{Ao}x_A$$

and differentiating with respect to z,

$$\frac{dC_A}{dz} = -C_{Ao}\frac{dx_A}{dz} \quad .....(A)$$

Now, if and only if the Diffusivity of carbon monoxide in the gas mixture is negligable (as proven in appendix 42), then we may write the Navier-Stokes equation of continuity in cylindrical coordinates as :

$$V_z \frac{dC_A}{dz} = -R_A$$

where the negative molar rate of production signifies the dissapearence of carbon monoxide. Using the relationship (A), above, this becomes :

$$V_z C_{Ao} \frac{dx_A}{dz} = +R_A$$

Now, if 'A' is the cross sectional area (radial) of the reactor, and if $F_{Ao}$ is the molar flowrate of pure CO into the reactor, then this equation becomes :

$$\frac{F_{Ao}}{A} \frac{dx_A}{dz} = R_A$$

Hence,

$$\frac{dx_A}{R_A} = \frac{Adz}{F_{Ao}} \qquad \text{and} \quad (Adz) = dV$$

Thus we arrive at the simple plug-flow design equation :

$$\frac{dV}{F_{Ao}} = \frac{dx_A}{R_A}$$

## APPENDIX 16

**Derivation of the energy balance equation used to model a non-isothermal reactor**

$$\left\{\begin{array}{c}\text{energy in streams}\\ \text{entering volume}\\ \text{element}\end{array}\right\} - \left\{\begin{array}{c}\text{energy in streams}\\ \text{leaving volume}\\ \text{element}\end{array}\right\} + \left\{\begin{array}{c}\text{energy transferred}\\ \text{from surroundings}\\ \text{into vol. element}\end{array}\right\}$$

$$= \left\{\begin{array}{c}\text{accumulation of energy}\\ \\ \text{in volume element}\end{array}\right\}$$

In chemical reactors, the energy exchange with the surroundings is denoted by Q. In a time interval dt, the energy transfer will be dQ. In a flow reactor, the energy in the flowing streams includes kinetic and potential energy contributions in addition to the enthalpy. However, when a reaction occurs, these two contributions are normally insignificant. Thus at steady state, the above equation becomes :

$$H_f - H_e + Q' = 0 \qquad \text{.....(A)}$$

where $H_f$ = rate of enthalpy in (feed stream)
$H_e$ = rate of enthalpy out (exit stream)
$Q'$ = rate of heat transfer

Under non-steady state operation, the accumulation term becomes important :

$$(H_f - H_e)\, dt + dQ = dH \qquad \text{.....(B)}$$

dH = accumulation of energy in volume element in time dt

If $F_t$ is the total molar feed flowrate through the reactor, and $C_p$ is the molar heat capacity of the reaction mixture,

$$dH = F_t C_p dT + H_R(rdV) \qquad .....(C)$$

where rdV = moles of reactant disappearing per unit time in the reactor volume dV

$H_R$ = heat of reaction

The heat transfer can be expressed in terms of an overall heat transfer coefficient, $h_o$, and the surrounding temperature $T_s$ then

$$dQ = h_o (T_s - T)\, dA_h \qquad .....(D)$$

where $dA_h$=effective heat transfer area in the volume element

Since a differential volume element is necessary for a tubular reactor, it is appropriate to write equation (B) as :

$$dQ = dH \qquad .....(E)$$

where the differentials refer to a change over a volume element rather than a time increment. That is, dH is the change in the energy rate between the streams entering and leaving the volume element and dQ is the rate of heat transfer into the differential volume element.

It should be noted that, for non-ideal reactors, axial dispersion contributions to the energy entering and leaving the reactor may be important. As this is most likely to occur in heterogeneous catalytic reactions, for purposes of this experiment, the assumptions of a simple plug flow reactor with no axial mixing and no radial gradients are retained. (Due to the absence of a catalyst bed in the reactor.)

Substituting equations (C) and (D) into equation (E) :

$$h_o (T_s - T)\, dA_h = H_R (r dV) + F_t C_p\, dT \quad ....(F)$$

Using the mass balance for a plug flow reactor :

$$F\, dx = r\, dV \quad .....(G)$$

Substituting equation (G) into equation (F)

$$h_o (T_s - T)\, dA_h = H_R F\, dx + F_t C_p\, dT$$

If z is the length and d is the diameter of the reactor tube, then

$$dA_h = \pi d\, dz$$
$$dV = \pi d^2\, dz$$

Substituting the above into equation (F) and dividing by dz, the energy equation results :

$$\frac{dT}{dz} = \frac{\pi d\, h_o (T_s - T) - H_R\, r\, (\pi d^2/4)}{F_t C_p}$$

```
M                       APPENDIX 17
M
M
M
M
EM ***************************************************************
EM
EM
EM          CALCULATING    :
EM
EM                      1)   ISO- AND NON-ISOTHERMAL REACTOR MODEL
EM
EM                      2)   HEAT REQUIRED TO HEAT ENTERING GAS FROM
EM                           ROOM TEMPERATURE TO THE REACTION TEMP.
REM                           ( PROVIDED BY THE HEATING COIL )
REM
REM                     3)   EVALUATION OF THE EQUILIBRIUM CONSTANT
REM                          AND THE GIBBS FREE ENERGY
REM
REM ***************************************************************
REM
REM
REM
REM DECLARATION OF VARIABLES USED IN PROGRAM
REM
REM XX                   :Coefficient of partial pressure of CO
REM Y                    :Coefficient of partial pressure of H2
REM PRESS                :System pressure
REM FLOWCO               :CO Flowrate
REM FLOWH2               :H2 Flowrate
REM PREX                 :Pre-exponential factor
REM EA                   :Activation energy
REM VOLFLOW             :Volumetric flowrates
REM TRXN                 :Reaction temperature(inherent temp. profile)
REM T                    :Actual reaction temperature
REM TWIRE                :Heating wire temp. profile
REM T50,T200             :Reference temp. profile to yield TWIRE profile
REM LMODEL(I)            :Theoretical length into catalyst
REM CONMOD(I)            :Theoretical conversion
REM LENGTH(I)            :Experimental length
REM CONVER(I)            :Experimental conversion
REM INCREMT(I)           :Length counter
REM GAP                  :0.2 cm. Incremental length
REM LE                   :Length counter
REM R1,R2                :Storage values for nass/energy balances
REM K0-K3,M0-M3          :Runge-kutta variables
REM XPOINT,YPOINT        :Graphics co-ordinates for exptl. points
REM XPT(I)<YPT(I)        :Graphics co-ordinates for theoretical points
REM ALPHA(I)             )
REM BETA(I)              }Storage variables for temp. coeff. in CP eqns.
REM GAMMA(I)             )
REM HEAT(I)              :Component heat of formation values
REM GIBB(I)              :Component Gibbs free energy
REM HEET                 :Heat of reactio at 298K
REM GIBBS                :Gibbs free energy at 298K
REM K                    :Equilibrium constant (function of T)
REM X                    :Conversion
REM VOLT,AMPS            :Voltage,current
REM LTUBE                :Section of tube with heating wire
REM RXNT                 :Reaction temp.to calc.heat for inlet gases
```

```
REM QCO,QH2          :Heat reqd. by CO and H2
REM Q                :Combined heat
REM RP               :Rate of reaction
REM MASS             :Mass balance soln.
REM ENERGY           :Energy balance soln.
REM K,GRASS,PR,GRP   :Air parameters (func(T)) to calc.heat trans.coeff.
REM
REM
REM
REM
CLS
KEY OFF
DIM CONVER(150),LENGTH(150),CONMOD(150),LMODEL(150),XPT(150),YPT(150)
DIM INCREMT(150),X(150),T(150)
REM
LOCATE 12,7:PRINT "ANALYSIS OF RATE DATA USING C.A.R.S. FOR A METHANATION
ON"
LOCATE 13,22:PRINT "ON SUPPORTED METAL CATALYSTS"
A$=INKEY$:IF A$="" THEN 730
CLS
PRINT "           M A I N    M E N U"
PRINT "           ------------------"
PRINT "           ------------------"
PRINT:PRINT
PRINT "A = calculation of equilibrium constant"
PRINT "B = fitting of a model to conversion-length data"
PRINT "C = heating of feed gas to correct operating temperature"
PRINT "D = end ?"
A$=INKEY$:IF A$="" THEN 830
IF A$="A" OR A$="a" GOTO 3320 ELSE IF A$="B" OR A$="b" GOTO 860 ELSE IF A
R A$="c" GOTO 4050 ELSE IF A$="D" OR A$="d" GOTO 5500
PRINT:PRINT "Incorrect key ! Wait....":FOR I=1 TO 1000:NEXT I:GOTO 740
CLS
REM
REM     ENTERING OF EXPERIMENTAL DATA POINTS
REM
PRINT "Number of conversion vs reactor length data points ? "
INPUT "( press <ENTER> for no points ) ",POINTS
PRINT:PRINT
FOR I=1 TO POINTS
INPUT "Conversion , reactor length  ? ",CONVER(I),LENGTH(I)
NEXT I
SCREEN 0,0,0
NONCOUNT=0
CLS
CCOUNT=0
 COUNT=0
 REM
 REM     OBTAINING RELEVANT PARAMETERS TO SET UP A THEORETICAL MODEL
 REM
 PRINT "Fitting a rate equation to a simple plug flow model for a homogen
action"
 LOCATE 4,18:PRINT "Simple power law given by :"
 LOCATE 6,20:PRINT "         -E"
 LOCATE 7,20:PRINT "         --   "
 LOCATE 8,20:PRINT "         RT     X     Y"
 LOCATE 9,20:PRINT "r   =  e     p      p"
 LOCATE 10,20:PRINT " CH           CO     H"
 LOCATE 11,20:PRINT "   4                   2"
 LOCATE 15,1:INPUT "Value of X ? ( -1 < X < .5 ) ",XX
```

```
INPUT "Value of Y ? ( approximately 1 ) ",Y
INPUT "Total pressure ( atm ) ? ",PRESS
INPUT "Flow rate of pure CO ( ml/min ) ? ",FLOWCO
INPUT "Flow rate of pure H2 ( ml/min ) ? ",FLOWH2
INPUT "Pre-exponential factor value ? ",PREX
INPUT "Activation energy ( between 7000 and 30000 [cal/mol] ) ? ",EA
INPUT "Temperature at beginning of catalyst ? ( K ) ",TEMP
INPUT "Increment in catalyst length for non-isothermal behaviour (cm) ?
MENT
INPUT "Inlet conversion ? ",VERSION
FOR I =1 TO 10
DOFF(I)=0
NEXT I
CLS:PRINT "Results to be : (P) rinted graphically"
PRINT "                    (T) abulated ? "
ZZ$=INKEY$:IF ZZ$="" THEN 1240
REM
REM
REM    CONVERSION OF ML/MIN TO MOL/SEC
REM
REM
VOLFLOW=FLOWCO/60/1000/22.414
VOLFH2=FLOWH2/60/1000/22.414
PRINT:PRINT
PRINT "A = Isothermal modelling"
PRINT "B = Non-isothermal modelling"
PRINT "C = Comparison of iso- and non-isothermal modelling "
PRINT "D = Return to main menu ?"
J$=INKEY$:IF J$="" THEN 1370
LOCATE 14,38:PRINT "BUSY"
REM CLS
IF J$="A" OR J$="a" GOTO 1430 ELSE IF J$="B" OR J$="b" GOTO 1690 ELSE IF
OR J$="c" GOTO 1430 ELSE IF J$="D" OR J$="d" GOTO 740
PRINT:PRINT"Incorrect key !  Wait....":FOR I=1 TO 1500:NEXT I
CLS:GOTO 1330
Q=0
REM
REM     GENERATING CONVERSION , LENGTH DATA POINTS USING A SIMPLE
REM     PLUG FLOW MODEL AND ASSUMING ISOTHERMAL BEHAVIOUR. IN IS THE
REM     VALUE OBTAINED FROM A NUMERICAL INTEGRATION
REM
JJ=VERSION*30
FOR I=1 TO 29-JJ
Q=Q+1
CONMOD(I)=(JJ+I-1)/30
GOSUB 2780
LMODEL(I)=12732.4*VOLFLOW*PRESS^-.7/PREX*EXP(EA/1.987/TEMP)*IN
IF LMODEL(I)>25 GOTO 1590
IF ZZ$="P" OR ZZ$="p" GOTO 1580
EE=CONMOD(I):LY=LMODEL(I):TT=TEMP:GOSUB 5150
NEXT I
IF ZZ$="P" OR ZZ$="p" GOTO 2180
LOCATE 23,1:PRINT "END OF RESULTS  ---  Hit any key to continue"
CCOUNT=0
SS$=INKEY$:IF SS$="" GOTO 1620
CLS
GOTO 2080
REM
REM
REM       CALCULATING CONVERSION , LENGTH , TEMPERATURE DATA FOR A
REM       SIMPLE PLUG FLOW MODEL BY ASSUMING NON-ISOTHERMAL BEHAVIOUR
```

```
REM       SIMULTANEOUS SOLUTION OF A MASS AND ENERGY BALANCE
REM
REM INCREMENT=1.5
TFEED=TEMP
GAP=INCREMENT
XBEGIN=VERSION
TBEGIN=TFEED:T=TFEED
X=0
Q=0
LE=0
FOR I=1 TO 400
Q=Q+1
GOSUB 4360:R1=ENERGY:KO=GAP*R1
GOSUB 4310:R2=MASS:MO=GAP*R2
T=TBEGIN+KO/2:X=XBEGIN+MO/2
GOSUB 4360:R1=ENERGY:K1=GAP*R1
GOSUB 4310:R2=MASS:M1=GAP*R2
T=TBEGIN+K1/2:X=XBEGIN+M1/2
GOSUB 4360:R1=ENERGY:K2=GAP*R1
GOSUB 4310:R2=MASS:M2=GAP*R2
T=TBEGIN+K2:X=XBEGIN+M2
GOSUB 4360:R1=ENERGY:K3=GAP*R1
GOSUB 4310:R2=MASS:M3=GAP*R2
T=TBEGIN+.16667*(KO+2*K1+2*K2+K3)
X=XBEGIN+.16667*(MO+2*M1+2*M2+M3)
TBEGIN=T:XBEGIN=X:T(I)=T:X(I)=X
INCREMT(I)=INCREMT(I-1)+GAP
CONMOD(I)=X(I):LMODEL(I)=INCREMT(I)
IF ABS(1-X(I))<.04 GOTO 2030
LE=LE+GAP
TRXN=ABS(T-TEMP)+TWIRE
IF ZZ$="P" OR ZZ$="p" GOTO 2020
LY=LE:TT=TRXN:EE=X:GOSUB 5150
NEXT I
REM FOR I = 1 TO POINTS
REM DOFF = ABS(CONVER(I)-CONMOD(I))
REM SUMDIF = DOFF+ DOFF
REM NEXT I
REM PRINT "      SUM OF RESIDUES = ";SUMDIF
FOR I = 2 TO POINTS
FOR J = 1 TO 30
IF LMODEL(J)=LENGTH(I) THEN DOFF(I) = ABS(CONVER(I)-CONMOD(J))
SUMDIF = SUMDIF + DOFF(I)
REM PRINT "LMODEL,CONMOD,J",LMODEL(J),CONMOD(J),J
REM PRINT "LENGTH,CONVER,I",LENGTH(I),CONVER(I),I
NEXT J
NEXT I
PRINT " SUM OF RESIDUES = ",SUMDIF
SUMDIF = 0
A$=INKEY$:IF A$="" THEN 2041
IF ZZ$="P" OR ZZ$="p" GOTO 2160
LOCATE 23,1:PRINT "END OF RESULTS  ---  Hit any key to continue"
SS$=INKEY$:IF SS$="" GOTO 2050
REM IF J$="C" GOTO 2120
REM
REM
REM       SETTING UP OF GRAPH TO PLOT CONVERSION VERSUS LENGTH
REM
REM
IF J$="C" GOTO 2140
```

```
IF J$<>"c" GOTO 960
NONCOUNT=NONCOUNT+1
IF NONCOUNT=2 GOTO 960 ELSE GOTO 1700
REM
IF J$="C" OR J$="c" GOTO 2510
SCREEN 2,0
LINE (100,24)-(625,144),,B
FOR I=1 TO 10
LINE (100,144-I*12)-(105,144-I*12)
LINE (620,144-I*12)-(625,144-I*12)
NEXT I
FOR I=1 TO 15
LINE (100+I*35,141)-(100+I*35,144)
LINE (100+I*35,24)-(100+I*35,27)
NEXT I
PRINT "    EXPERIMENTAL AND THEORETICAL PLOT OF CONVERSION VERSUS REACTO
H"
PRINT "    ------------------------------------------------------------
-"
LOCATE 20:PRINT "            0        2        4        6        8
 12       14"
LOCATE 21:PRINT "                                Length down reactor tube (

LOCATE 7:PRINT "C":PRINT "O":PRINT "N":PRINT "V"
PRINT "E":PRINT "R":PRINT "S":PRINT "I"
PRINT "O":PRINT "N"
LOCATE 19,10:PRINT "0":LOCATE 16,9:PRINT ".2":LOCATE 13,9:PRINT ".4":LOC
9:PRINT ".6":LOCATE 7,9:PRINT ".8":LOCATE 4,10:PRINT "1"
LINE (15,173)-(20,176),,B
LINE (1,181)-(20,181)
LOCATE 22,7:PRINT "experimental point"
LOCATE 23,7:PRINT "theoretical curve fit"
REM
REM
REM    CALCULATING THE COORDINATES OF THE EXPERIMENTAL POINTS
REM
FOR I=1 TO POINTS
XPOINT=LENGTH(I)*35+100
YPOINT=-CONVER(I)*120+144
LINE (XPOINT-3,YPOINT-2)-(XPOINT+2,YPOINT+1),,B
NEXT I
REM
REM
REM     CALCULATING THE COORDINATES OF THE THEORETICAL CONVERSION,
REM     LENGTH DATA POINTS IN ORDER TO PLOT THEM GRAPHICALLY
REM
FOR I=2 TO Q
XPT(I)=LMODEL(I)*35+100
YPT(I)=-CONMOD(I)*120+144
REM PSET (XPT(I),YPT(I))
NEXT I
XPT(1)=LMODEL(1)*35+100:YPT(1)=-CONMOD(1)*120+144
FOR I=2 TO Q
IF XPT(I)>625 GOTO 2650
IF YPT(I)<24 GOTO 2650
LINE (XPT(I),YPT(I))-(XPT(I-1),YPT(I-1))
NEXT I
COUNT=COUNT+1
IF COUNT>1 GOTO 2700
IF J$="C" GOTO 2690
IF J$<>"c" GOTO 2700
```

```
0 LOCATE 23,72:PRINT "BUSY":GOTO 1690
0 LOCATE 23,72:PRINT "    "
0 A$=INKEY$:IF A$="" THEN 2710
0 GOTO 960
0 REM
0 REM
0 REM
0 REM    SUBROUTINE TO PERFORM A NUMERICAL INTEGRATION
0 REM
0 A=VERSION
0 B=CONMOD(I)
0 E=.0001
0 M=(A+B)/2
0 IF M=0 THEN M=8E-08
0 H1=(B-A)/40
0 IF H1<>0 GOTO 2860
0 H1=1E-08
0 GOSUB 3070
0 N=((B-A)^5*D/E/180)^.25
0 N=2*INT(N/2+1)
0 S=0
0 X=A
0 H=(B-A)/N
0 FOR J=1 TO N/2
0 GOSUB 3040
0 S=S+F
0 X=X+H
0 GOSUB 3040
0 S=S+4*F
0 X=X+H
0 GOSUB 3040
0 S=S+F
0 NEXT J
0 IN=S*H/3:RETURN
0 REM  ******  DEFINE USER FUNCTION  *********
0 F=(((1-X)/(4-2*X))^-XX)*((3*(1-X)/(4-2*X))^-Y)
0 RETURN
0 REM *****  EVALUATION OF ERRORS  *******
0 D=0
0 X=M-2*H1
0 GOSUB 3040
0 D=D+F
0 X=M-H1
0 GOSUB 3040
0 D=D-4*F
0 X=M
0 GOSUB 3040
0 D=D+6*F
0 X=M+H1
0 GOSUB 3040
0 D=D-4*F
0 X=M+2*H1
0 GOSUB 3040
0 D=D+F
0 D=ABS(D)/H1^4
0 RETURN
```

```
50 REM
50 REM
70 REM    SECTION CALCULATING THE EQUILIBRIUM CONSTANT FOR THE METHANATION
80 REM    REACTION AT DIFFERENT TEMPERATURES USING Cp DATA WHICH IS A
90 REM    FUNCTION OF THE TEMPERATURE. ONCE THE K VALUE HAS BEEN OBTAINED,
00 REM    A CONVERSION IS CALCULATED USING NEWTONS METHOD
10 REM
20 CLS
30 PRINT "         Calculation of the equilibrium constant K using Cp value
40 LOCATE 4,9:PRINT " Carbon monoxide     Methane          Hydrogen
er"
50 LOCATE 5:PRINT "-------------------------------------------------------
-----------"
60 PRINT:PRINT "alpha":PRINT "beta":PRINT "gama":PRINT "del H":PRINT "del G
70 FOR I=1 TO 6
80 LOCATE 5+I,9:PRINT "|":LOCATE 5+I,25:PRINT "|":LOCATE 5+I,41:PRINT "|":L
 5+I,57:PRINT "|":LOCATE 5+I,73:PRINT "|"
90 NEXT I
00 FOR I=1 TO 4
10 READ ALPHA(I),BETA(I),GAMA(I),HEAT(I),GIBB(I)
20 NEXT I
30 REM    CO DATA
40 REM DATA 6.555,.15046E-02,-.30846E-06,-26416,-32781
50 DATA 6.636,1.4376E-03,-3.2229E-07,-26416,-32781
60 REM    METHANE DATA
70 DATA 3.381,18.044E-03,-4.3E-06,-17889,-12140
80 REM    HYDROGEN DATA
90 REM DATA 6.776,2.0768E-04,3.36499E-07,0,0
00 DATA 6.688,2.7578E-04,3.557E-07,0,0
10 REM    WATER DATA
20 REM DATA 7.3,2.46E-03,0,-57798,-54635
30 DATA 7.3,2.459E-03,0,-57798,-54635
40 FOR I=0 TO 3
50 LOCATE 7,10+17*I-I:PRINT " ";ALPHA(I+1)
60 NEXT I
70 FOR I=0 TO 3
80 LOCATE 8,10+17*I-I:PRINT " ";BETA(I+1)
90 NEXT I
00 FOR I=0 TO 3
10 LOCATE 9,10+17*I-I:PRINT " ";GAMA(I+1)
20 NEXT I
30 FOR I=0 TO 3
40 LOCATE 10,10+17*I-I:PRINT " ";HEAT(I+1)
50 NEXT I
60 FOR I=0 TO 3
70 LOCATE 11,10+17*I-I:PRINT " ";GIBB(I+1)
80 NEXT I
90 DELAL=ALPHA(2)+ALPHA(4)-ALPHA(1)-3*ALPHA(3)
00 DELBE=BETA(2)+BETA(4)-BETA(1)-3*BETA(3)
10 DELGA=GAMA(2)+GAMA(4)-GAMA(1)-3*GAMA(3)
20 HEET=HEAT(2)+HEAT(4)-HEAT(1)-3*HEAT(3)
30 GIBBS=GIBB(2)+GIBB(4)-GIBB(1)-3*GIBB(3)
40 REM LOCATE 12:INPUT "Heat of reaction at 298 K ? ",HEAT
50 REM INPUT "Molar Gibbs free energy at 298 K ?  ",GIBBS
60 H0=HEET-DELAL*298-DELBE/2*298*298-DELGA/3*298*298*298
70 II=H0-DELAL*298*LOG (298)-DELBE/2*298*298-DELGA/6*298*298*298-GIBBS
80 III=II/1.987/298
90 LOCATE 12:PRINT "Ho = ",H0:PRINT "I = ",III
00 PRINT:INPUT "Temperature ( K ) ? ",TE
```

```
3810 K=EXP(-H0/1.987/TE+DELAL/1.987*LOG(TE)+DELBE/1.987/2*TE+DELGA/6/1.987*TE
^II)
3820 REM
3830 REM     NEWTONS METHOD
3840 REM
3850 X=.999
3860 F=X*X*((4-2*X)^2)/27/((1-X)^4)-K
3870 DF=((2*X*((4-2*X)^2)-X*X*4*(4-2*X))*((1-X)^4)+X*X*4*((4-2*X)^2)*((1-X)^3
(1-X)^8)/27
3880 XN=X-F/DF
3890 IF ABS(XN-X)<.0001 GOTO 3930
3900 X=XN
3910 GOTO 3860
3920 REM
3930 PRINT "K = ",K
3940 PRINT "X = ",X
3950 PRINT:PRINT "A = New temperature "
3960 PRINT "B = Return to main menu ?"
3970 A$=INKEY$:IF A$="" THEN 3970
3980 IF A$="A" OR A$="a" GOTO 3800 ELSE GOTO 740
3990 END
4000 REM
4010 REM
4020 REM     CALCULATING IF THE HEAT RELEASED BY THE HEATING WIRE IS SUFFICIEN
4030 REM     TO HEAT THE ENTERING GASES TO THE REACTION TEMPERATURE
4040 REM
4050 CLS
4060 INPUT "Flow rate of Carbon Monoxide ? ( ml/min ) ",FLOWCO
4070 INPUT "Flow rate of Hydrogen ? ( ml/min ) ",FLOWH2
4080 INPUT "Voltage ? ",VOLT
4090 INPUT "Current ? ",AMPS
4100 INPUT "Length of tube containing the heating wire ? ( cm ) ",LTUBE
4110 INPUT "Temperature at which reaction will occur ? ( K ) ",RXNT
4120 VOLCO=FLOWCO*7.43583E-07
4130 VOLH2=FLOWH2*7.43583E-07
4140 T=RXNT
4150 QCO=4.184*VOLCO*(6.636*T+.0014376/2*T*T-3.2229E-07/3*T*T*T-6.636*298-.00
6/2*298*298+3.2229E-07/3*298*298*298)
4160 QH2=4.184*VOLH2*(6.688*T+2.7578E-04/2*T*T+3.557E-07/3*T*T*T-6.688*298-2.
E-04/2*298*298-3.557E-07/3*298*298*298)
4170 Q=QCO+QH2
4180 RESIS=LTUBE/23.4*51.2
4190 P=RESIS*AMPS*AMPS
4200 REM
4210 CLS
4220 PRINT "Power supplied by heating wire = ";P;" watts"
4230 PRINT "Entering gases require ";Q;" watts to reach reaction temperature"
4240 PRINT:PRINT:PRINT "Hit any key to continue"
4250 A$=INKEY$:IF A$="" THEN 4250
4260 GOTO 740
4270 REM
4280 REM
4290 REM       EQUATIONS FOR RUNGE KUTTA
4300 REM
4310 REM     MASS BALANCE
4320 F=(((1-X)/(4-2*X))^XX)*((3*(1-X)/(4-2*X))^Y)
4330 RP=PREX*EXP(-EA/1.987/T)*F
4340 MASS=RP*7.854E-05/(VOLFLOW):RETURN
4350 REM
4360 REM     ENERGY BALANCE
```

```
0 F=(((1-X)/(4-2*X))^XX)*((3*(1-X)/(4-2*X))^Y)
0 RP=PREX*EXP(-EA/1.987/T)*F
0 REM PRINT T
0 REM PRINT "DIST",LE
0 GOSUB 4700:GOSUB 4750:GOSUB 4810:GOSUB 4860:GOSUB 4930:GOSUB 5060:GOSUB

0 REM PRINT "K,PR,GR,VOLT,REST,T200,T50",K,PR,GRP,VOLT,REST,T200,T50
0 POWER=VOLT^2/REST
0 FLUXIN=POWER*.0116789
0 THERMAL=(LOG(17/12))/2/3.1415926#/.24/K
0 DELT=FLUXIN/THERMAL
0 GRASS=GRP*(.012^3)*DELT:RAD=GRASS*PR
0 STORE1=.387*(RAD^(1/6))
0 STORE2=(.559/PR)^(9/16)
0 STORE3=(STORE2+1)^(8/27)
0 NU=(.6+(STORE1/STORE3))^2
0 HO=K*NU/.012
0 TWIRE=T50+(TEMP-323)*(T200-T50)/159
0 REM PRINT T200,T50,TWIRE
0 REM PRINT "TWIRE,T200,T50=",TWIRE,T200,T50
0 REM ENERGY=(.141*(TWIRE-T)+RP*16.18)/4184/7/(VOLFLOW+VOLFH2)
0 ENERGY=(3.1415926#*.012*HO*(TWIRE-T)+RP*16.18)/4184/7/(VOLFLOW+VOLFH2)
0 REM PRINT ENERGY,ENERGY2
0 REM PRINT ENERGY,RP,T
0 RETURN
0 REM
0 REM
0 END
0 REM
0 REM    AIR FILM PARAMETERS TO CALCULATE Ho
0 REM
0 REM
0 REM    K FUNCTION
0 REM
0 K=-2.33E-08*T*T+8.91233E-05*T+.0016083377#
0 RETURN
0 REM
0 REM      Pr FUNCTION
0 REM
0 PR=2.465E-07*T*T-3.21571E-04*T+.7820605
0 RETURN
0 REM
0 REM      Gr FUNCTION
0 REM
0 IF T>440 GOTO 4830
0 GRP=ABS(.513721*T^4-946.44*T^3+631197.85#*T*T-181750335#*T+19225687912#)
0 RETURN
0 GRP=25447625#-27413*T
0 RETURN
0 REM
0 REM      RESISTANCE FUNCTION
0 REM
0 REST=.005974*T+47.59
0 RETURN
0 REM
0 REM      VOLTAGE FUNCTION
0 REM
```

```
0 REM
0 VOLT=.13076506#*T-26.3978981#
0 RETURN
0 REM
0 REM      T200 TEMPERATURE PROFILE
0 REM
0 IF LE>5.5 GOTO 5010
0 T200=-.011655*LE^4+.548718*LE^3-5.797086*LE^2+21.5992*LE+480.577
0 RETURN
0 T200=.64045594#*LE^2-12.678564#*LE+557.02403#
0 RETURN
0 REM
0 REM       T50 TEMPERATURE PROFILE
0 REM
0 IF LE>6 GOTO 5090
0 T50=.0228438*LE^4-.2574981*LE^3+.517366*LE^2+1.701671*LE+324.05303#
0 RETURN
0 T50=.146103*LE^2-2.7446322#*LE+338.25184#
0 RETURN
0 REM
0 REM
0 REM
0 REM     TABULATION SUBROUTINE
0 REM
0 CCOUNT=CCOUNT+1
0 IF CCOUNT=1 GOTO 5240 ELSE GOTO 5400
0 REM   NO. OF LINES PER PAGE  LPP = 12
0 REM QCOUNT=INT(CCOUNT/12)*12
0 REM IF QCOUNT<=12 GOTO 4740
0 LOCATE 23,1:PRINT "Hit any key to continue"
0 SS$=INKEY$:IF SS$="" THEN 5220
0 CLS
0 CLS:NL=0:IF J$="A" OR J$="a" GOTO 5260
0 GOTO 5290
0 LOCATE 1,21:PRINT "ISOTHERMAL ANALYSIS"
0 LOCATE 2,21:PRINT "--------------------"
0 GOTO 5360
0 IF J$="B" OR J$="b" GOTO 5310
0 GOTO 5340
0 LOCATE 1,19:PRINT "NON-ISOTHERMAL ANALYSIS"
0 LOCATE 2,19:PRINT "-----------------------"
2 FOR I =1 TO POINTS
3 DIFF = ABS(CONVER(I)-CONMOD(I))
4 SUMDIF = SUMDIF + DIFF
5 NEXT I
0 GOTO 5360
0 LOCATE 1,2:PRINT "COMBINED ANALYSIS ( ISO- AND NON-ISOTHERMAL BEHAVIOUR
0 LOCATE 2,2:PRINT "-----------------------------------------------------
0 PRINT
0 PRINT "  Length ( cm )       Temperature ( K )         Conversion "
0 PRINT "  -------------       ----------------          ---------- "
0 PRINT:PRINT
0 LOCATE NL+6,6:PRINT USING "###.##";LY
0 LOCATE NL+6,28:PRINT USING "###.##";TT
0 LOCATE NL+6,47:PRINT USING "##.#######";EE
0 NL=NL+1
0 IF NL=15 GOTO 5460
0 GOTO 5490
0 LOCATE 23,1:PRINT "Hit any key to continue"
0 SS$=INKEY$:IF SS$="" THEN 5470
0 CLS:CCOUNT=0
0 RETURN
0 END
```

## APPENDIX 18

Flow sheet of the Basic computer program showing the logic behind the various calculations.

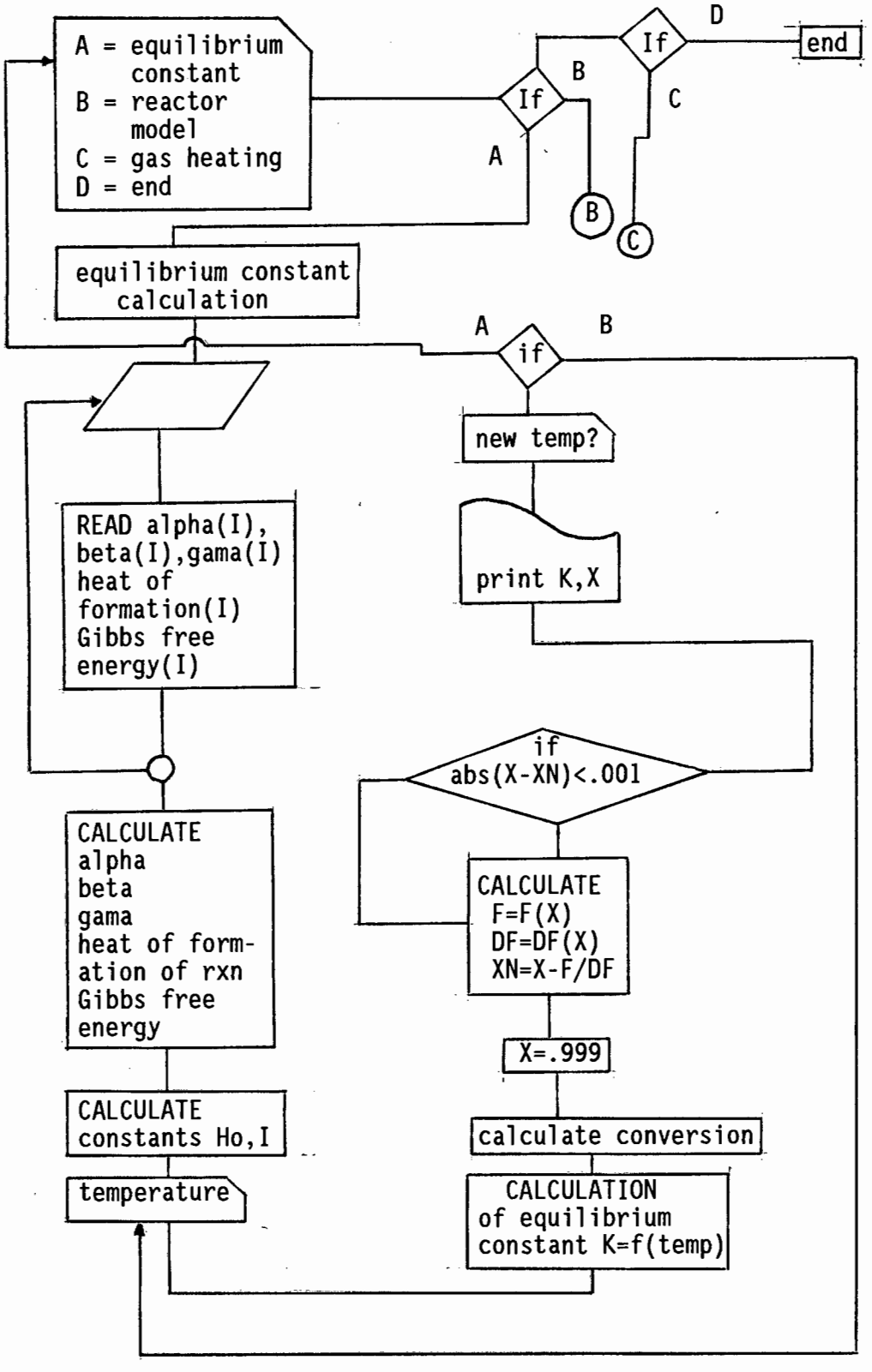

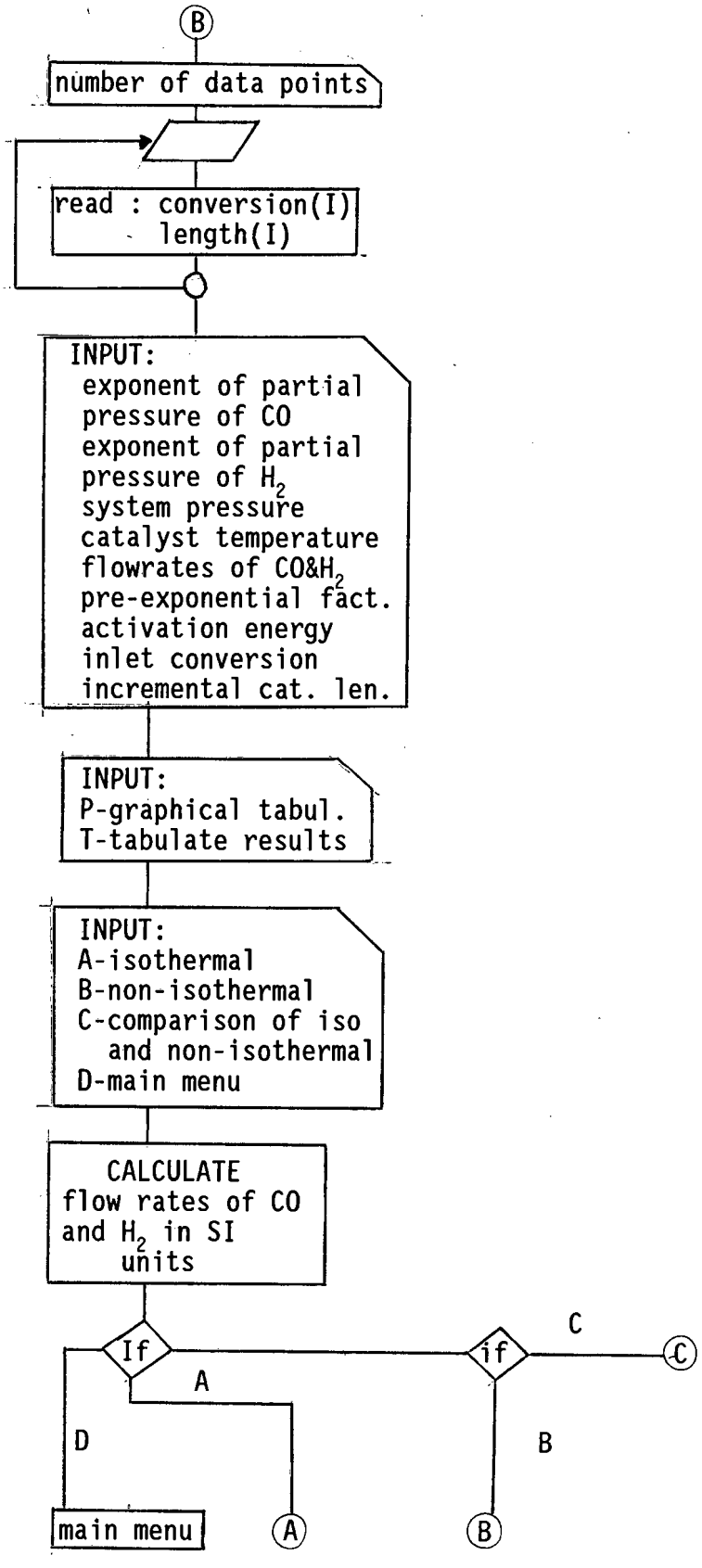
B
number of data points
read : conversion(I)
length(I)
INPUT:
exponent of partial
pressure of CO
exponent of partial
pressure of $H_2$
system pressure
catalyst temperature
flowrates of CO&$H_2$
pre-exponential fact.
activation energy
inlet conversion
incremental cat. len.
INPUT:
P-graphical tabul.
T-tabulate results
INPUT:
A-isothermal
B-non-isothermal
C-comparison of iso
and non-isothermal
D-main menu
CALCULATE
flow rates of CO
and $H_2$ in SI
units
If
A
D
main menu
A
if
C
C
B
B

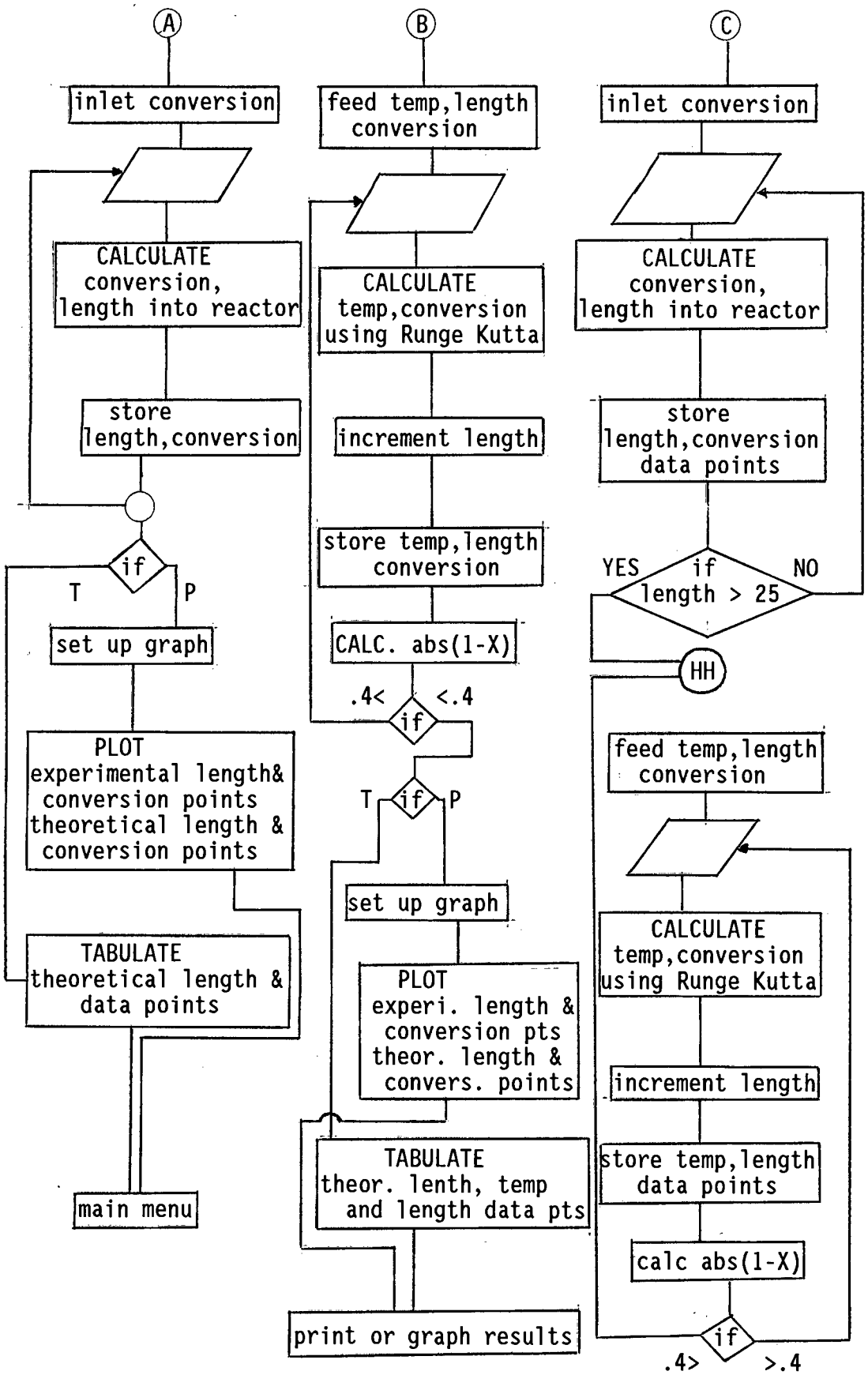
A
inlet conversion
CALCULATE conversion, length into reactor
store length,conversion
if
T
P
set up graph
PLOT experimental length& conversion points theoretical length & conversion points
TABULATE theoretical length & data points
main menu
B
feed temp,length conversion
CALCULATE temp,conversion using Runge Kutta
increment length
store temp,length conversion
CALC. abs(1-X)
.4<
<.4
if
T
if
P
set up graph
PLOT experi. length & conversion pts theor. length & convers. points
TABULATE theor. lenth, temp and length data pts
print or graph results
C
inlet conversion
CALCULATE conversion, length into reactor
store length,conversion data points
YES
if length > 25
NO
HH
feed temp,length conversion
CALCULATE temp,conversion using Runge Kutta
increment length
store temp,length data points
calc abs(1-X)
if
.4>
>.4

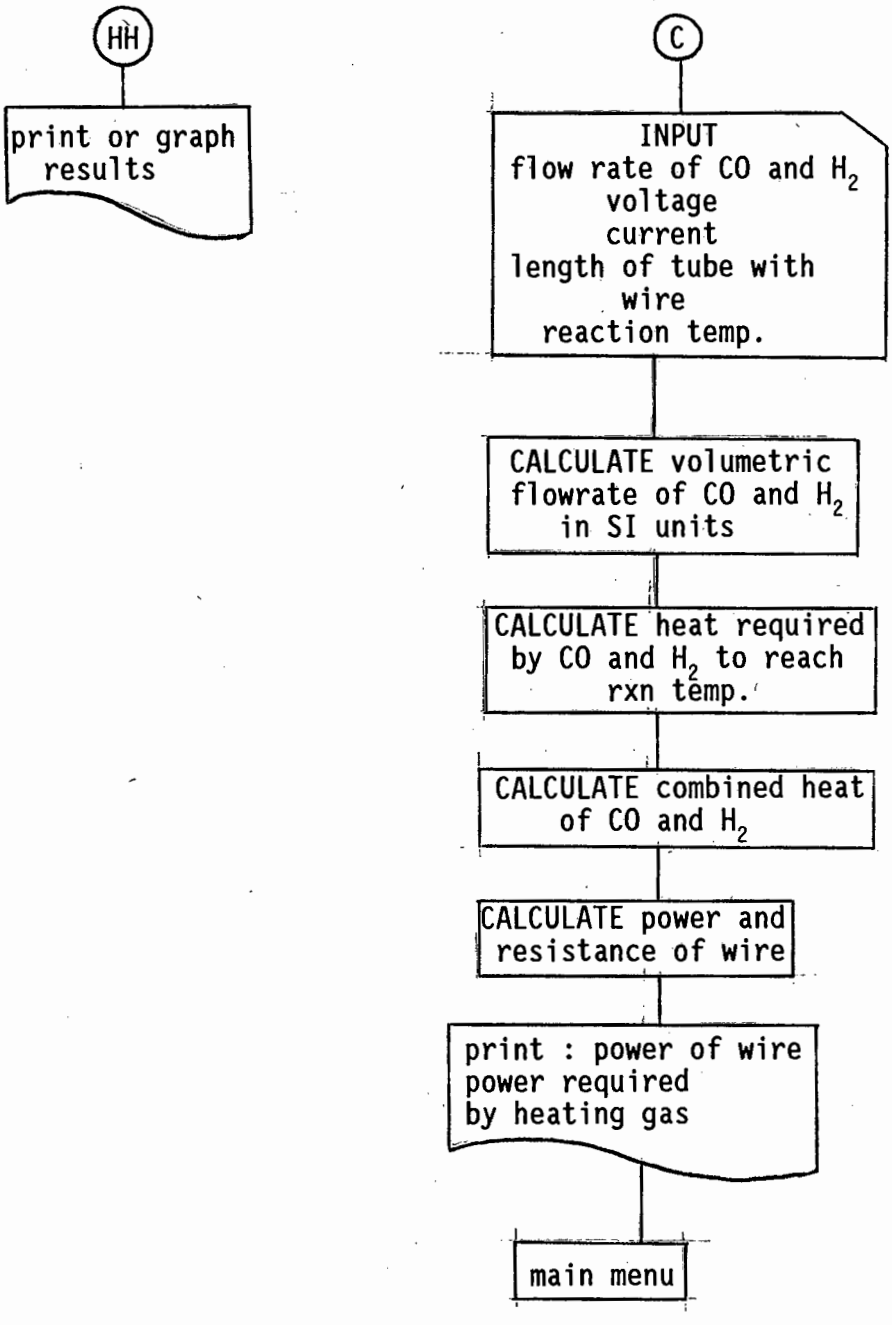
HH
print or graph results
C
INPUT
flow rate of CO and $H_2$
voltage
current
length of tube with wire
reaction temp.
CALCULATE volumetric flowrate of CO and $H_2$ in SI units
CALCULATE heat required by CO and $H_2$ to reach rxn temp.
CALCULATE combined heat of CO and $H_2$
CALCULATE power and resistance of wire
print : power of wire
power required
by heating gas
main menu

**APPENDIX 19**

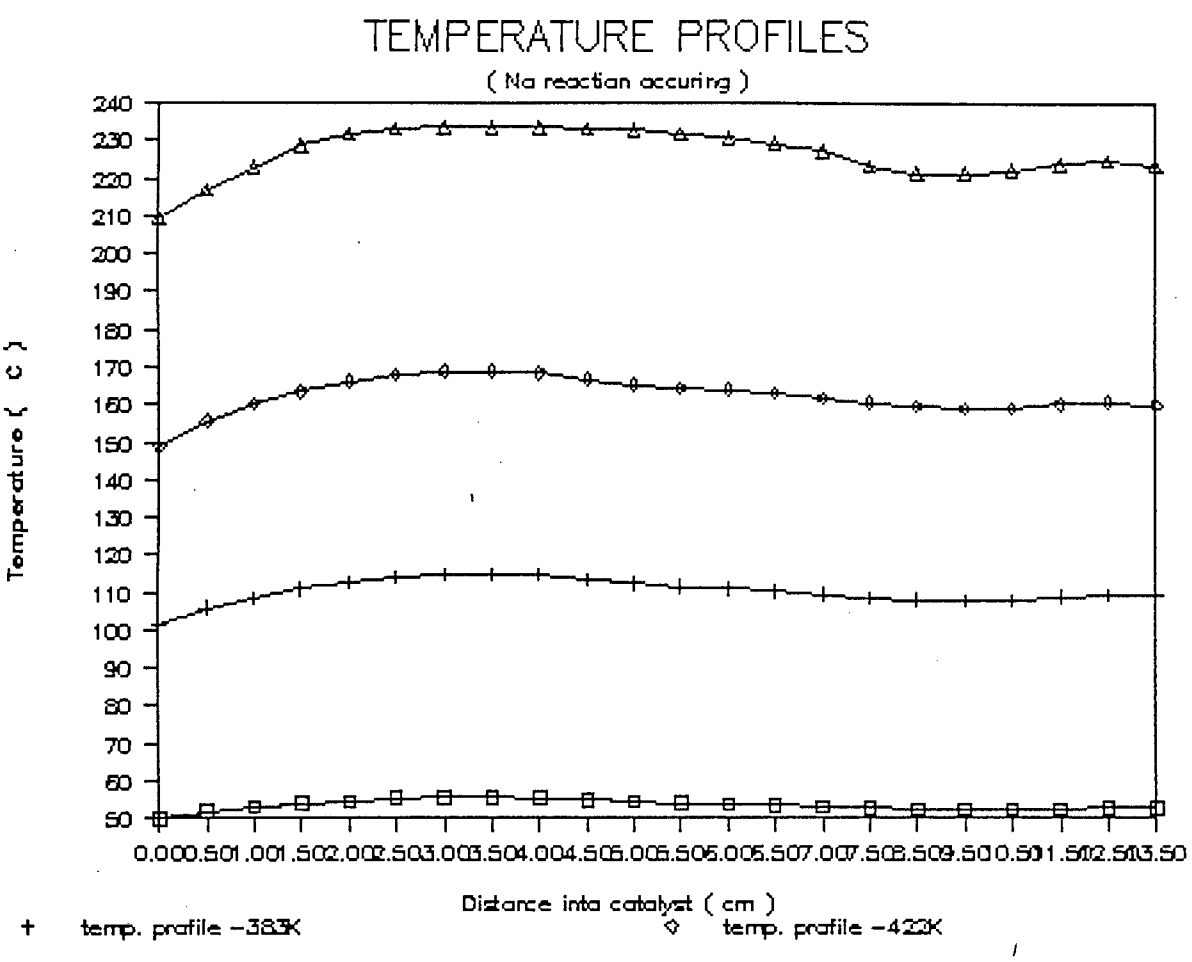
TEMPERATURE PROFILES
( No reaction occuring )
Temperature ( C )
240
230
220
210
200
190
180
170
160
150
140
130
120
110
100
90
80
70
60
50
0.00 0.50 1.00 1.50 2.00 2.50 3.00 3.50 4.00 4.50 5.00 5.50 6.00 6.50 7.00 7.50 8.00 8.50 9.00 9.50 10.00 10.50 11.00 11.50 12.00 12.50 13.00 13.50
Distance into catalyst ( cm )
+ temp. profile -383K
◇ temp. profile -422K

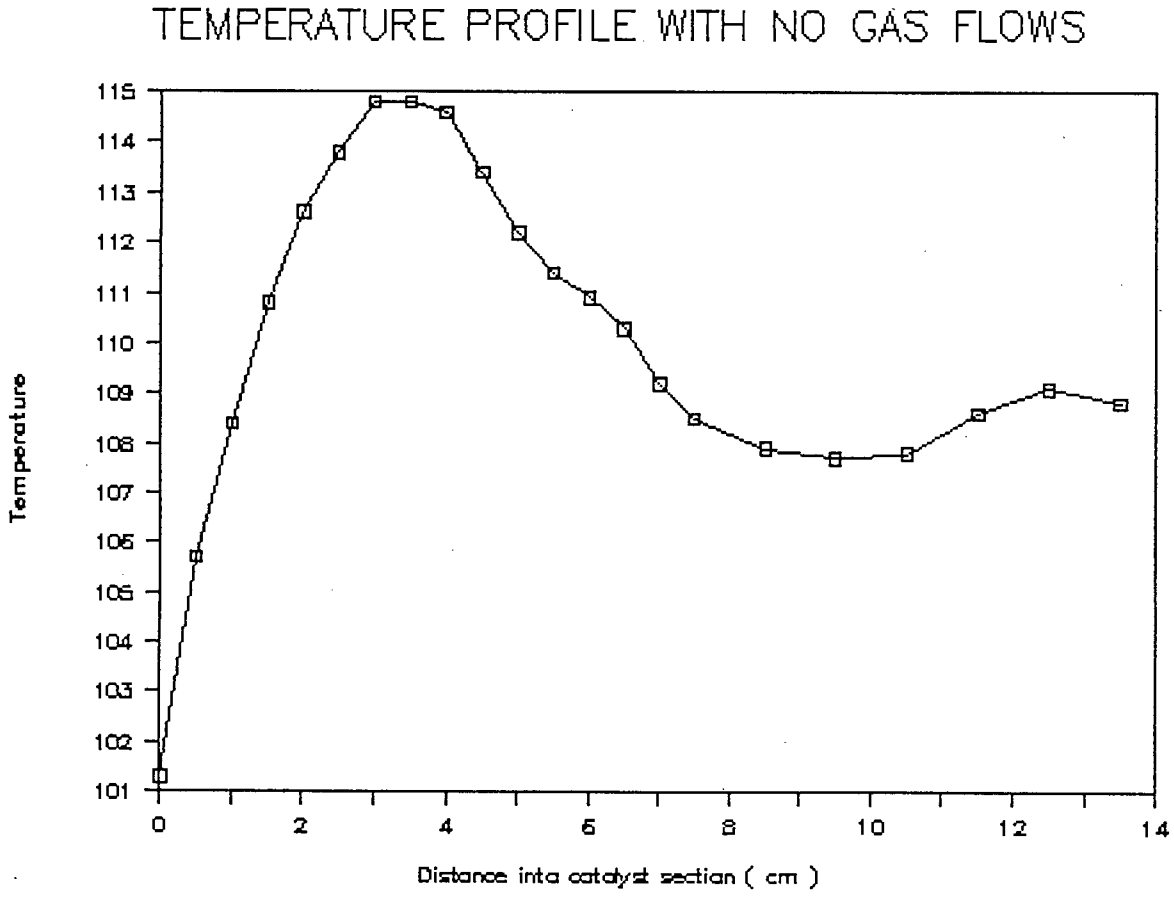
TEMPERATURE PROFILE WITH NO GAS FLOWS
Temperature
115
114
113
112
111
110
109
108
107
106
105
104
103
102
101
0
2
4
6
8
10
12
14
Distance into catalyst section ( cm )

**APPENDIX 20**

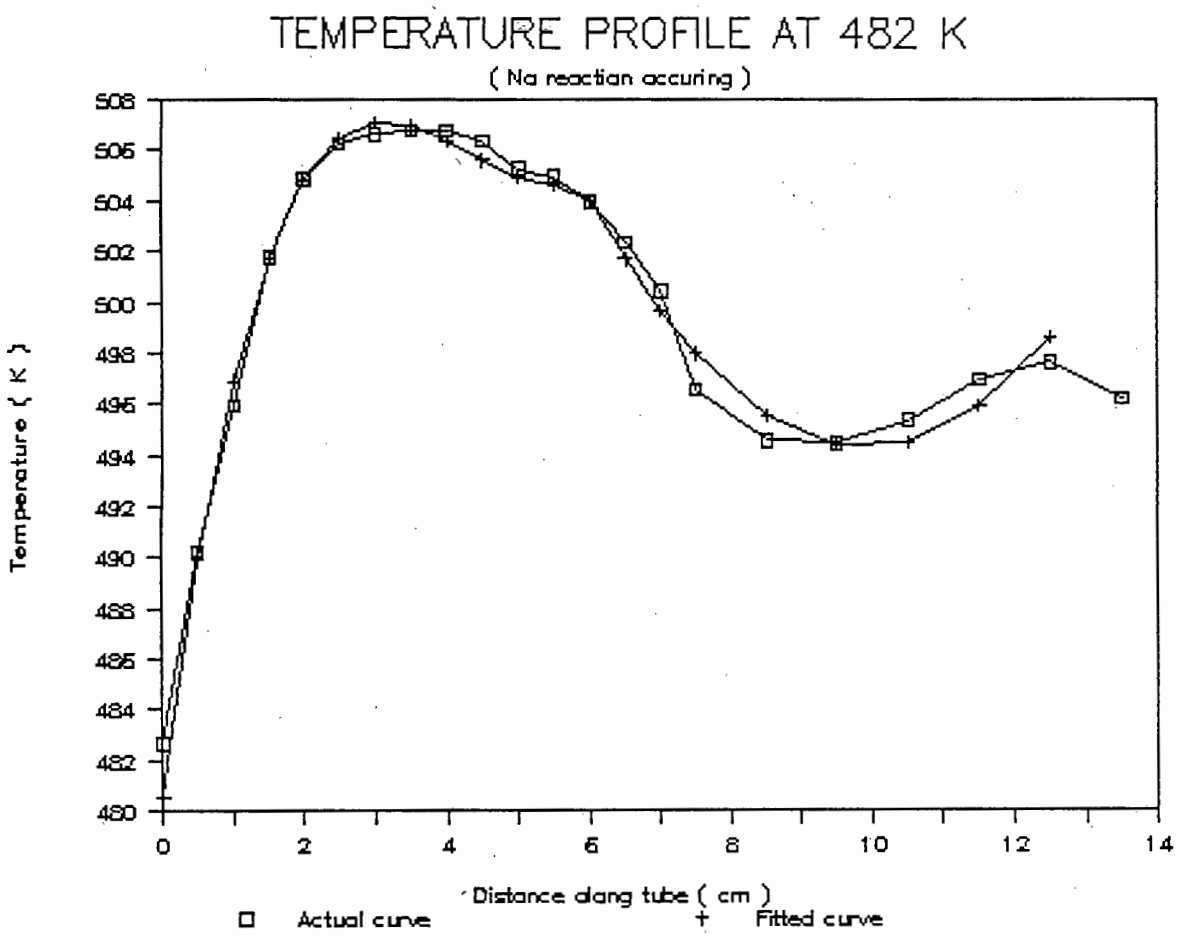
TEMPERATURE PROFILE AT 482 K
( No reaction occuring )
Temperature ( K )
508
506
504
502
500
498
496
494
492
490
488
486
484
482
480
0
2
4
6
8
10
12
14
Distance along tube ( cm )
Actual curve
Fitted curve

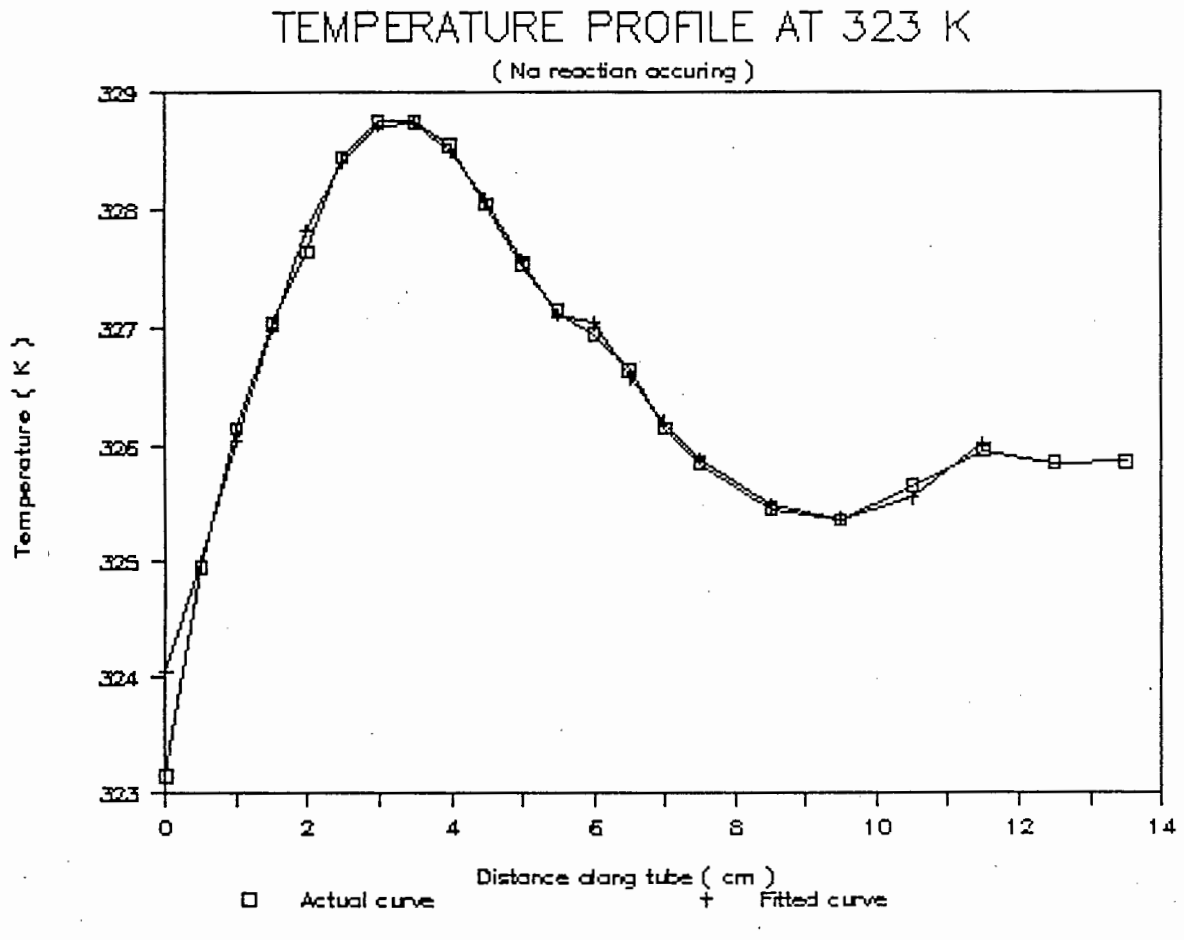
TEMPERATURE PROFILE AT 323 K
( No reaction occuring )
Temperature ( K )
329
328
327
326
325
324
323
0
2
4
6
8
10
12
14
Distance along tube ( cm )
Actual curve
Fitted curve

**APPENDIX 21**

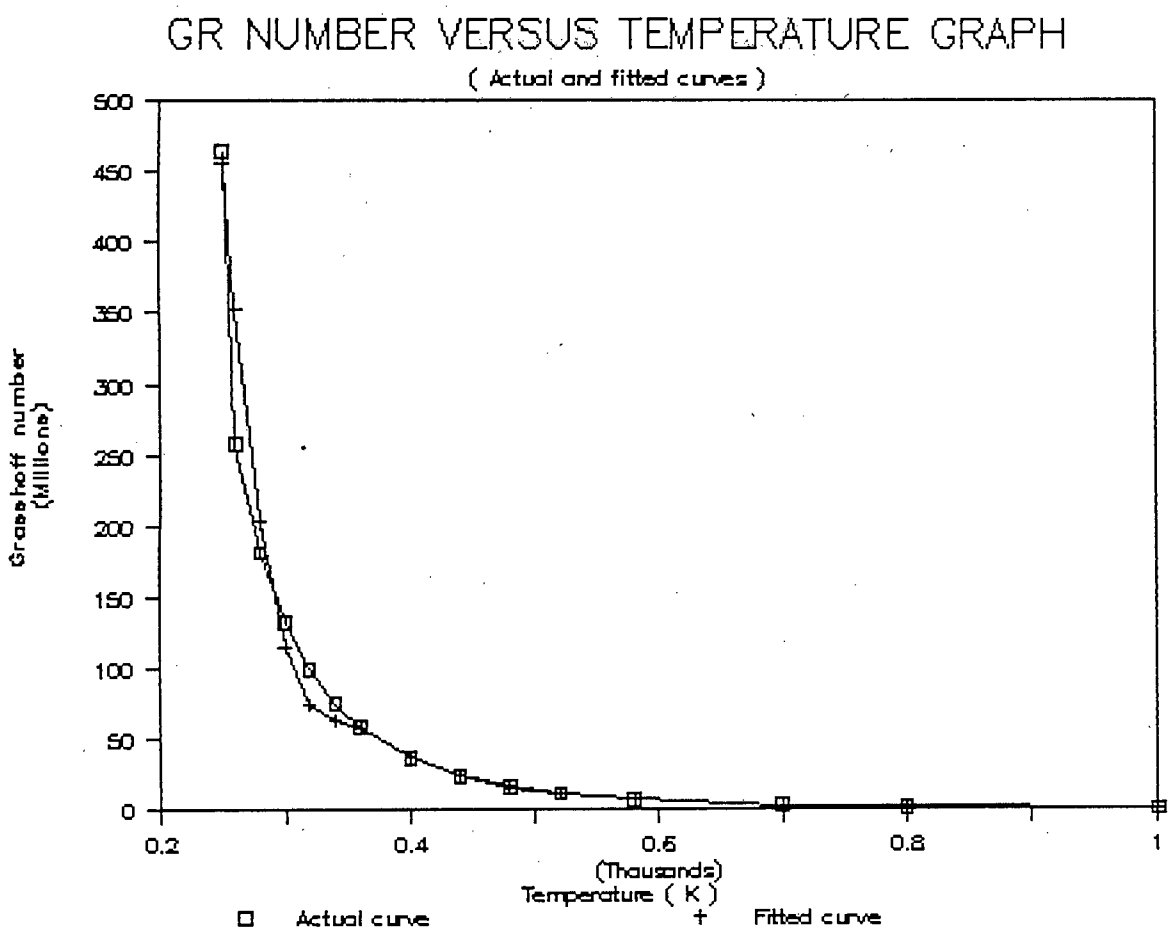
GR NUMBER VERSUS TEMPERATURE GRAPH
( Actual and fitted curves )
Grasshoff number (Millions)
500
450
400
350
300
250
200
150
100
50
0
0.2
0.4
0.6
0.8
1
(Thousands)
Temperature ( K )
Actual curve
Fitted curve

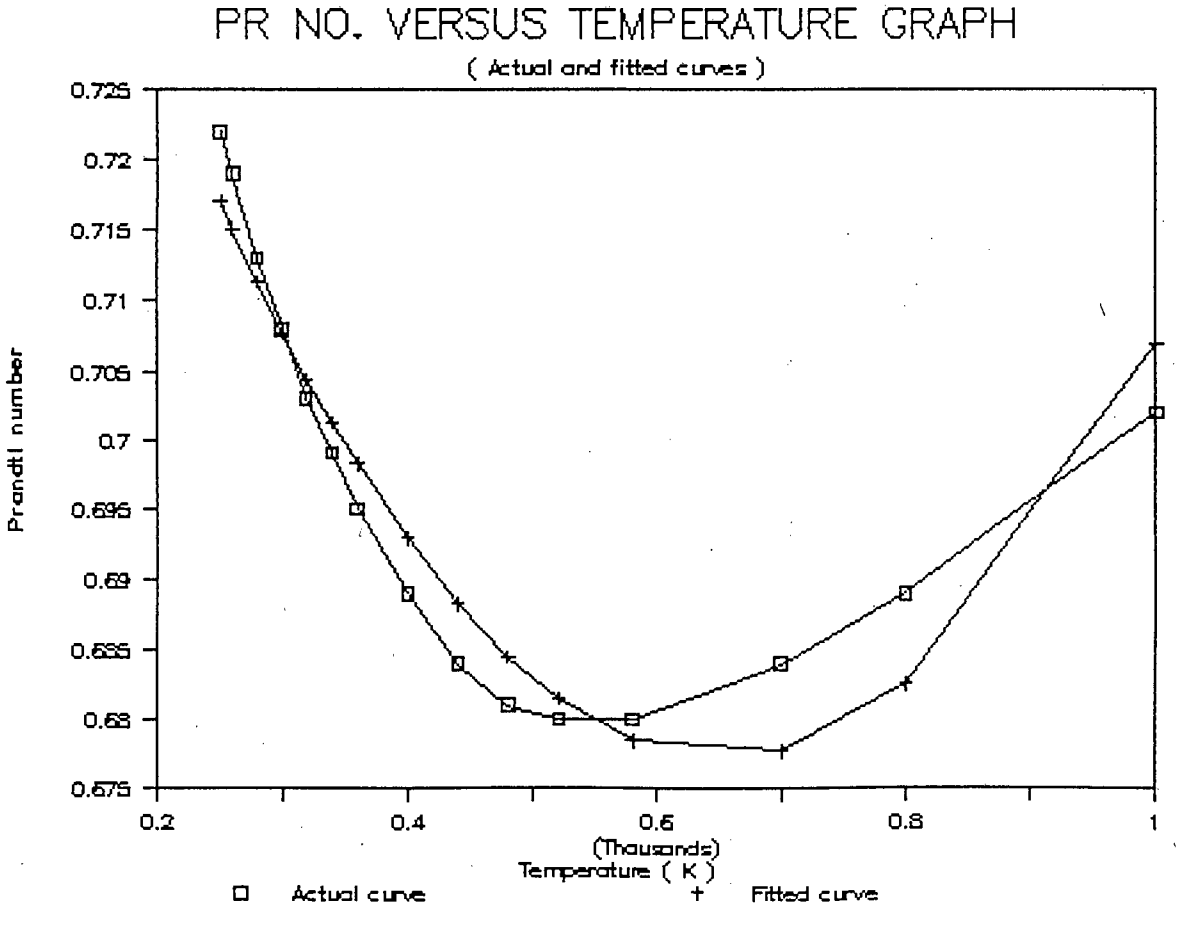
PR NO. VERSUS TEMPERATURE GRAPH
( Actual and fitted curves )
Prandtl number
0.725
0.72
0.715
0.71
0.705
0.7
0.695
0.69
0.685
0.68
0.675
0.2
0.4
0.6
0.8
1
(Thousands)
Temperature ( K )
Actual curve
Fitted curve

## APPENDIX 22

Calculation of the compressibility factor and the fugacity coefficient to determine the approach to ideal behaviour. Thermodynamic equations taken from (Smith J.M. and van Ness H.C., 1975) are used for the property evaluations. Subsequent development of the conversion based on the equilibrium constant follows.

The ideal equation adapted for non ideal behaviour may be written as :

$PV = nZRT$ where Z = compressibility factor

Critical constants are taken from Appendix B (Smith and van Ness)

| | $T_c$ (K) | $P_c$ (atm) | w |
|---|---|---|---|
| CO | 132.9 | 34.5 | 0.041 |
| $CH_4$ | 190.6 | 45.4 | 0.007 |
| $H_2$ | 33.2 | 12.8 | 0.000 |
| $H_2O$ | 647.1 | 217.6 | 0.348 |

Z may be calculated using the equation :

$$Z = 1 + \left[\frac{BP_c}{RT_c}\right] \frac{P_r}{T_r}$$

where $P_c$ , $T_c$ are the critical values

$P_r$ , $T_r$ are reduced values

Also $$\frac{BP_c}{RT_c} = B^o + wB^1$$

where $$B^o = 0.083 - \frac{0.422}{T_r}$$

$$B^1 = 0.139 - \frac{0.172}{T_r}$$

Using a temperature of 200°C or 473 K and a pressure of 1 atm (similar to reaction conditions), the following table can be constructed :

| | $P_r$ | $T_r$ | $B^o$ | $B^1$ | Z |
|---|---|---|---|---|---|
| CO | 0.02899 | 3.559 | 0.0276 | 0.1382 | 1.000 |
| $H_2$ | 0.07813 | 14.247 | 0.07698 | 0.139 | 1.000 |
| $CH_4$ | 0.02203 | 2.482 | -0.01557 | 0.1352 | 0.999 |
| $H_2O$ | 0.00459 | 0.731 | -0.6138 | -0.5025 | 0.995 |

Hence all species may be assumed to be ideal.

**Calculation of the fugacity coefficient of each gas in the mixture.**

The test to see if the mixture may be assumed to be ideal is to determine the value of the fugacity coefficient. A value of unity confirms this assumption of ideal behaviour.

The equation to be used is :

$$\text{Ln } \hat{\Phi}_i = P/RT\{B_{ii} + 0.5B_{jk}[y_j y_k(2S_{ji} - S_{jk})]\}$$

where $S_{ji} = 2B_{ji} - B_{jj} - B_{ii}$

$S_{jk} = 2B_{jk} - B_{jj} - B_{kk}$

Also : $B_{ij} = RT_{cij}/P_{cij}(B^o + w_{ij}B^1)$

where $B^o$ and $B^1$ are as defined earlier

$w_c$ , $T_c$ , $P_c$ , $T_c$ , $V_c$ and $Z_c$ are the critical parameters, defined as below :

$w_{ij} = 0.5(w_i + w_j)$

$T_{cij} = (T_{ci}T_{cj})^{1/2}$

$$P_{cij} = \frac{Z_{cij} RT_{cij}}{V_{cij}}$$

$$Z_{cij} = 0.5(Z_{ci} + Z_{cj})$$

$$V_{cij} = \left[\frac{V_{ci}^{1/3} + V_{cj}^{1/3}}{2}\right]^3$$

In order to solve the above equations, a computer program was written. A listing is provided in Appendix 24. The critical constants were entered in a data statement and read into the program. Using the program to calculate the fugacity coefficients, the following values were obtained :

fugacity coefficient of CO = 0.99947
fugacity coefficient of $H_2$ = 0.99962
fugacity coefficient of $CH_4$ = 0.99939
fugacity coefficient of $H_2O$ = 0.99984

Thus the gas mixture may be assumed to be ideal.

**Development of the equilibrium constant in terms of the conversion.**

System pressure : 1 atm
Basis : Conversion x of CO to $CH_4$

| Species | Moles initially present | Moles formed/ used | Moles at equilib. | Mole fr. |
|---|---|---|---|---|
| CO | 1 | x | 1-x | $\frac{1-x}{4-2x}$ |
| $H_2$ | 3 | 3-3x | 3(1-x) | $\frac{3(1-x)}{4-2x}$ |
| $H_2O$ | 0 | x | x | $\frac{x}{4-2x}$ |
| $CH_4$ | 0 | x | x | $\frac{x}{4-2x}$ |
| | | | 4-2x | |

From (Smith and van Ness), the equilibrium constant K for an ideal gas phase reaction may be written as :

$$K = \pi \hat{f}^{vi} \qquad \ldots\ldots\ldots(A)$$

where $\hat{f}^{vi}$ is defined by the equation $\hat{f}^{vi} = y_i \, P\hat{\Phi}_i$

Since $\hat{\Phi}_i$ is approximately unity, equation (A) reduces to :

$$K = \pi y_i^{vi} p^{vi}$$

Since P = 1 atm, $K = \pi y_i^{vi}$. This equation may be rewritten as

$$K = \frac{\text{product of mole fractions of products}}{\text{product of mole fractions of reactants}}$$

$$= \frac{x^2(4-2x)^2}{3(1-x)^2}$$

## APPENDIX 23

Determination of the equilibrium constant as a function of temperature. All derivations and calculations are taken from a thermodynamics text by (Smith J.M and van Ness H.C., 1975)

The equilibrium constant is related to temperature as follows :

$$\text{Ln } K = \frac{-G^o}{RT}$$

$$\text{also } \frac{d}{dT}\left[\frac{G^o}{RT}\right] = \frac{-\Delta H}{RT^2}$$

$$\text{Substituting : } \frac{d}{dT}(\text{Ln } K) = \frac{\Delta H}{RT^2}$$

Integrating gives :

$$\text{Ln } K = 1/R \int \frac{\Delta H}{T^2} dT + I \quad .....(A)$$

where I = constant of integration

$$\Delta H = H_o + \int \Delta C_p \, dT$$

$$\Delta H = H^o_{298} + \Sigma_{prod}(n \int C_p \, dT) - \Sigma_{react} (n \int C_p dT)$$

$$= H^o_{298} + \int \Delta C_p \, dT \quad .....(B)$$

where $\Delta C_p = \Sigma_{prod} \, nC_{pi} - \Sigma_{react} \, nC_{pi}$

A general form of $C_p$ is as shown below :

$$C_{pi} = \alpha_i + \beta_i T + \gamma_i T^2$$

where $\alpha_i$ , $\beta_i$ , $\gamma_i$ are constants for species i

This implies that :

$$\Delta C_p = \Delta\alpha + (\Delta\beta)T + (\Delta\gamma)T^2$$

where $\Delta\alpha = \Sigma_{prod}\, n\alpha - \Sigma_{react}\, n\alpha$
where $\Delta\beta = \Sigma_{prod}\, n\beta - \Sigma_{react}\, n\beta$
where $\Delta\gamma = \Sigma_{prod}\, n\gamma - \Sigma_{react}\, n\gamma$

Substituting the above into equation (B) and integrating gives :

$$\Delta H^o = \Delta H_o + \Delta\alpha T + \frac{\Delta\beta T^2}{2} + \frac{\Delta\gamma T^3}{3} \quad .....(C)$$

Substituting equation (C) into equation (A) gives K :

$$\text{Ln } K = \frac{-H_o}{RT} + \frac{\Delta\alpha \text{Ln } T}{R} + \frac{\Delta\beta T}{2R} + \frac{\Delta\gamma T^2}{6R} + I \quad ...(D)$$

Since $G^o = -RT \text{ Ln } K$ , substituting into equation (D) gives :

$$\Delta G^o = \Delta H_o - \Delta\alpha T \text{ Ln } T - \frac{\Delta\beta T^2}{2} - \frac{\Delta\gamma T^3}{6} - IRT \quad (E)$$

By evaluating $\Delta H$ and $\Delta G^o$ at 298 K using Tables 4-4 and 9-1 (44) respectively, the constants I and $H_o$ could be solved for. Hence equations (C), (D) and (E) may be written as :

$$\Delta H = -45262.6 - 16.019T + 0.009119T^2 - 1.6819*10^{-6}T^3$$

$$\text{Ln } K = 22774T^{-1} - 8.0619\text{Ln } T + 4.589*10^{-3}T - 0.004232T^3 + 25.57$$

$$\Delta G^{\circ} = -45262.6 + 16.019 T \ln T - 0.009119 T^2 + 8.408 * 10^{-7} T^3 - 50.806 T$$

where $\Delta H$ and $\Delta G^{\circ}$ have the units of cal/gmol

As an example at a temperature of 500 K :

$\ln K = 14.564$ $\qquad$ $G^{\circ} = -17363$ cal/gmol

$K = 2113899$

```
REM ************************************************************************
REM
REM          CALCULATION OF THE FUGACITY COEFFICIENTS FOR A MIXTURE
REM           OF GASES. ( TO CHECK THE ASSUMPTION OF AN IDEAL GAS
REM                              MIXTURE )
REM
REM ************************************************************************
REM
REM
 REM   Declaration of variables used
 REM
 REM   TC(I)                      Critical temp of gas i
 REM   PC(I)                      Critical pressure of gas i
 REM   ZC(I)                      Critical compressibility factor of gas i
 REM   VC(I)                      Critical volume factor of gas i
 REM   W(I)                       Accentric factor of gas i
 REM   TC(I,J)                    Critical temp of gas i wrt gas j
 REM   PCRIT(I,J)                 Critical press of gas i wrt gas j
 REM   ZCRIT(I,J)                 Critical compress.  of gas i wrt gas j
 REM   VCRIT(I,J)                 Critical volume of gas i wrt gas j
 REM   WW(I,J)                    Accentric factor of gas i wrt gas j
 REM   B0,B1,                     Functions of the reduced temp.
 REM   TPC                        Pseudo. crit. temp. for mixture
 REM   PPC                        Pseudo. crit. press. for mixture
 REM   TR                         Reduced temp. for mixture
 REM   PPR                        Reduced pseudo. press. for mixture
 REM
 REM
 REM
 REM CALCULATION OF FUGACITY COEFFICIENTS
 REM
 REM
 KEY OFF:CLS
 DIM TC(4),PC(4),W(4),ZC(4),VC(4),WW(4,4),PCRIT(4,4),X(4)
 DIM TCRIT(4,4),VCRIT(4,4),ZCRIT(4,4),B(4,4),DELJI(5,5),DELJK(4,4)
 DIM THI(4),ANSWER$(4)
 LOCATE 12,20 :PRINT"CALCULATION OF FUGACITY COEFFICIENTS"
 REM A$=INKEY$:IF A$=""THEN 80
 REM
 REM CRITICAL CONSTANTS
 REM
 REM CO - DATA
 DATA 132.9,34.5,0.041,.295,93.1,"CO"
 REM
 REM H2 - DATA
 DATA 33.2,12.8,0,.305,65,"H2"
 REM
 REM CH4 - DATA
 DATA 190.6,45.4,.007,.288,99,"CH4"
 REM
 REM H2O - DATA
 DATA 647.1,217.6,.348,.23,56,"H2O"
 REM
 REM  MOLE FRACTION DATA
 DATA .25,.25,.25,.25
 FOR I= 1 TO 4
 READ TC(I),PC(I),W(I),ZC(I),VC(I),ANSWER$(I)
 NEXT I
 REM
 REM
 REM DEFINING FUNCTIONS B0,B1
 REM
 DEF FNB0(TR)=.083-.422/(TR^1.6)
 DEF FNB1(TR)=.139-.172/(TR^4.2)
```

```
REM
REM
FOR I=1 TO 4
READ X(I)
FOR J=1 TO 4
TCRIT(I,J)=(TC(I)*TC(J))^.5
VCRIT(I,J)=((VC(I)^.333333 + VC(J)^.333333)/2)^3
ZCRIT(I,J)=(ZC(I)+ZC(J))/2
PCRIT(I,J)=ZCRIT(I,J)*TCRIT(I,J)/VCRIT(I,J)*82.05
WW(I,J)=(W(I)+W(J))/2
NEXT J
NEXT I
TPC=0:PPC=0
FOR I=1 TO 4
TPC=TPC+X(I)*TC(I)
PPC=PPC+X(I)*PC(I)
NEXT I
TR=473/TPC:PR=1/PPC
FOR I=1 TO 4
FOR J=1 TO 4
B(I,J)=82.05*TCRIT(I,J)/PCRIT(I,J)*(FNB0(TR)+WW(I,J)*FNB1(TR))
NEXT J
NEXT I
FOR J=1 TO 4
FOR I=1 TO 4
IF I<>J GOTO 920
DELIJ(J,I)=0:GOTO 930
DELIJ(J,I)=2*B(J,I)-B(J,J)-B(I,I)
NEXT I
NEXT J
FOR I=1 TO 4
STORE=0
FOR J=1 TO 4
FOR K=1 TO 4
STORE=STORE+X(J)*X(K)*DELJI(J,K)
 NEXT K:NEXT J
 NEWSTORE=1/82.05/473*(B(I,I)+.5*STORE)
 THI(I)=EXP(NEWSTORE)
 NEXT I
 REM
 REM
 REM   PRINTING OF THE RESULTS
 CLS:LOCATE 5:FOR I=1 TO 4
 PRINT "Fugacity coefficient of ";ANSWER$(I);" = ";THI(I)
 NEXT I
 END
```

## APPENDIX 25

Data for the methanation reaction over 11% nickel on silica alumina.

Catalyst : 11% Nickel/Silica-Alumina
Temperature : 250°C
CO Flowrate : 6 ml/min
$H_2$ Flowrate : 18 ml/min

| File no. CE | Dist. into Catalyst | Temperature (°C) | Corrected Conc. | Conversion of CO |
|---|---|---|---|---|
| | (cm) | | | (%) |
| 501 | 0 | 249.2 | 1.950 | 4.01 |
| 502 | 1 | 267.1 | 1.794 | 8.02 |
| 503 | 2 | 278.6 | 1.721 | 11.76 |
| 504 | 3 | 289.2 | 1.675 | 14.08 |
| 505 | 4 | 296.0 | 1.585 | 18.73 |
| 506 | 5 | 299.0 | 1.533 | 21.37 |
| 507 | 6 | 302.0 | 1.357 | 30.39 |
| 509 | 8 | 302.0 | 1.188 | 39.06 |

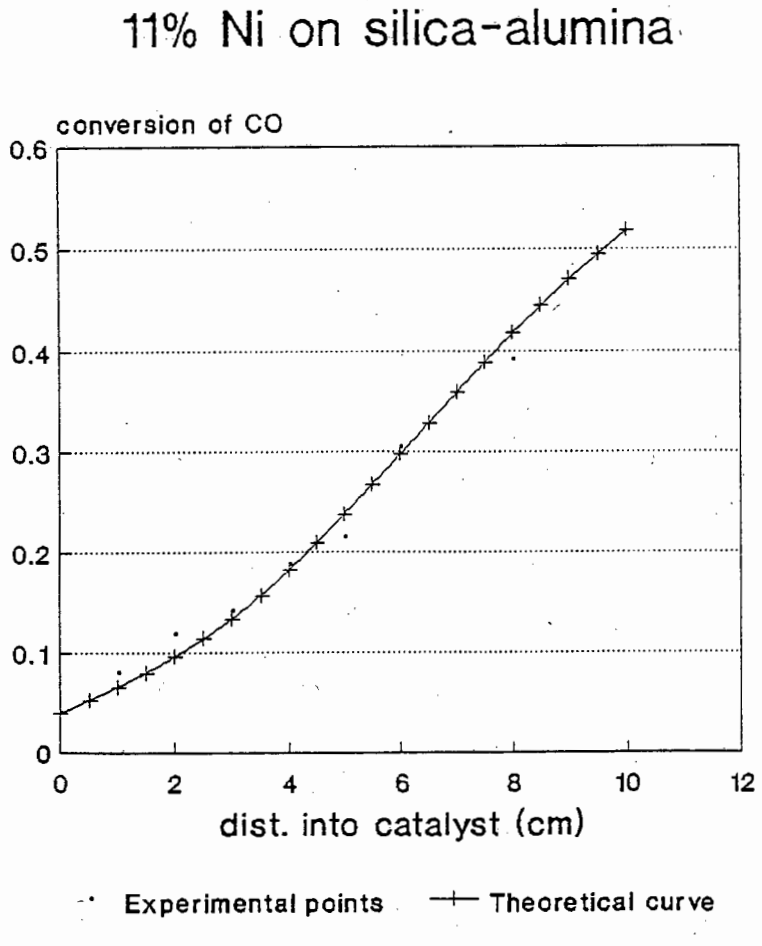

## APPENDIX 26

Data for the methanation reaction over 7% nickel on Zeolite-Y

Catalyst : 7% Nickel/Zeolite-Y
Temperature : 250°C
CO Flowrate : 6 ml/min
$H_2$ Flowrtate : 18 ml/min

| File no. CE | Dist. into Catalyst | Temperature (°C) | Corrected Conc. | Conversion of CO |
|---|---|---|---|---|
| | (cm) | | | (%) |
| 550 | 0 | 254.9 | 1.098 | 8.32 |
| 551 | 1 | 268.8 | 1.069 | 10.72 |
| 552 | 2 | 280.1 | 1.056 | 11.84 |
| 553 | 3 | 286.3 | 1.049 | 12.36 |
| 554 | 4 | 292.1 | 1.001 | 16.44 |
| 555 | 5 | 295.5 | 0.983 | 17.97 |
| 556 | 6 | 296.8 | 0.955 | 20.30 |
| 557 | 7 | 299.7 | 0.943 | 21.25 |
| 558 | 8 | 299.8 | 0.921 | 23.14 |

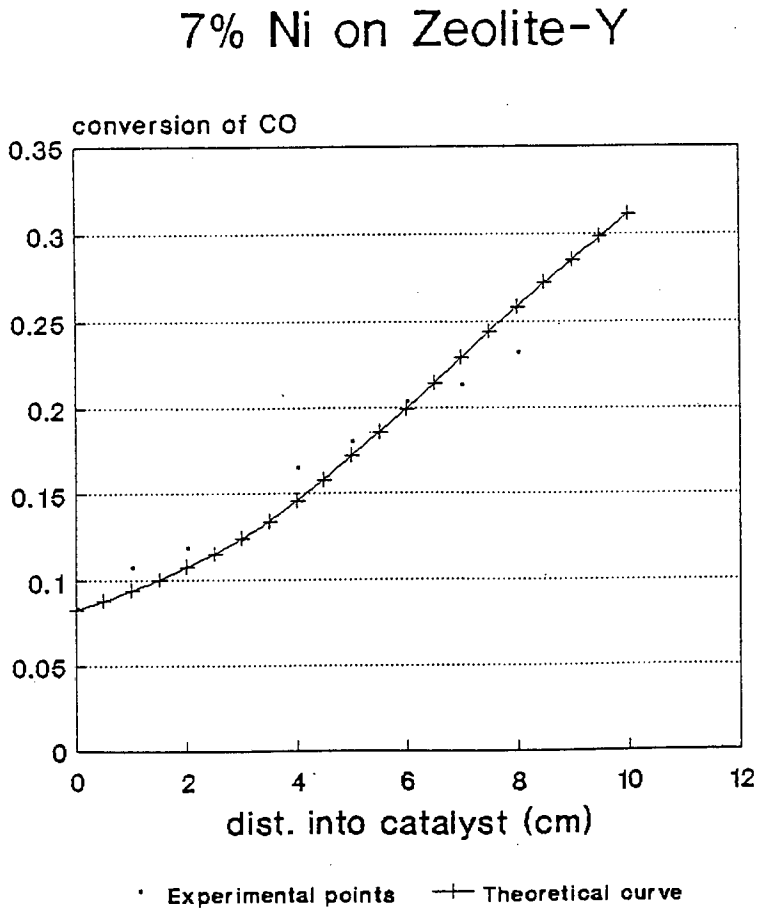

## APPENDIX 27

Data for the methanation reaction over 7% nickel on alumina

Catalyst : 7% Nickel/Alumina
Temperature : 250°C
CO Flowrate : 6 ml/min
$H_2$ Flowrate : 18 ml/min

| File no. CE | Dist. into Catalyst | Temperature (°C) | Corrected Conc. | Conversion of CO |
|---|---|---|---|---|
| | (cm) | | | (%) |
| 590 | 0 | 252.1 | 1.021 | 5.53 |
| 591 | 1 | 260.5 | 0.979 | 9.43 |
| 592 | 2 | 268.6 | 0.944 | 12.67 |
| 593 | 3 | 273.5 | 0.889 | 13.77 |
| 594 | 4 | 276.7 | 0.871 | 18.52 |
| 595 | 5 | 277.0 | 0.860 | 19.46 |
| 596 | 6 | 277.3 | 0.819 | 24.25 |
| 597 | 7 | 278.5 | 0.801 | 25.92 |
| 598 | 8 | 277.3 | 0.772 | 28.62 |

7% Ni on alumina

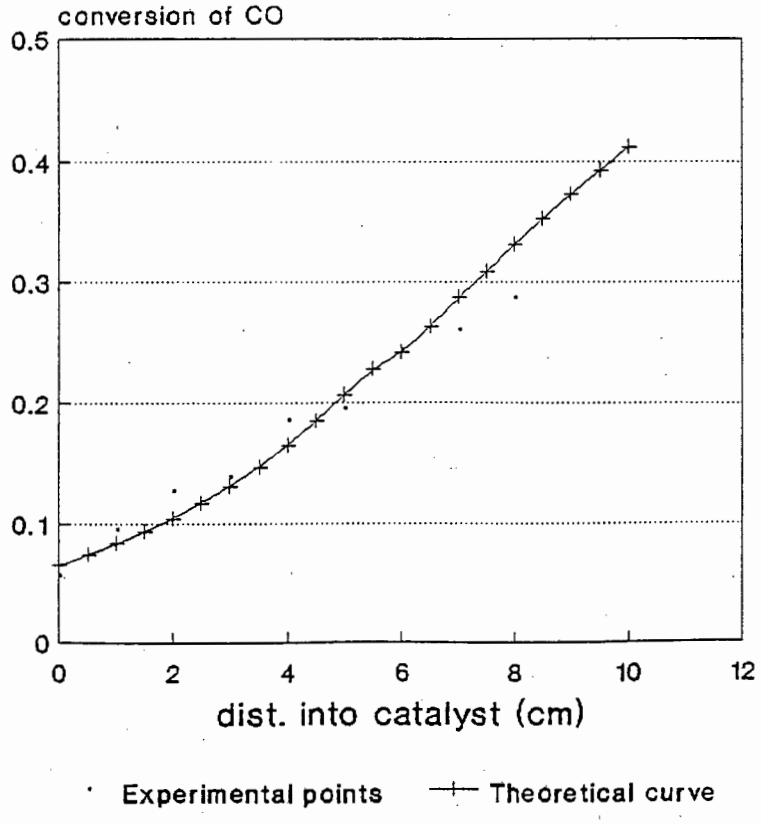

## APPENDIX 28

Data for the methanation reaction over 7% nickel on alumina

Catalyst : 7% Ni/Alumina
Temperature : 250°C
CO Flowrate : 13 ml/min
$H_2$ Flowrate : 39 ml/min

| File no. CE | Dist. into Catalyst (cm) | Temperature (°C) | Corrected Conc. | Conversion of CO (%) |
|---|---|---|---|---|
| 580 | 0 | 251.0 | 1.134 | 10.87 |
| 581 | 1 | 266.0 | 1.112 | 12.60 |
| 582 | 2 | 278.6 | 1.087 | 14.61 |
| 583 | 3 | 287.1 | 1.071 | 15.02 |
| 584 | 4 | 291.8 | 1.013 | 20.37 |
| 585 | 5 | 294.6 | 0.988 | 22.34 |
| 586 | 6 | 297.5 | 0.935 | 26.48 |
| 587 | 7 | 300.4 | 0.922 | 27.48 |
| 588 | 8 | 300.2 | 0.877 | 31.06 |

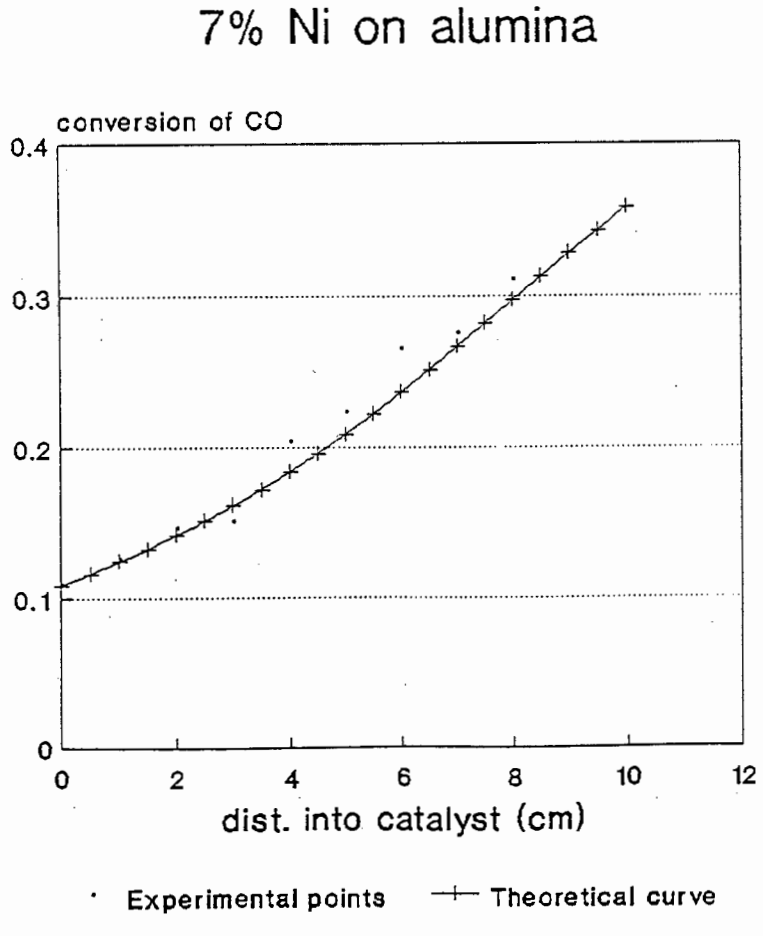

## APPENDIX 29

Data for the methanation reaction over 0.5% nickel on ZSM-5

Catalyst : 0.5% Ni/ZSM-5
Temperature : 250°C
CO Flowrate : 13 ml/min
$H_2$ Flowrate : 39 ml/min

| File no. CE | Dist. into Catalyst (cm) | Temperature (°C) | Corrected Conc. | Conversion of CO (%) |
|---|---|---|---|---|
| 720 | 0 | 252.4 | 1.322 | 6.11 |
| 721 | 1 | 261.6 | 1.266 | 7.01 |
| 722 | 2 | 271.0 | 1.255 | 10.87 |
| 723 | 3 | 277.2 | 1.205 | 13.41 |
| 724 | 4 | 281.4 | 1.199 | 14.86 |
| 725 | 5 | 284.4 | 1.176 | 16.51 |
| 726 | 6 | 285.5 | 1.214 | 16.86 |
| 727 | 7 | 287.5 | 1.164 | 17.29 |
| 728 | 8 | 286.7 | 1.351 | 19.39 |

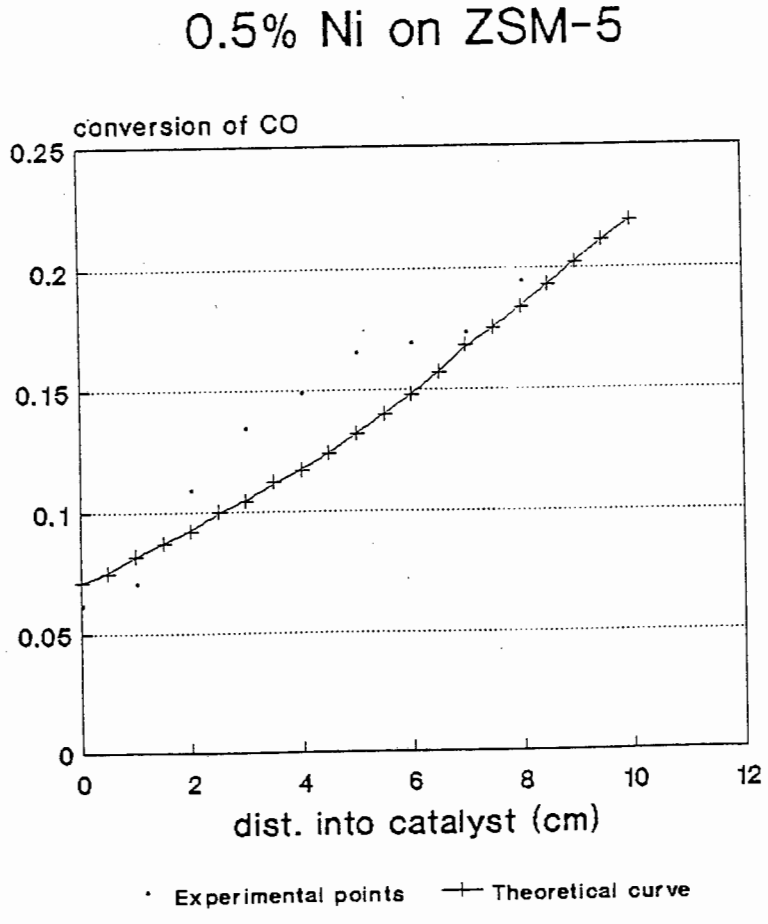

## APPENDIX 30

Data for the methanation reaction over 7% cobalt on alumina

Catalyst : 7% Co/Alumina
Temperature : 250°C
CO Flowrate : 6 ml/min
$H_2$ Flowrate : 18 ml/min

| File no. CE | Dist. into Catalyst (cm) | Temperature (°C) | Corrected Conc. | Conversion of CO (%) |
|---|---|---|---|---|
| 811 | 0 | 253.8 | 0.985 | 3.14 |
| 812 | 1 | 256.6 | 0.962 | 5.46 |
| 813 | 2 | 256.5 | 0.925 | 8.07 |
| 815 | 4 | 258.2 | 0.911 | 10.46 |
| 816 | 5 | 257.4 | 0.855 | 15.94 |
| 817 | 6 | 256.1 | 0.838 | 17.59 |
| 818 | 7 | 256.0 | 0.816 | 19.75 |

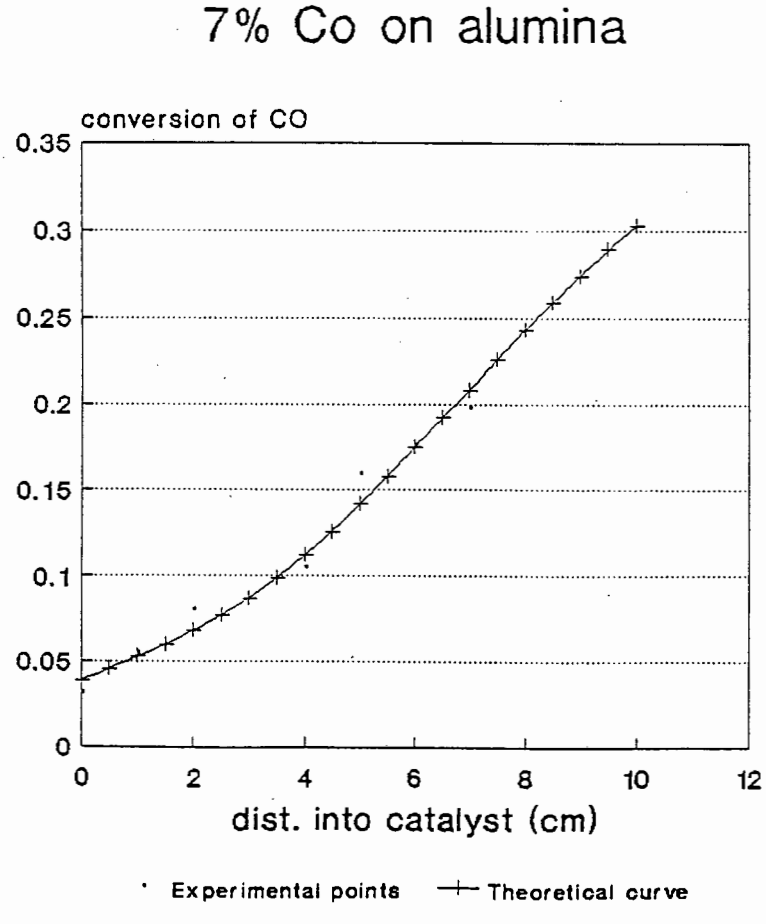

## APPENDIX 31

Data for the methanation reaction over 7% cobalt on silica-alumina.

Catalyst : 7% $Co/SiO_2$-$Al_2O_3$
Temperature : 250°C
CO Flowrate : 6 ml/min
$H_2$ Flowrate : 18 ml/min

| File no. CE | Dist. into Catalyst (cm) | Temperature (°C) | Corrected Conc. | Conversion of CO (%) |
|---|---|---|---|---|
| 910 | 0 | 253.8 | 1.088 | 6.77 |
| 911 | 1 | 261.8 | 1.043 | 9.71 |
| 912 | 2 | 266.8 | 1.016 | 11.13 |
| 913 | 3 | 269.5 | 0.981 | 15.20 |
| 914 | 4 | 270.5 | 0.965 | 16.61 |
| 915 | 5 | 272.7 | 0.939 | 18.87 |
| 916 | 6 | 270.7 | 0.915 | 21.09 |
| 918 | 8 | 267.7 | 0.891 | 23.22 |

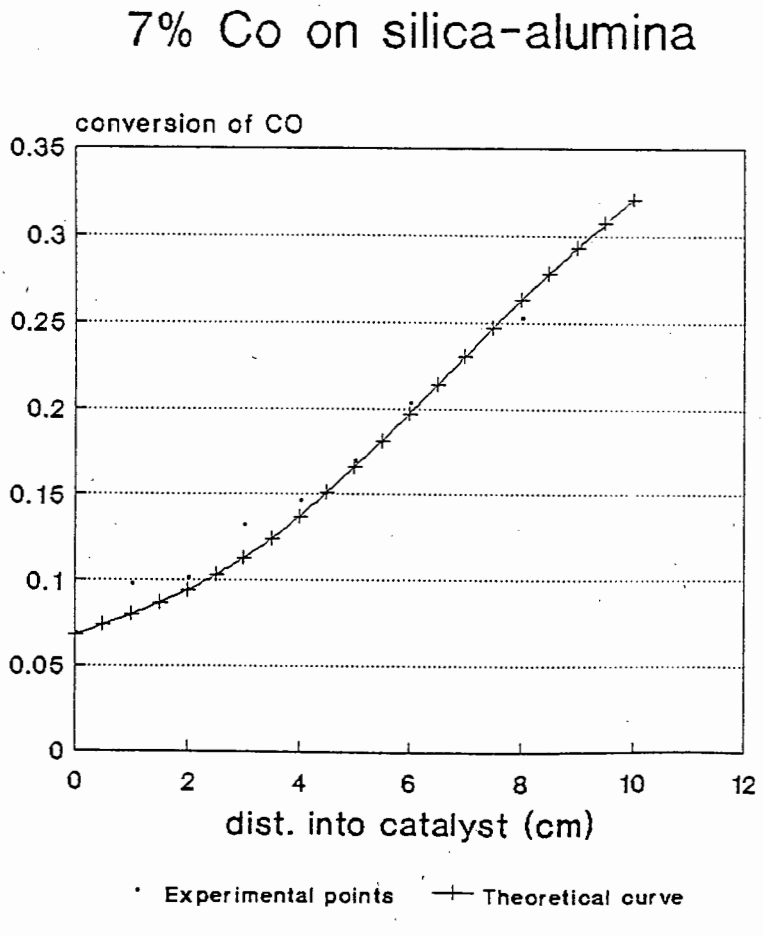

## APPENDIX 32

Data for the methanation reaction over cobalt on alumina

Catalyst : 7% Co/Alumina
Temperature : 250°C
CO Flowrate : 6 ml/min
$H_2$ Flowrate : 18 ml/min

| File no. CE | Dist. into Catalyst (cm) | Temperature (°C) | Corrected Conc. | Conversion of CO (%) |
|---|---|---|---|---|
| 951 | 0 | 245.2 | 0.968 | 4.89 |
| 952 | 1 | 250.1 | 0.949 | 6.76 |
| 953 | 2 | 256.2 | 0.935 | 8.22 |
| 954 | 3 | 254.7 | 0.925 | 9.17 |
| 955 | 4 | 257.0 | 0.883 | 13.22 |
| 956 | 5 | 252.3 | 0.864 | 15.19 |
| 957 | 6 | 250.9 | 0.842 | 17.32 |
| 958 | 7 | 248.9 | 0.814 | 20.09 |
| 959 | 8 | 245.1 | 0.801 | 21.32 |

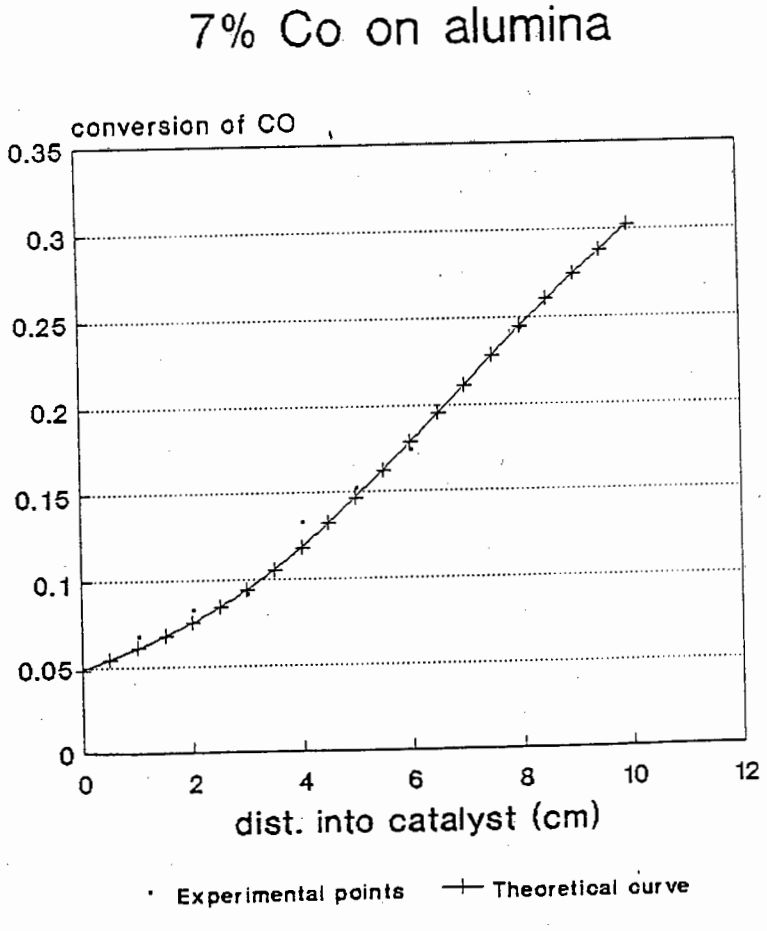

## APPENDIX 33

Data for the methanation reaction over 0.5% cobalt on silica-alumina.

Catalyst : 0.5% Co/Silica-Alumina
Temperature : 250°C
CO Flowrate : 6 ml/min
$H_2$ Flowrate : 18 ml/min

| File no. CE | Dist. into Catalyst | Temperature (°C) | Corrected Conc. | Conversion of CO |
|---|---|---|---|---|
| | (cm) | | | (%) |
| 71 | 0 | 251.9 | 0.766 | 2.89 |
| 72 | 1 | 256.9 | 0.743 | 5.74 |
| 73 | 2 | 259.7 | 0.730 | 7.24 |
| 74 | 3 | 262.0 | 0.715 | 9.02 |
| 75 | 4 | 262.6 | 0.697 | 11.23 |
| 76 | 5 | 261.0 | 0.682 | 13.02 |
| 77 | 6 | 261.4 | 0.666 | 15.01 |
| 78 | 7 | 262.0 | 0.645 | 16.70 |

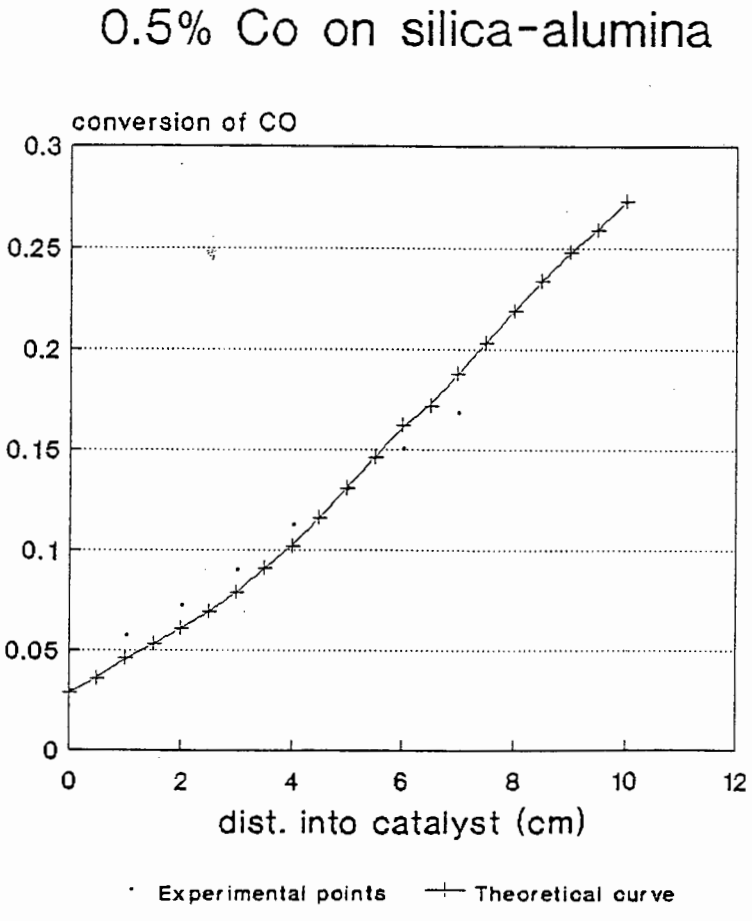

## APPENDIX 34

Data for the methanation reaction over 7% cobalt on Zeolite-Y

Catalyst : 7% Co/Zeolite-Y
Temperature : 250°C
CO Flowrate : 6 ml/min
$H_2$ Flowrate : 18 ml/min

| File no. CE | Dist. into Catalyst | Temperature (°C) | Corrected Conc. | Conversion of CO |
|---|---|---|---|---|
| | (cm) | | | (%) |
| 110 | 0 | 251.9 | 1.418 | 5.38 |
| 111 | 1 | 255.9 | 1.394 | 7.83 |
| 112 | 2 | 258.7 | 1.363 | 10.89 |
| 113 | 3 | 259.4 | 1.325 | 14.69 |
| 114 | 4 | 261.4 | 1.287 | 18.53 |
| 115 | 5 | 261.2 | 1.263 | 20.91 |
| 116 | 6 | 258.9 | 1.244 | 22.84 |
| 117 | 7 | 258.8 | 1.206 | 26.53 |
| 118 | 8 | 259.1 | 1.164 | 30.84 |

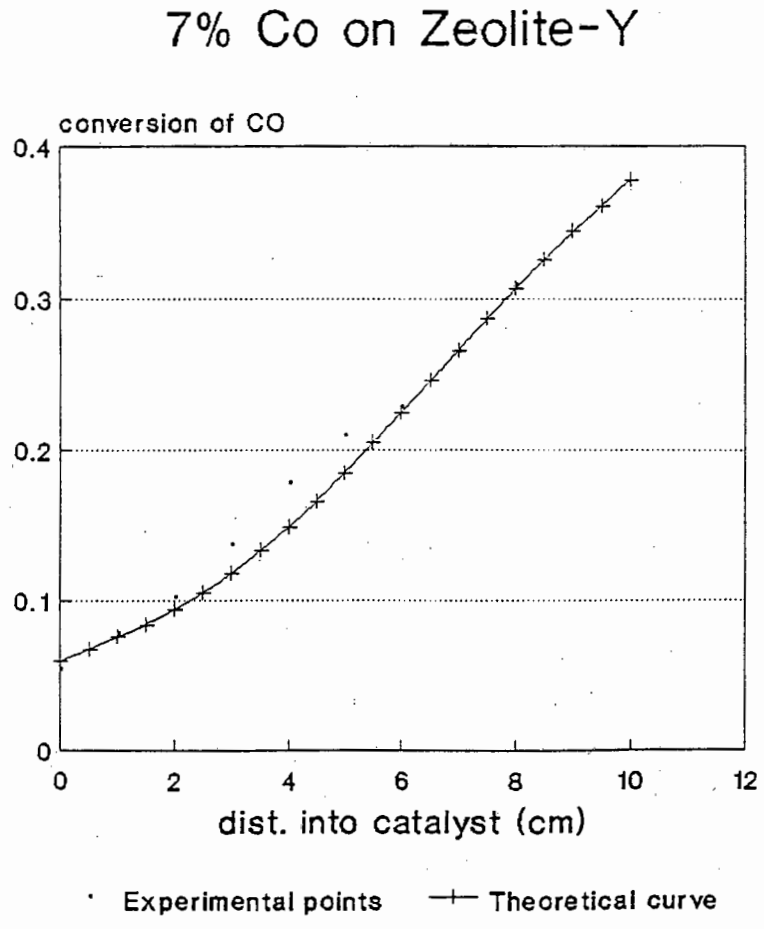

## APPENDIX 35

Data for the methanation reaction over 7% ruthenium on silica-alumina.

Catalyst : 7% Ru/Silica-Alumina
Temperature : 250°C
CO Flowrate : 13 ml/min
$H_2$ Flowrate : 39 ml/min

| File no. CE | Dist. into Catalyst (cm) | Temperature (°C) | Corrected Conc. | Conversion of CO (%) |
|---|---|---|---|---|
| 140 | 0 | 253.8 | 1.259 | 5.43 |
| 141 | 1 | 258.3 | 1.166 | 12.77 |
| 142 | 2 | 281.0 | 1.129 | 18.48 |
| 143 | 3 | 286.7 | 1.058 | 25.61 |
| 144 | 4 | 285.8 | 1.024 | 29.00 |
| 145 | 5 | 289.9 | 0.935 | 37.91 |
| 146 | 6 | 288.8 | 0.914 | 39.95 |
| 147 | 7 | 290.8 | 0.886 | 47.74 |
| 148 | 8 | 298.0 | 0.789 | 52.51 |

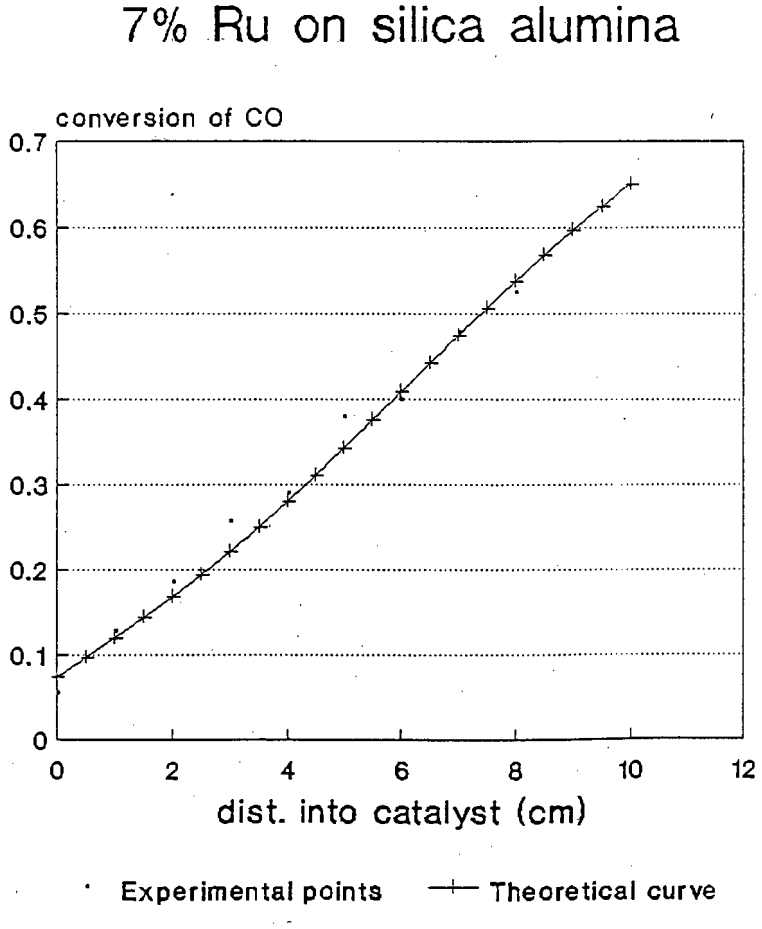

## APPENDIX 36

Data for the methanation reaction over 7% ruthenium on alumina

Catalyst : 7% Ru/Alumina
Temperature : 250°C
CO Flowrate : 6 ml/min
$H_2$ Flowrate : 18 ml/min

| File no. CE | Dist. into Catalyst (cm) | Temperature (°C) | Corrected Conc. | Conversion of CO (%) |
|---|---|---|---|---|
| 190 | 0 | 250.9 | 1.277 | 7.32 |
| 191 | 1 | 253.5 | 1.248 | 9.48 |
| 192 | 2 | 254.6 | 1.227 | 10.95 |
| 193 | 3 | 254.8 | 1.198 | 13.10 |
| 195 | 5 | 253.5 | 1.172 | 14.99 |
| 196 | 6 | 251.9 | 1.159 | 15.88 |
| 197 | 7 | 251.7 | 1.074 | 22.00 |

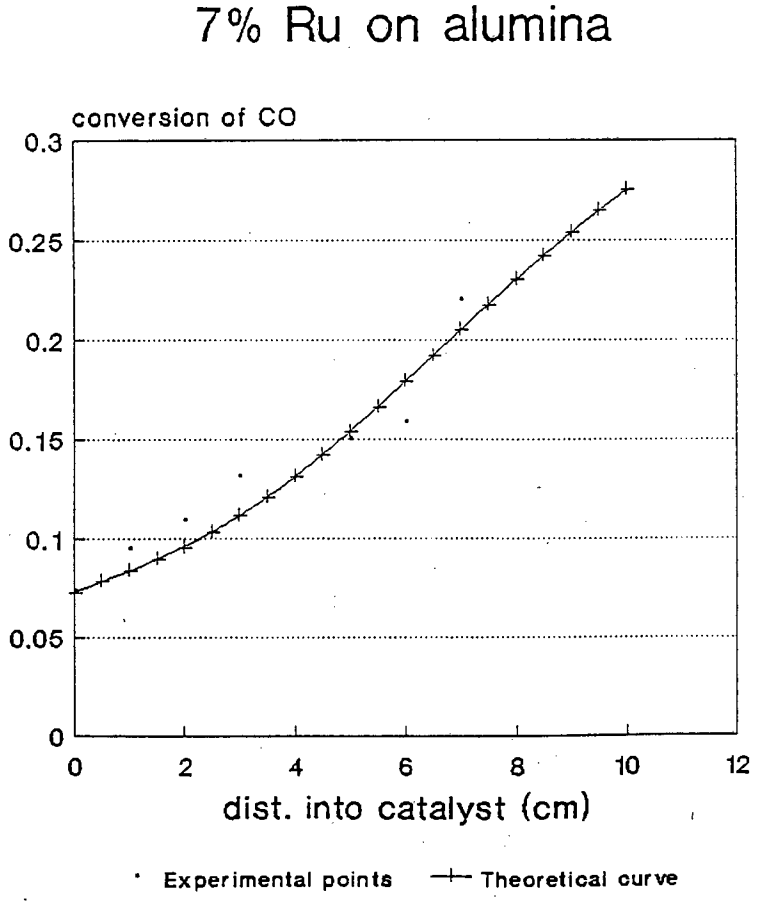

## APPENDIX 37

Data for the methanation reaction over 7% ruthenium on Zeolite-Y

Catalyst : 7% Ru/Zeolite-Y
Temperature : 250°C
CO Flowrate : 13 ml/min
$H_2$ Flowrate : 39 ml/min

| File no. CE | Dist. into Catalyst | Temperature (°C) | Corrected Conc. | Conversion of CO |
|---|---|---|---|---|
| | (cm) | | | (%) |
| 260 | 0 | 252.9 | 1.635 | 2.05 |
| 261 | 1 | 256.4 | 1.597 | 5.87 |
| 262 | 2 | 257.8 | 1.585 | 7.13 |
| 263 | 3 | 262.6 | 1.546 | 10.99 |
| 264 | 4 | 268.5 | 1.502 | 15.39 |
| 265 | 5 | 274.4 | 1.462 | 19.38 |
| 266 | 6 | 277.7 | 1.440 | 21.56 |
| 267 | 7 | 285.9 | 1.392 | 26.39 |
| 268 | 8 | 287.0 | 1.386 | 26.99 |

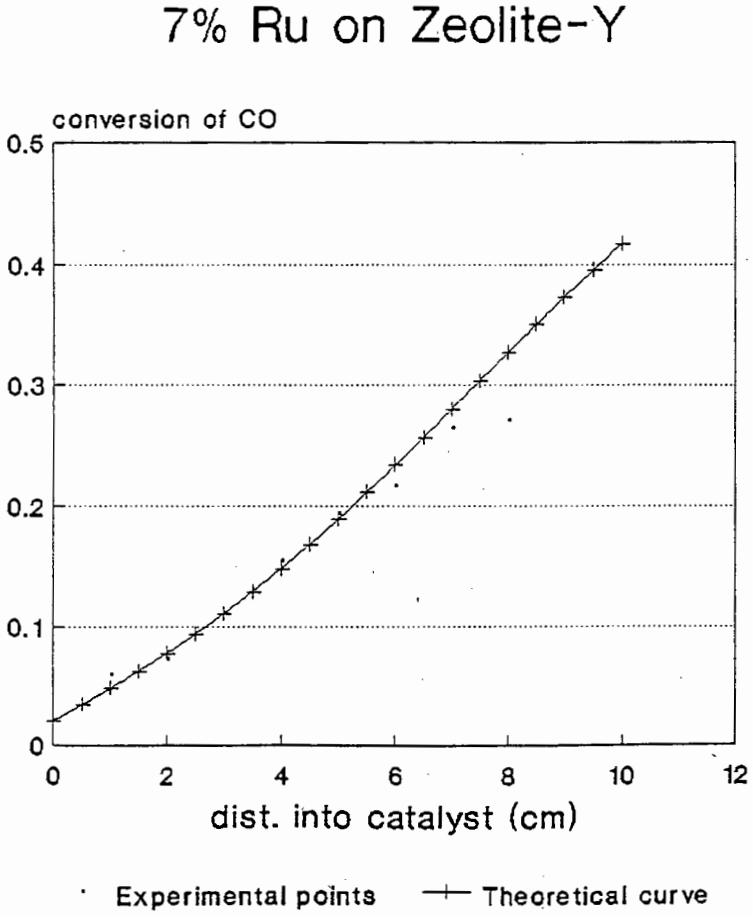

## APPENDIX 38

Data for the methanation reaction over 7% ruthenium on Zeolite-Y

Catalyst : 7% Ru/Zeolite-Y
Temperature : 250°C
CO Flowrate : 6 ml/min
$H_2$ Flowrate : 18 ml/min

| File no. CE | Dist. into Catalyst (cm) | Temperature (°C) | Corrected Conc. | Conversion of CO (%) |
|---|---|---|---|---|
| 270 | 0 | 255.2 | 1.672 | 5.15 |
| 271 | 1 | 257.5 | 1.653 | 7.06 |
| 272 | 2 | 265.1 | 1.595 | 12.79 |
| 273 | 3 | 271.0 | 1.555 | 16.84 |
| 275 | 5 | 270.0 | 1.492 | 23.09 |
| 276 | 6 | 281.3 | 1.492 | 23.15 |
| 277 | 7 | 289.4 | 1.448 | 27.55 |
| 278 | 8 | 292.3 | 1.404 | 31.89 |

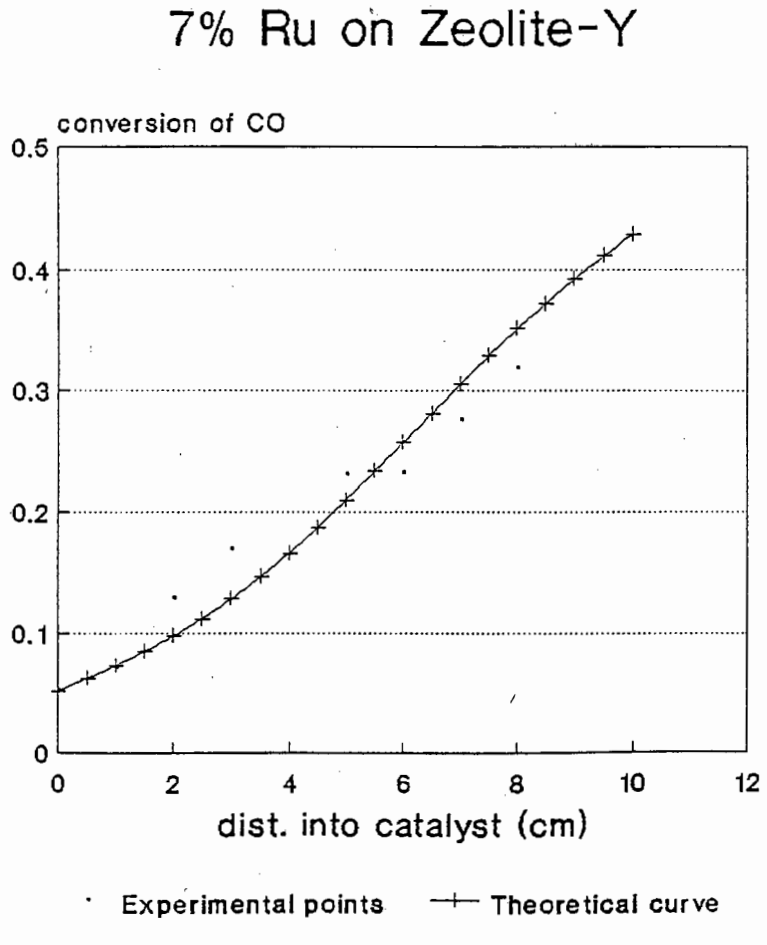

## APPENDIX 39

Data for the methanation reaction over 0.5% ruthenium on ZSM-5

Catalyst : 0.5% Ru/ZSM-5
Temperature : 250°C
CO Flowrate : 6 ml/min
$H_2$ Flowrate : 18 ml/min

| File no. CE | Dist. into Catalyst | Temperature (°C) | Corrected Conc. | Conversion of CO |
|---|---|---|---|---|
| | (cm) | | | (%) |
| 310 | 0 | 251.5 | 1.095 | 4.98 |
| 311 | 1 | 253.9 | 1.073 | 6.92 |
| 312 | 2 | 254.2 | 1.021 | 11.40 |
| 314 | 4 | 255.1 | 0.974 | 15.47 |
| 315 | 5 | 253.3 | 0.856 | 25.78 |
| 316 | 6 | 253.5 | 0.801 | 30.49 |
| 317 | 7 | 254.1 | 0.769 | 33.26 |
| 318 | 8 | 252.2 | 0.709 | 38.48 |

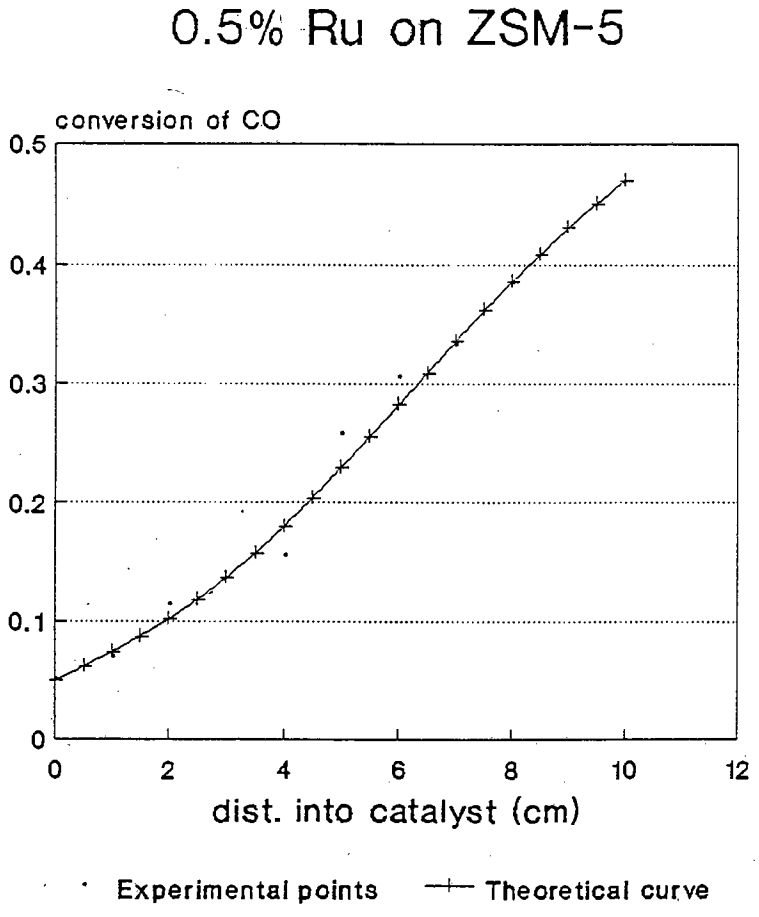

# Appendix 40

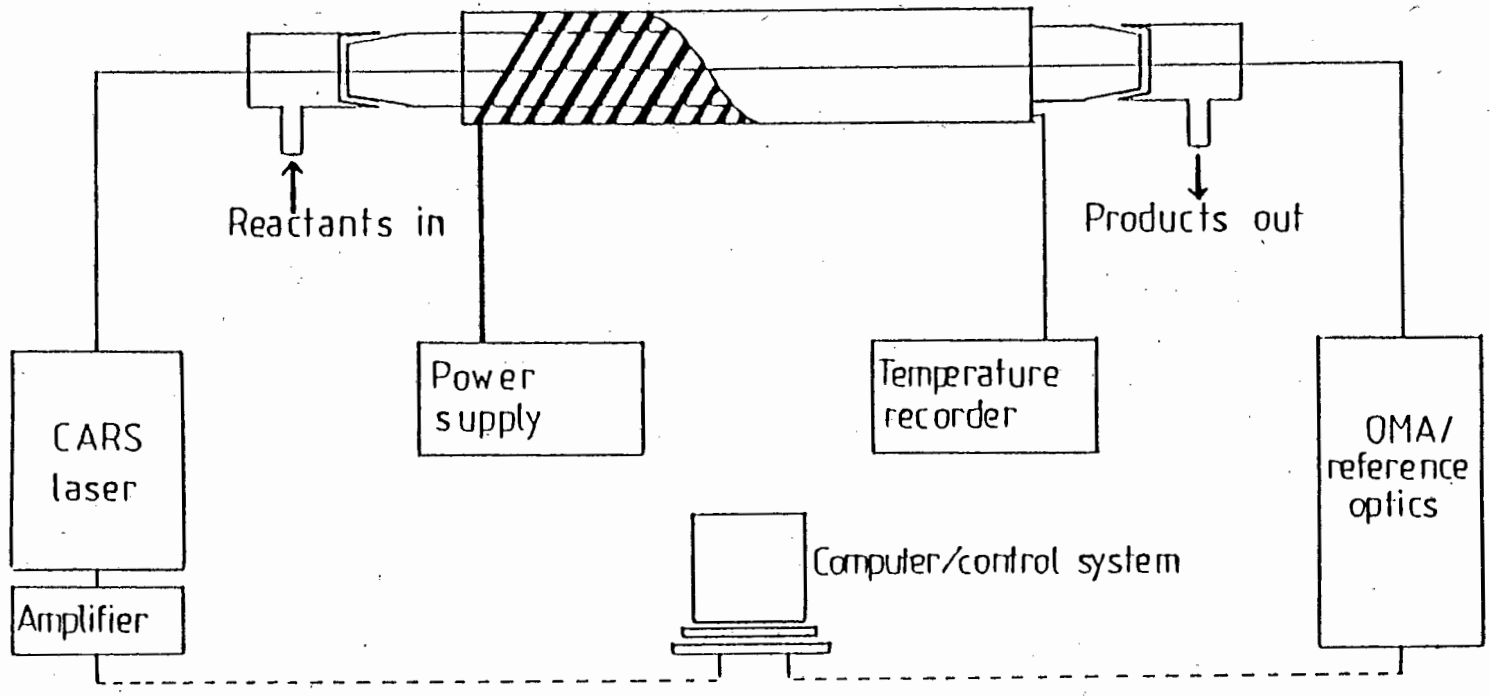


Schematic flowsheet of CARS experimental arrangement.

LASER PROPERTIES - Doubled Nd:YAG beam ($\omega_p$) - 200 mJ pulses; Broadband dye laser ($\omega_s$) - 5 mJ pulses; Pulse length - 15 ns; Beam diameter - 8 mm; Repetition rate - 1 to 10 Hz.

## APPENDIX 41

Modifying the rate for surface reaction.

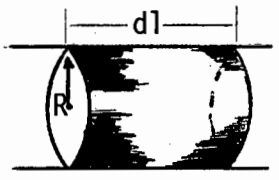


Volume = $\pi R^2 dl$

Rate (r) : Units $[mol/m^3\ sec]$

The catalyst, however, is only coated onto the mesh around the outer surface of the reactor tube. The normal units for the rate equation do not have any physical significance in the case of a tube-wall reactor. The rate thus has to be modified for surface reaction. This can be done as follows:

Surface where reaction occurs = $2\pi R dl$

$$r_{surface} = r_{volume} * \frac{\pi R^2\ dl \quad m^3\ (reactor)}{2\pi R\ dl \quad m^2\ (surface)}$$

$$= \underline{A\ e^{-Ea/RT}\ p_{CO}{}^{X} p_{H}{}^{Y} * R/2 \qquad mol/m^2\ sec}$$

## APPENDIX 42

Calculation of the external diffusion and internal diffusion resistances to determine the rate controlling step.

Calculation of the external diffusion

Using the equation :

$$r_p = k_m a_m (C_b - C_s) \qquad \text{.....(A)}$$

where $k_m$ = mass transfer coefficient
$a_m$ = effective catalyst surface area
$C_b$ = bulk concentration
$C_s$ = catalyst surface concentration

also :

$$j_D = \frac{k_m a_m}{G\ a_t} \left[\frac{\mu}{\rho D}\right]^{2/3} \qquad \text{.....(B)}$$

$$= \frac{0.458\ Re^{-0.407}}{\epsilon_B}$$

where $\epsilon_B$ = void fraction of interparticle space

Incorporating (A) into (B) :

$$(C_b - C_s) = \frac{r_p (\mu/\rho D)^{2/3}}{a_t (G/\rho)}\ j_D$$

where $(\mu/\rho D)$ = Prandtl number

At a temperature of 200°C, the following table may be drawn up :

| Species | flowrate (ml/min) | density ($kg/m^3$) | viscosity (Pa s) |
|---|---|---|---|
| CO | 4 | 0.7583 | $2.419*10^{-5}$ |
| $H_2$ | 12 | 0.0546 | $14.5*10^{-6}$ |

To calculate the bulk diffusivity, the following equation was used :

$$D_{AB} = \frac{0.0018583\ T^{3/2}\ (1/M_A + 1/M_B)^{1/2}}{P_t\ \sigma_{AB}^2 \Omega_{AB}}$$

where $M_A$ = molecular mass of A
$M_B$ = molecular mass of B
$T$ = temperature ( K )
$\sigma_{AB}$ = constants
$\Omega_{AB}$ = collision integral

where $\sigma_{AB} = 0.5\ (\sigma_A + \sigma_B)$
$= f(k_B T/\varepsilon)$

where $k_B$ = Boltzman's constant

Knudsen diffusivity may be calculated using the equation :

$$D_k = 9.70*10^3\ a\ (T/M_A)^{1/2}$$

where 'a' is in Angstrom units

Using the values in Table 11-1 (Smith and van Ness , p 455), the bulk diffusivity works out to be 0.181 $cm^2\ s^{-1}$

Using a pore diameter of 55 angstrom, the Knudsen diffusivity works out to be 0.0221 $cm^2\ s^{-1}$

The overall diffusivity may be calculated as follows :

$$D = \frac{1}{1/D_b + 1/D_k}$$

Substituting the above values, the combined diffusivity works out to be $0.0196\ cm^2\ s^{-1} = 1.96*10^{-6}\ m^2\ s^{-1}$

$$G = \left[\begin{array}{|c|c|c|c|c|c|} \hline X\ ml & 1\ min & l & kgmol & Y\ kg & \\ \hline min & 60\ sec & 1000\ ml & 22414\ l & kgmol & \pi 0.005^2 \\ \hline \end{array}\right]$$

$$= 9.47*10^{-6}\ X\ Y\ \ kg\ m^{-2}\ s^{-1}$$

$$d_p = 25*10^{-6}\ \ m$$

$$Re_{co} = \frac{d_p G}{\mu}$$

$$= \frac{(25*10^{-6})(9.47*10^{-6})(28)(4)}{2.419*10^{-5}}$$

$$= 0.001$$

$$j_D = (0.458)\ Re^{-0.407}$$

$$= 7.34$$

$$a_t = 200\ \frac{m^2}{g} \quad \frac{1000\ g}{kg}$$

$$= 2*10^5\ m^2\ kg^{-1}$$

Using $r_p = 1*10^9\ e^{-25575/1.987/481} \left[\frac{1-x}{4-2x}\right]^{-0.35} \left[\frac{3(1-x)}{4-2x}\right]^{0.85}$

For $x = 0.1$ , $r_p = 0.002961\ mol\ m^{-3}\ s^{-1}$

$= 2.961*10^{-6}\ kgmol\ m^{-3}\ s^{-1}$

$$\text{Prandtl number} = \frac{2.419*10^{-5}}{(0.7583)(1.96*10^{-6})}$$

$$= 16.276$$

$$Pr^{2/3} = 6.422$$

$G = 1.06*10^{-3}$ kg $m^{-2}$ $s^{-1}$

Using equation (A) :

$$(C_b - C_s)_{co} = \frac{(2.961*10^{-6})(6.422)(0.7583)}{(7.34)(2*10^5)(1.06*10^{-3})}$$

$$= 9.267*10^{-9} \text{ kgmol } m^{-3}$$

$$(p_b - p_s)_{co} = RT(9.267*10^{-9})$$

$$= \underline{3.6495*10^{-7} \text{ atm}}$$

Similarly for hydrogen, $(p_b - p_s)_{H2} = \underline{3.312*10^{-7} \text{ atm}}$

Calculation of the internal diffusion

Using the equation $\phi = r_p/3 * (k_1\rho/D_e)^{1/2}$

$k_1 = 0.00239$

$r_p = 25*10^{-6}$ m

also $0 < D_e < 1$

thus

$$r_p << (k_1\rho/ D_e)^{1/2}$$

hence $\phi \rightarrow 0$ and $n \rightarrow 1$

Appendix 43

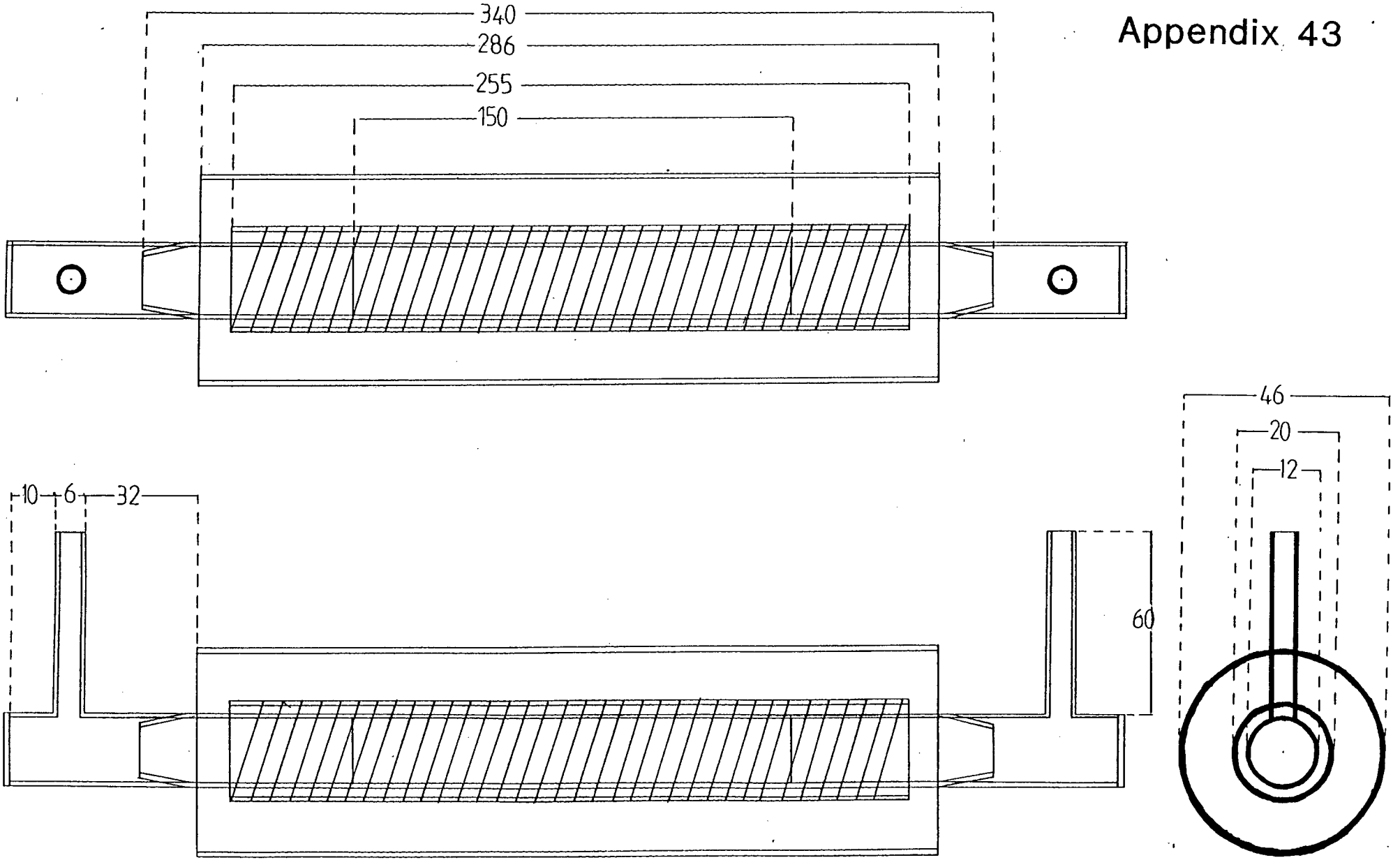


**Methanation Reactor** **Dimensions in mm**

# Appendix 44

# The Methanation Reactor

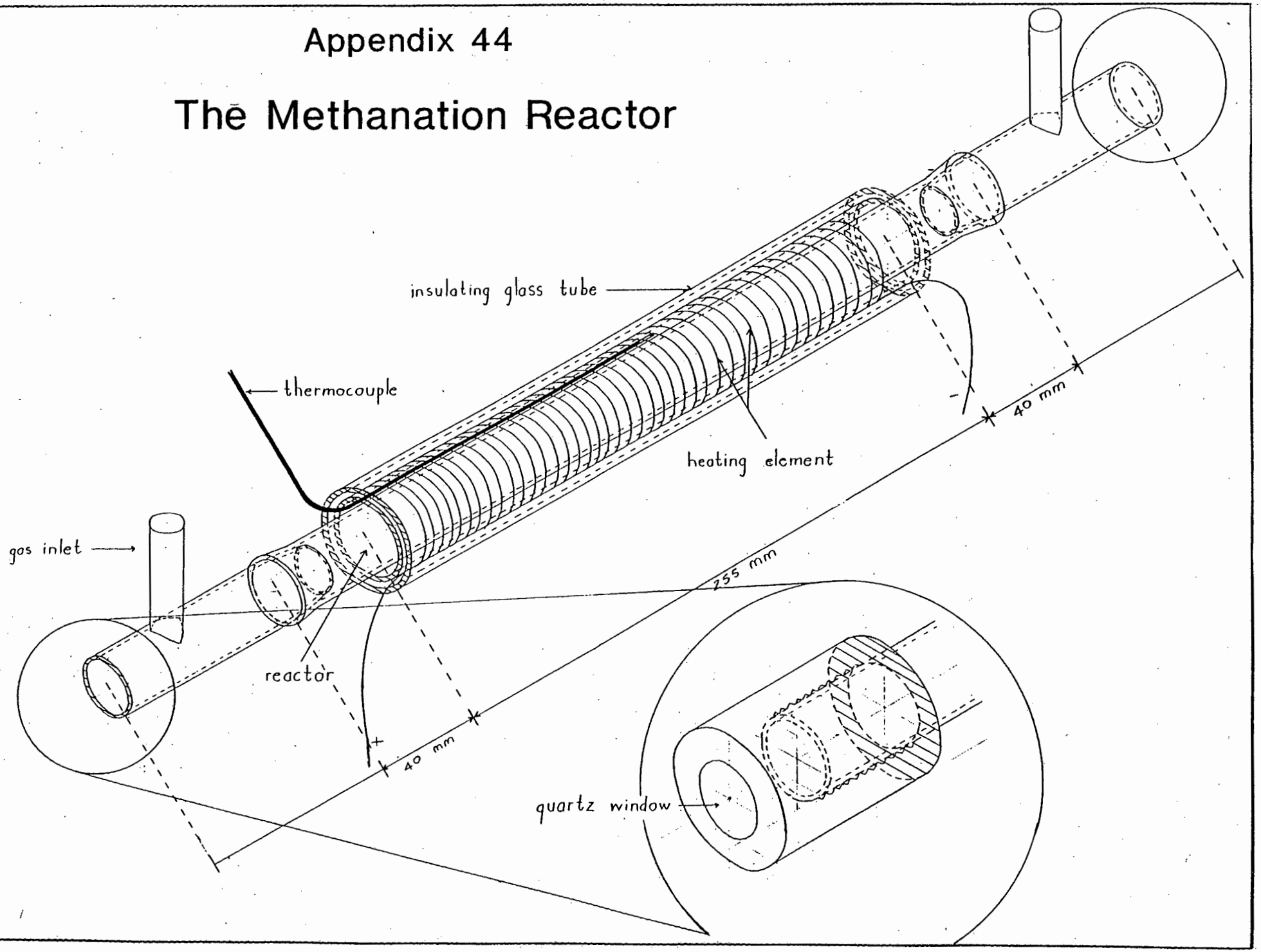

# Appendix 45

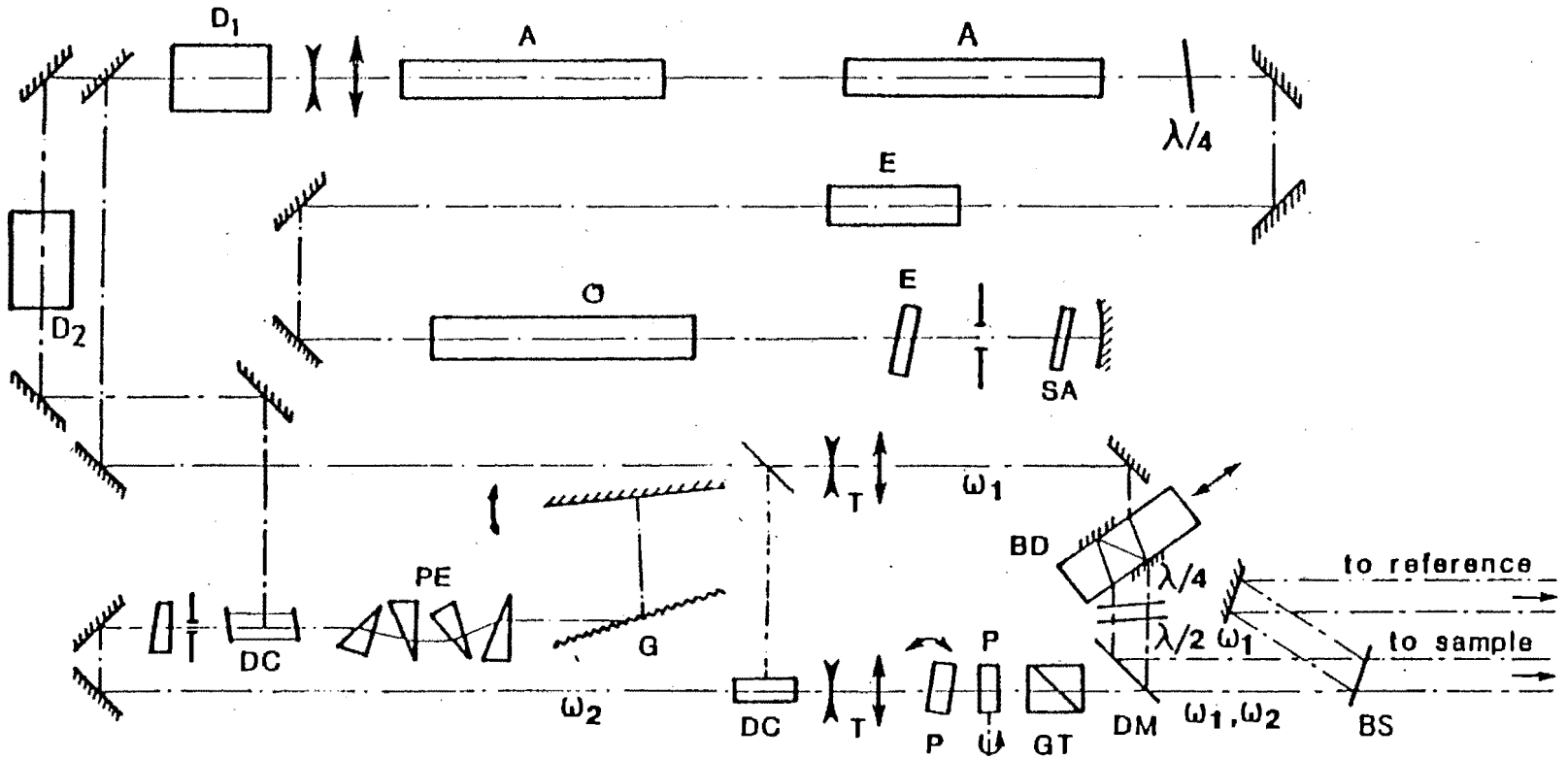


*Laser source assembly. A : Nd YAG amplifier — BD : parallel plate for production of parallel beams for BOXCARS (BOXCARS arrangement shown, translation of the plate allows passage to collinear arrangement without loss of alignment) — BS : beam splitter for reference channel — D : KDP doubler — DC : dye cell — DM : dichroic mirror — E : Fabry-Pérot étalon — G : grating — GT : Glan-Thompson prism — P : AR coated parallel plate for beam translation — PE : prism expander — SA : saturable absorber — T : telescope. λ/4 and λ/2 are quarter-wave and half-wave plates respectively.*